Field and Numerical Investigation of Mixing and Transport of Ammonia in the Ottawa River

By

Ivana Vouk

A thesis submitted under supervisions of
Dr. Majid Mohammadian, Dr. Colin Rennie and Dr. Robert Delatolla
in partial fulfilment of the requirements for the degree of

Masters of Applied Science in Civil Engineering

Department of Civil Engineering
University of Ottawa
Ottawa, Canada
August 2015

The M.A.S.c in Civil Engineering is a joint program
with Carleton University administrated
by Ottawa-Carleton Institute for Civil Engineering

Dedication

To my husband Dave for helping pave the way for this chapter of my life; for providing endless support, encouragement and guidance.

To my family for believing that I could do whatever I set my mind to and for cheering me on every step of the way.

To Hudson for already having an infectious personality.

Abstract

Wastewater treatment plants discharge effluents containing a number of constituents whose concentrations may negatively affect the receiving waters. Current research in mixing and transport between a point source discharge and the ambient environment attempts to reduce these effects through a better understanding of the physical processes involved and development of numerical models to better predict the fate of the effluents under different conditions. This thesis examined the mixing and transport of ammonia discharged from a multiport diffuser of a municipal wastewater treatment plant into the Ottawa River. The river reach was surveyed using an M9 acoustic Doppler current profiler to obtain spatially distributed measurements of depth and velocity. Water samples were collected at and downstream of the diffuser at multiple depths. The samples were analyzed for ammonia concentration and kinetics. The river reach was also simulated in the FLOW-3D model using available turbulence closure schemes. Comparisons were made between measured and modelled results, as well as some empirical and semi-empirical approximations. A combination of measured and modelled results helped describe (quantitatively and qualitatively) the mixing and transport between the discharged effluent and receiving river. Unionized ammonia was tested for regulatory compliance. Both measured and modelled results showed that although the regulatory end-of-pipe discharge concentrations were met, downstream regulations were not met.

Résumé

Les stations de traitement des eaux usées déversent des effluents contenant des substances à des concentrations qui impactent négativement l'étendue d'eau. La recherche actuelle qui porte sur le mélange et le transport d'une décharge d'une source ponctuelle vers l'environnement vise à réduire les effets négatifs sur l'étendue d'eau qui reçoit les eaux résiduelles. À cette fin, la recherche d'actualité cherche à prédire le parcours des effluents sous des conditions variées avec une meilleure compréhension des processus physiques et avec de la modélisation numérique. Ce mémoire étudie le mélange et le transport de l'ammoniac évacué par un diffuseur à port multiple d'une station de traitement des eaux usées de la municipalité qui se trouve sur la rivière des Outaouais. La portée de la rivière est mesurée en utilisant un courantomètre Doppler M9 afin d'obtenir des données réparties dans l'espace de la profondeur et de la vitesse. Des échantillons d'eau sont recueillis à plusieurs profondeurs à la position du diffuseur et en aval de celui-ci afin de déterminer la concentration d'ammoniac de l'eau ainsi que son comportement cinétique. La portée de la rivière est simulée utilisant le modèle FLOW-3D à l'aide des modèles de régimes de turbulence disponibles. Les simulations et les modèles empiriques et semi-empiriques sont validés avec les résultats mesurés. Cette combinaison de résultats mesurés et modélisés permet de décrire le mélange et le transport entre l'eau évacuée et l'étendue d'eau d'une façon quantitative et qualitative. La quantité d'ammoniac non ionisé est vérifiée afin de mesurer la conformité réglementaire. Les résultats mesurés et modélisés montrent que les concentrations de décharge à la fin de la conduite sont conformes alors que les concentrations en aval ne le sont pas.

Acknowledgments

I would like to thank my supervisors for giving me the opportunity to touch upon a variety of aspects in Water Resource Engineering. I would not have learned as much without their continuous support, guidance, patience and a limitless number of discussion sessions.

My field and lab work was only possible thanks to the help of the following staff, students and friends: Elizabeth Jamieson, Melanie Paré, June Harada, Marc Lapointe, Kate Davis, Vahid Pilechi and Matthew Ruta.

My gratitude goes out to my Environment Canada colleagues for encouraging me to go back to school.

Table of Contents

List of Figures

List of Tables

List of Symbols

A_x, A_y, A_z	Fractional area of control volume sides open to flow in the x, y and z directions [m^2]
B	Plume width [m]
b	Gaussian half-width [m]
b	Buoyancy flux per unit diffuser length [m^3/s^3]
b	Discharge line source width [m]
$C_{\varepsilon 1}, C_{\varepsilon 2}, C_{\varepsilon 3}, C_\mu$	Dimensionless constants of equations 5b and 6
C	Concentration [mg-N/L]
C, C_2, c	Dimensionless constants of equations 27, 25 and 7, respectively
C_0	Effluent initial concentration [mg-N/L]
C_C	Centerline concentration [mg-N/L]
C_a	Ambient concentration [mg-N/L]
C_x	Plume concentration at length x from the diffuser [mg-N/L]
D	Nozzle diameter [m]
$Diff_k$	FLOW-3D's diffusion of k term
$Diff_\varepsilon$	FLOW-3D's diffusion of ε term
d	Distance [m]
e_{ij}	Strain rate tensor [1/s]
F	Densimetric Froude number
F	Fluid fraction of a cell in the VOF method
f	Fraction of total unionized ammonia
G_T	Buoyancy production term in FLOW-3D

g_z	Gravitational acceleration [m/s^2]
g'_i	Modified gravitational acceleration [m/s^2]
H	Depth of water at the diffuser [m]
k	Turbulent kinetic energy
L, l	Turbulent length scale [m]
NH_3	Unionized ammonia
NH_4^+	Ammonium
NO_2^-	Nitrite
NO_3^-	Nitrate
$n, n_{Manning}$	Manning's n
P, p	Pressure [N/m^2]
P_T	Turbulent kinetic energy of production term in FLOW-3D
pK_a	Dissociation constant of ammonia
q	Effluent discharge per unit diffuser length [m^2/s]
r	Transverse location of concentration along a given cross-section [m]
S_n	Dilution
s	Distance between ports of a diffuser [m]
T	Temperature [K]
t	Time [s]
U_i, U_j	Mean velocity in tensor notation [m/s]
u_*	Shear velocity [m/s]
u, v, w	Velocity in the x, y, z direction respectively [m/s]
u_i, u_k	Fluctuating velocity in tensor notation [m/s]

V_F	Fractional volume of control volume that is open to flow [m^3]
$v_{magnitude}$	Velocity magnitude [m/s]
v_e, v_n	Easting and northing velocities [m/s]
v_u, v_u	Streamwise and transverse velocities [m/s]
x_n	Near-field length [m]
x, y, z	Coordinates
ε	Rate of dissipation of k
ε_t	Transverse mixing coefficient [m^2/s]
κ	von Karman constant
μ	Dynamic viscosity [kg/(m·s)]
υ	Kinematic viscosity [m^2/s]
υ_τ	Eddy viscosity [m^2/s]
ρ	Fluid density of the computational mesh [kg/m^3]
ρ_0	Reference fluid density [kg/m^3]
ρ_a	Ambient (river) density [kg/m^3]
ρ_e	Effluent density [kg/m^3]

1. Introduction

Wastewater treatment systems often result in the release of high concentrations of organic and inorganic pollutants into open bodies of water. Over the last 100 years growing concern over anthropogenic impacts on the natural environment has resulted in more stringent government regulations leading to the lessening of impacts on receiving waters (Benidickson, 2007). In 2012, Canada introduced legislation regulating effluent releases from wastewater treatment plants (WWTP) (Fisheries Act, 1985). While effluent quality has been improving, it continues to consist of a complex mixture of pollutants, the fate of which is partially determined by the flow patterns, mixing and transport of the effluent when discharged into ambient waters. The impacts, fate and transport of these pollutants in the environment are of interest to science, but more importantly to those populations being served by the receiving waters. Scientists and engineers can play a significant role in predicting the flow patterns when discharged and ambient waters meet, as well as the transport and the fate of the pollutants contained within.

1.1. Objective

This thesis examines the mixing and transport of an effluent discharged into a river (in particular from a municipal WWTP which discharges into the Ottawa River) and how well these processes can be simulated using existing off-the-shelf numerical modeling. The main mechanism of comparison was ammonia, a constituent already present in the discharging effluent. The thesis set out to:

1. describe and predict ammonia concentration at and downstream of a WWTP using both field and numerical modeling methods;
2. collect spatially distributed measurements of depth and velocity, and water samples, to gain insight to the fate of ammonia in the field;
3. determine whether ammonia releases and its presence in the receiving environment meet new regulations;

4. use 3D computational fluid dynamic (CFD) modelling to describe the flow field and ammonia concentration distribution in the river;
5. study the performance of available turbulence models; and
6. compare 3D CFD modelling results to collected data and empirical approximations.

1.2. Novelty of the study

Mixing of effluent discharges and the receiving (ambient) waters is highly dependent on the design of the outfall, which itself is based on effluent characteristics and the receiving environment (as will be shown in this thesis). Many studies have concentrated on understanding mixing principles using laboratory setup and developing semi-empirical equations. Even when CFD modelling has been applied, it has rarely been used to study multiport diffuser discharges in rivers (shallow, moving flows). Instead, diffusers in coastal areas, submerged in deep waters, have been the focus. Whenever riverine studies have been conducted, Rhodamine WT was used in the field to collect fluorescence concentrations – data which would help enable the setup and validation of the models.

To the best knowledge of the author, the use of the FLOW-3D modelling software to study the mixing between a diffuser discharge and ambient flow; and the collection of ammonia (already found in a WWTP effluent) to determine effluent concentrations at and downstream of a diffuser's discharge has not been tried yet.

2. Background

2.1. Description of the Study Reach & ROPEC's Discharge Pipe

2.1.1. Study reach

The Ottawa River drainage basin at 148,000km^2 (NRCAN, 2010) is important economically, socially and ecologically, in both the provinces of Ontario and Quebec. It provides source water for a number of cities and towns lining its shores; it contains a number of hydropower plants; it is used recreationally by locals and tourists; and it is rich with an abundant number of aquatic species and waterfowl. It also acts as a receiving environment for discharges from combined sewer overflows and wastewater treatment facilities.

The study was conducted along the right bifurcation channel around Lower Duck Island (UTM East 453400m to 454600m) on the Ottawa River, downstream of the city of Ottawa (Figure 2.1). The river substrate in the study reach is 100% fine sand with no obvious vegetation, rocks or logs in the mid-channel (WEPP, 2007). The pH of the river is slightly basic (pH >7).

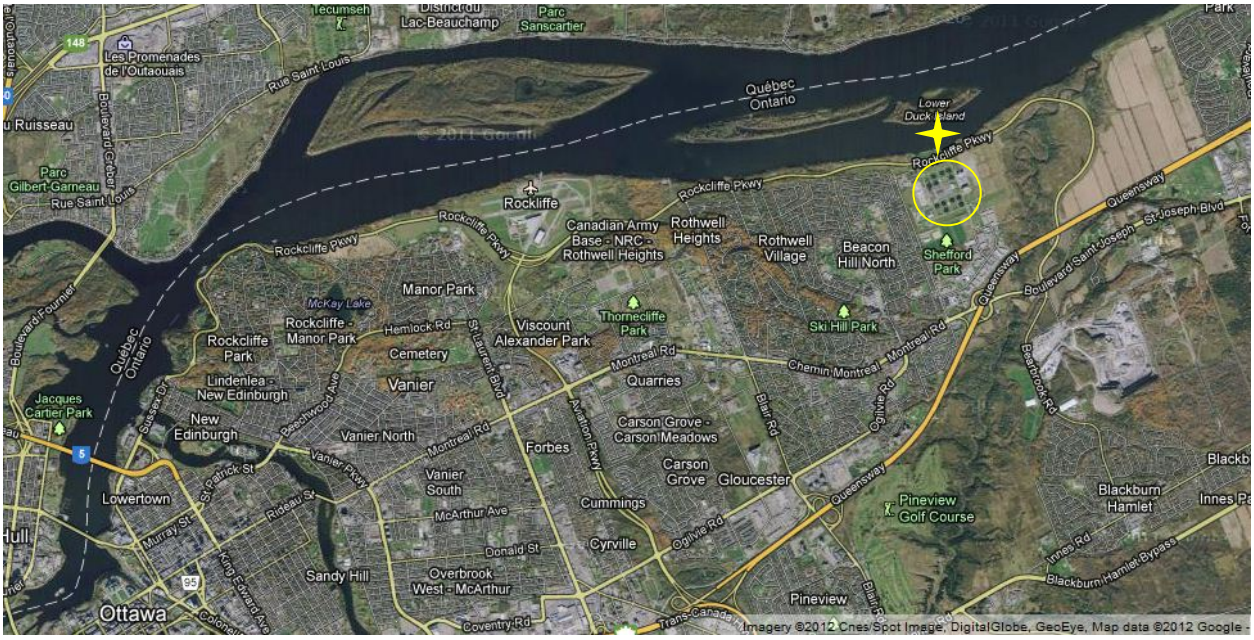

Figure 2.1: Areal image of the North-East sector of the city of Ottawa (Google, 2012). Location of the study area is indicated by the yellow star. The ROPEC wastewater treatment plan is located directly south of the study area (circled in yellow).

The surveyed area was approximately 1.2km long (streamwise) and 300m wide (transverse). The study reach flows east, with a slight meander (curvature). The 31 year average (available period of record) flow for the Ottawa River, for the month of August is 648m^3/s with a low of 540m^3/s and a high of 738m^3/s (EC, 2015). These flows were measured at the nearest gauge (02KF005) located 20km upstream of the study reach at Britannia Bay.

2.1.2. ROPEC's discharge

City of Ottawa's wastewater treatment plant (WWTP) – named Robert O. Pickard Environmental Centre (ROPEC) – is situated approximately 10km downstream of downtown Ottawa (see Figure 2.1). The plant discharges its treated effluent into a portion of the Ottawa River that is dissected by two islands, Upper and Lower Duck Islands, whose lengths are parallel to the river flow. The discharge point lies in the channel between Lower Duck Island and the south bank of the river. Major tributaries upstream of the study reach are the Rideau and Gatineau Rivers, discharging from the south and north banks, respectively. The confluences of each of the rivers are more than 6km upstream of the study reach. Four combined sewer discharges are located immediately upstream of the ROPEC diffuser along the south bank of the river (WEPP, 2007).

ROPEC uses a multiport diffuser, hereon in referred to as a diffuser, to discharge its treated effluent into the river. A diffuser consists of a linear manifold containing a multiple number of ports used to discharge treated effluent. The principle of the diffuser is to promote quicker fluid mixing in the discharge environment by releasing the effluent at a high discharge rate across a larger cross sectional area of the river contributing to rapid dilution of the effluent (Kim & Seo, 2000). Wastewater effluent diffuser designs vary and are optimized to take into account the composition of the effluent mixture and the dynamics of the receiving environment.

ROPEC's diffuser (Figure 2.2) contains 9 ports and is 42m long (from first to last port). Each port is 900mm in diameter with 5.25m spacings between each port. The ports release the effluent vertically, perpendicular to the river bottom and to the ambient flow. The first

port of the diffuser is 112m from the river bank. The manifold is 2400mm in diameter up to the 5th port at which point it tapers through three eccentric reducers to a diameter of 1350mm by the end of the pipe. This reduction in the manifold is conventionally designed to ensure equivalent discharge through all ports compensating for the pressure decrease in the downstream end of the diffuser. The manifold is housed in a trench under the river bed with individual ports emerging perpendicularly from the bed bottom. Riprap covers the manifold to prevent bed erosion or scour. The manifold is lateral to the river flow, and estimated to be at an angle of 89.1° from the river bank downstream of the manifold. Due to a lack of information, port heights were approximated during the field campaign.

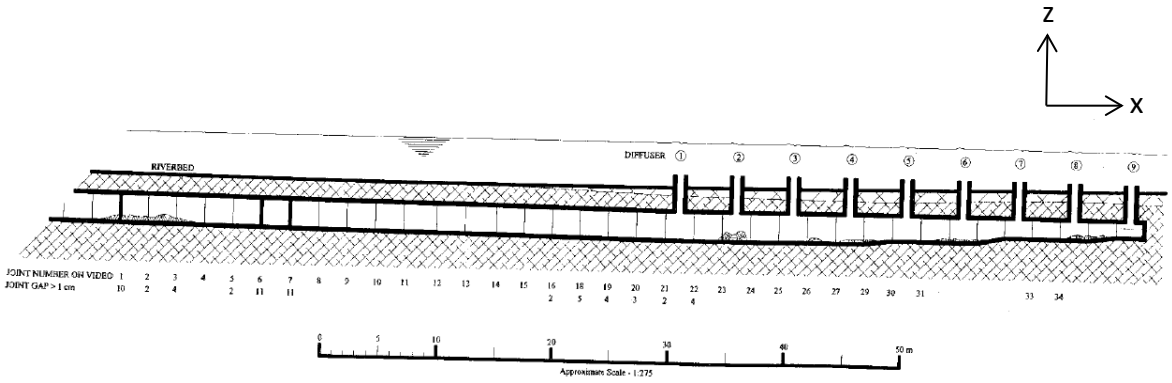

Figure 2.2 A schematic of the ROPEC diffuser as provided by ROPEC. The diffuser discharge inside the manifold is flowing in the x-direction and exiting in the z-direction, vertically. In this schematic, the river flow is in the y-direction, flowing out of the page.

ROPEC is a Class IV WWTP, which is dependent on a point system for classification as described in the Ontario Water Resources Act (1990). The point system is based on a large number of details including the size of population served, the size of the facility, types of treatments available, etc. ROPEC serves residential, commercial and institutional premises as well as local industry. ROPEC is one of the largest treatment facilities in Canada, with average daily flows of 545,000m^3/d and peak daily flows as high as 1,200,000m^3/d (Kennedy & McHarg, 2007). It contains preliminary, primary and secondary biological treatment enhanced for chemical phosphorous removal with disinfection of the final effluent.

2.2. Modelling Review

This thesis examines whether a computational fluid dynamic (CFD) model is capable of simulating mixing of ammonia in an ambient flow of a river upon diffuser discharge from a wastewater treatment plant. The FLOW-3D (v. 10) model developed by Flow Science Inc., USA is used for this purpose. It is a numerical model that can simulate transient or steady-state 1-, 2- and 3-dimensional problems using a finite volume approximation. The model employs Navier-Stokes equations as explained in the following section.

2.2.1. Navier-Stokes equations

Fluid motion is governed by Navier-Stokes equations which include the continuity (equation 1) and momentum equations (2), below. Continuity ensures that flow coming into a system equals the flow coming out of that system. Momentum describes the change in velocity over time and its change over space with respect to advection, diffusion, pressure changes, buoyancy, and other effects. The following are a set of Navier-Stokes equations for incompressible Newtonian fluids, in form particular to the work done in this thesis:

$$\frac{\partial u}{\partial x}+\frac{\partial v}{\partial y}+\frac{\partial w}{\partial z}=0 \tag{1}$$

$$\frac{\partial u}{\partial t}+u\frac{\partial u}{\partial x}+v\frac{\partial u}{\partial y}+w\frac{\partial u}{\partial z}=-\frac{1}{\rho}\frac{\partial p}{\partial x}+\upsilon\left(\frac{\partial^2 u}{\partial x^2}+\frac{\partial^2 u}{\partial y^2}+\frac{\partial^2 u}{\partial z^2}\right) \tag{2.a}$$

$$\frac{\partial v}{\partial t}+u\frac{\partial v}{\partial x}+v\frac{\partial v}{\partial y}+w\frac{\partial v}{\partial z}=-\frac{1}{\rho}\frac{\partial p}{\partial y}+\upsilon\left(\frac{\partial^2 v}{\partial x^2}+\frac{\partial^2 v}{\partial y^2}+\frac{\partial^2 v}{\partial z^2}\right) \tag{2.b}$$

$$\frac{\partial w}{\partial t}+u\frac{\partial w}{\partial x}+v\frac{\partial w}{\partial y}+w\frac{\partial w}{\partial z}=-\frac{1}{\rho}\frac{\partial p}{\partial z}+\upsilon\left(\frac{\partial^2 w}{\partial x^2}+\frac{\partial^2 w}{\partial y^2}+\frac{\partial^2 w}{\partial z^2}\right)+g_z\left(\frac{\rho-\rho_0}{\rho}\right) \tag{2.c}$$

Variables u, v and w represent the velocities in the x, y and z (streamwise, transverse and vertical) directions, respectively; while p, g, ρ, ρ_0 and υ represent the pressure component, gravity acceleration, fluid density, reference fluid density and kinematic viscosity, respectively. Note that the equations are divided by density and the buoyancy term is applied to the vertical (in the z-direction) gravitational acceleration.

The Navier-Stokes equations cannot be solved analytically except for some special cases. Instead, numerical methods are widely used to solve these equations.

2.2.2. Turbulence modelling

Understanding turbulent flows is of great significance in studies of open-channel flows. Their highly random, three-dimensional and unsteady flows are difficult to predict (Rodi, 1993). Turbulent motion in rivers creates eddies, whose sizes range so greatly they become difficult to resolve by any one model. Thus, solutions to solving for most effective scales have become of interest, where turbulence modelling plays a large role (Rodi, 1993; Versteeg & Malalasekera, 2007). Much research has been conducted on finding the most accurate and economical solution to describe the effects of turbulence on flows.

Temporal averaging

One method to aid in the description of turbulence is by time averaging the Navier-Stokes equations. This technique simplifies the equations to a form commonly known as Reynold's Averaged Navier-Stokes (RANS) equations. When using RANS, the continuity equation only requires mean velocities. Thus, momentum equations are simplified to the following equation, where g' takes into consideration the buoyancy effect as in equation (2):

$$U_j \frac{\partial U_i}{\partial x_j} = -\frac{1}{\rho}\frac{\partial P}{\partial x_i} + \frac{\partial}{\partial x_k}\left(\upsilon \frac{\partial U_i}{\partial x_k} - \overline{u_i u_k}\right) + g'_i \qquad (3)$$

For simplification, the equation was written in tensor notation, where the $U_i = (U, V, W)$ and $u_i = (u, v, w)$ terms represent the mean and fluctuating velocities in tensor notation, respectively. Here, the pressure term P is also averaged. Although simplified, six new variables are introduced (stemming from the $\overline{u_\iota u_k}$ term) whose solutions are required before the RANS equations can be solved. These variables are known as Reynold's stresses, which represent momentum transfer caused by velocity fluctuations. They are solved using turbulence modelling.

In 1877, Boussinesq introduced the concept of eddy viscosity, where turbulent stresses are assumed to be proportional to mean velocity gradients (e.g. Rodi, 1993). In turbulent flows, momentum exchange increases. Thus, the virtual viscosity, termed eddy viscosity, is introduced to represent the increased momentum exchange (Versteeg & Malalasekera, 2007). In the RANS equations, Reynold's stress in the gradient of the shear stress term is replaced with eddy viscosity, υ_τ, times the velocity gradient:

$$\upsilon \frac{\partial U_i}{\partial x_k} - \overline{u_\iota u_k} = (\upsilon + \upsilon_\tau) \frac{\partial U_i}{\partial x_k} \tag{4}$$

Using the eddy viscosity concept, a range of methods has been developed for turbulence modelling, some of which are discussed further.

The simplest forms of turbulence models are called zero-equation turbulence models, where the eddy viscosity is calculated from given flow variables. These are algebraic in form and consider the eddy viscosity by means of experimental measurements, physical estimates, empirical formulas or relationship to the mean-velocity distribution (Rodi, 1993). One-equation turbulence models solve turbulent energy transport using an additional (partial differential) equation which generally solves for turbulent kinetic energy taking into account diffusion and advection of kinetic energy. Two-equation models

solve for turbulent viscosity using one equation for turbulent kinetic energy and another for the scale of turbulence e.g. energy dissipation rate (ε). A large number of models have been developed, but this thesis will discuss only those models that have been utilized in the FLOW-3D model.

k-ε model

The *k-ε* turbulence scheme models turbulence by examining the turbulent kinetic energy (k) and the rate of dissipation of turbulent kinetic energy (ε). Both equations take into account advection, diffusion, production and destruction of the variable. The turbulent kinetic energy and the rate of dissipation of the turbulent kinetic energy of the *k-ε* model used in FLOW-3D are as follows, respectively:

$$\underbrace{\frac{\partial k}{\partial t}}_{\text{I}} + \underbrace{\frac{1}{V_F}\left\{uA_x\frac{\partial k}{\partial x} + vA_y\frac{\partial k}{\partial y} + wA_z\frac{\partial k}{\partial z}\right\}}_{\text{II}} = \underbrace{P_T + G_T + Diff_k - \varepsilon}_{\text{III}} \tag{5a}$$

$$\underbrace{\frac{\partial \varepsilon}{\partial t}}_{\text{I}} + \underbrace{\frac{1}{V_F}\left\{uA_x\frac{\partial \varepsilon}{\partial x} + vA_yR\frac{\partial \varepsilon}{\partial y} + wA_z\frac{\partial \varepsilon}{\partial z}\right\}}_{\text{II}} = \underbrace{\frac{C_{\varepsilon 1}\cdot\varepsilon^2}{k}(P_T + C_{\varepsilon 3}\cdot G_T) + Diff_\varepsilon - \frac{C_{\varepsilon 2}\cdot\varepsilon^2}{k}}_{\text{III}} \tag{5b}$$

Term I describes the change of *k* and *ε* over time; term II describes advection of *k* and *ε*, and term III is the rate of destruction of *k* and *ε*. P_T is the rate of production of *k* and *ε*, G_T is the buoyancy production term, and $Diff_k$ and $Diff_\varepsilon$ describe the diffusion of k and ε, respectively. For a full definition of P_T, G_T, $Diff_{k_T}$ and $Diff_\varepsilon$ please refer to the FLOW-3D manual (Flow Science, 2010). The constants C_μ, $C_{\varepsilon 1}$, $C_{\varepsilon 2}$ and $C_{\varepsilon 3}$ are empirical constants whose values are: 0.09, 1.44, 1.92 and 0.2, respectively. Variables A_x, A_y and A_z are the "fractional area of control volume sides open to flow in x-, y- or z-direction" (Flow Science, 2014) corresponding to the FLOW-3D's FAVOR functions, while V_F is the "fractional volume

of control volume that is open to flow" (Flow Science, 2014) relating to the VOF method. Both will be discussed in Section 2.2.3.

RNG k-ε model

The Renormalized Group (RNG) k-ε model (Yakhot & Orszag, 1986) renormalizes the Navier-Stokes equations. It uses equations similar to the standard k-ε model, but through mathematical filtering and modifications to viscosity will describe the small scale turbulence in terms of larger scale motions (Versteeg & Malalasekera, 2007). In this way, most of the empirically derived k-ε equations coefficients are explicitly derived from the model itself (Flow Science Inc., 2010).

For both the k-ε and RNG k-ε models, the eddy viscosity υ_τ in FLOW-3D is equal to:

$$\upsilon_\tau = C_\mu \frac{k^2}{\varepsilon} \tag{6}$$

In the RNG k-ε model the constants C_μ and $C_{\varepsilon 1}$ are mathematically derived to: 0.085 and 1.42, respectively.

Spatial averaging

Large Eddy Simulation approach

A Large Eddy Simulation (LES) uses a spatial filter to separate small scale eddies from large ones. Here, instead of temporal averaging taking place (as in RANS models), spatial averaging takes place. Small scale eddies are approximated, while large scale eddies are calculated with respect to changes in time and space. This theory assumes that small eddies are isotropic, having a universal behaviour, whereas large eddies depend on mean velocity, the system's geometry and boundary flow conditions (Versteeg & Malalasekera, 2007). Here, the concept of sub-grid-scale (SGS) stresses arises, as it serves a function to

parametrize the small length-scales which cannot be resolved by the large scale mesh of LES. In FLOW-3D, small scale eddy approximations in the LES model are represented by the following equation for v_τ, which is the LES kinematic eddy viscosity (Flow Science, 2010):

$$v_\tau = (cL)^2 \sqrt{2e_{ij}2e_{ij}} \tag{7}$$

Variable c represents a constant with values between 0.1 and 0.2, while e_{ij} represents the strain rate tensor and is mathematically described as:

$$e_{ij} = \frac{1}{2}\left(\frac{\partial \overline{u_i}}{\partial x_j} + \frac{\partial \overline{u_j}}{\partial x_i}\right) \tag{8}$$

L is the length scale calculated by the mean cell size:

$$L = (\delta x \delta y \delta z)^{\frac{1}{3}} \tag{9}$$

2.2.3. Numerical method

FLOW-3D exploits some explicit and implicit schemes to solve for relevant parameters. A special method for employing an Eulerian staggered grid is used by incorporating the Volume of Fluid (VOF) method and Fractional Area/Volume Obstacle Representation (FAVOR) function. This section provides a summary of FLOW-3D's functionality and some concepts particular to the model.

Numerical solution of Navier-Stokes equations

A pressure correction approach is used to solve the Navier-Stokes equations. For three-dimensional incompressible flows, pressure in FLOW-3D can be approximated using several different implicit schemes, the most common being the successive over-relaxation

(SOR) method. This method is used for solving a linear set of equations resulting in faster convergence. An implicit solver is used to ensure the solution's stability. The momentum advection terms may be approximated using first or second order accuracy. The viscous stress, heat transfer and advection solvers may be modeled using explicit or implicit schemes. FLOW-3D will solve the Navier-Stokes equation with continuity, but also provides the user with an option to use constant or zero velocity.

Computational mesh

Simulations in FLOW-3D are performed exclusively using a rectangular Cartesian or cylindrical mesh. Structures or obstacles (or necessary portions thereof) within a study domain are fully enveloped by the mesh, which does not need to conform owing to the FAVOR function (described below). In fact, any required geometry (e.g. topography) is fully embedded into the mesh.

Modelling wall boundaries and obstacles

The FLOW-3D model utilizes a Fractional Area/Volume Obstacle Representation (FAVOR) method, which makes use of a variable porosity to identify obstacles to fluid flow, such as solid structures in the way of flow. This way, a simple rectangular (or a brick) mesh is employed, as opposed to a mesh whose cell sizes change to accommodate the shape of the obstructing structure. For this reason, the mesh size may be coarser than that required in other models. Obstacles are characterized by the model as fractions of areas and volumes of each cell, and are given a value for porosity. The model calculates the fraction of an area and volume open to flow for each cell surface and brick volume, respectively. The fraction is identified as porosity, which is equal to 0 for solid (or obstacle) regions and 1 (or unity) for fluid regions (Hirt & Sicilian, 1985). The porosity values are used in all of the fluid dynamics equations; see equation (5) (k-ε model) for an example. This method improves the solution accuracy of the numerical modelling near walls (Barkhudarov, 1997).

Modelling free surface

In order to track free surfaces (or interfaces between two fluids – which are not discussed in this thesis) the Volume of Fluid (VOF) method is used in FLOW-3D. In this method, a transport equation is solved for a fluid fraction function *F*:

$$\frac{\partial F}{\partial t} + \frac{1}{V}\nabla \cdot (\mathbf{Au}\mathrm{F}) = 0 \tag{10}$$

This function identifies whether a mesh cell is empty ($F = 0$), full of fluid ($F = 1$) or partially filled ($0 < F < 1$). A partially filled cell is an indication that the cell contains a free-surface. Through identification of closest neighbouring mesh cells, the free surface boundary is determined. FLOW-3D assigns zero shear stress and uniform pressure to this boundary.

Boundary conditions

An important factor to a successful simulation of a numerical model requires that proper initial and boundary conditions are assigned. For this reason conditions imposed on the studied system must be understood and translated to initial and boundary conditions of a model. Initial conditions are values of variables to be computed by a model, at time equal 0. Boundary conditions are further discussed below.

Boundary conditions for flow

Boundary conditions for flow are assigned at the mesh edge or around obstacles, where free-slip or no-slip boundaries can be identified. Free-slip boundaries identify surfaces which have zero tangential stress. FLOW-3D ensures these are met by equating velocity gradients to zero for all cell faces which have zero flow or have been identified as free-surface areas. All rigid wall and free boundary surfaces have free-slip boundaries in FLOW-3D. No-slip conditions, on the other hand, are created using a wall shear-stress, which will be discussed further in section *Boundary conditions for turbulence models*.

Boundary conditions in FLOW-3D are imposed on all six sides of a rectangular mesh. A variety of options are available, so only those that are used in this thesis are described:

- A rigid wall boundary identifies a boundary where normal velocity is equal to zero. Here, tangential velocities can be assigned zero or some other value, depending on whether free-slip or no-slip conditions are required, respectively.
- A symmetrical boundary option assumes that conditions at the boundary also extend outside of it, without any flux. Thus, a study domain may be assumed to extend beyond the given mesh. This boundary option also allows for transfer of information between adjacent meshes. When applied to a water surface, this boundary option is known as a rigid lid.
- Fixed velocity boundaries accept a single value for the velocity normal (which is defined by the user) across the boundary. Fluid elevation must also be specified at this boundary condition. Tangential velocities are defined if cross-flow at the boundary exists. Pressure conditions are not and, in general, cannot be specified since velocities will depend on pressure gradients. Here, fluid fraction is assumed to be unity (unless modified by the user) everywhere except at free surfaces and where obstacles exist.
- Grid overlay is a special boundary condition which is only used in a restart simulation (a new simulation which uses the final flow details of a preceding simulation). This becomes extremely useful for analysis of a smaller portion of a study domain. The mesh overlay boundary interpolates the flow solution of the preceding simulation along a newly identified boundary in the following simulation. Boundary conditions can vary spatially, but are held constant for the restart simulation (Flow Science Inc., 2010).
- Outflow boundary in FLOW-3D is an option available to model uniform flows at the outflowing mesh border(s). In order to ensure this, normal velocity gradients at the boundary are set to zero (Flow Science Inc., 2012).

Where applicable, most flow boundaries can be time dependent, but since steady-state modelling was applied in this thesis, this option and the relevant theory is not discussed.

Boundary conditions for concentration and temperature

Depending on the study requirement, temperature or concentration values may be specified at the input boundary. The values are used to help initiate the problem solving at the boundary and carry on forward (downstream) throughout the mesh. For the remaining boundaries, values are calculated based on internally calculated values of internal cells. Thermal conditions might change along rigid walls due to friction caused by fluid and wall interaction. In some cases even slight changes might contribute to large variations in results. Concentration might also be affected along the boundary.

For point source inflows, a function known as the mass-momentum source may be invoked in FLOW-3D. Point sources (or sinks) introduce new flow to (or from) the modelling domain. A two-dimensional surface of any geometry can be created and directed at any direction in the Cartesian coordinate system from which a specified mass or discharge is introduced (or removed) at user specified temperature and concentration values. The mass-momentum source can be placed anywhere within the model domain, even at the mesh boundary.

Boundary conditions for turbulence models

Advection and diffusion fluxes are assigned values of 0 at rigid walls and tangential stress is assigned 0 at the free-surface. Inflow boundaries can be user specified, but if not, ε is calculated using equation:

$$\varepsilon = C_{\mu}\sqrt{\frac{3}{2}}\frac{k^{3/2}}{l} \tag{11}$$

where l is the turbulent length scale. FLOW-3D defines l as 7% of the smallest cell size, but the recommended value is 7% of the depth (for rivers) (Flow Science, 2010).

For cells containing rigid walls, FLOW-3D assigns values to k and ε, based on the log-law, which leads to the following equations:

$$k = \frac{u_*^2}{\sqrt{C_\mu}} \quad \text{and} \quad \varepsilon = \frac{u_*^3}{\kappa d} \tag{12}$$

where u_* is the shear velocity arising from the log-law described in FLOW-3D as:

$$u = u_* \left[\frac{1}{\kappa}\ln\left(\frac{\rho u_* d}{\mu}\right) + 5.0\right] \tag{13}$$

The velocity u is the component parallel to the wall, κ represents the von Karman constant 0.41, μ represents the dynamic viscosity and d is the perpendicular distance of the velocity u from the wall. Note that the FAVOR method only approximates the location of the wall within any given cell, thus further approximations are made to calculate u, u_* and d.

2.2.4. Model based on empirical functions

The numerical model used in this thesis was compared to a model commonly used for simulating mixing and transport of pollutants from a point-source discharge. This model, called the Cornell Mixing Zone Expert System (CORMIX) was originally developed by the United States Environmental Protection Agency (USEPA) and Cornell University to use for prediction and regulatory compliance of continuous point source discharges, such as wastewater effluent discharges. In other words, CORMIX was created to model the mixing between point source discharges and the receiving (ambient) environment, as well as to aid in the design of discharge ports. The model is based on semi-empirical equations, developed through laboratory and field research. It is data driven in that it allows the user

to specify the discharge and ambient conditions, as well as the configuration of the discharge ports. The model deduces which hydrodynamic method (or semi-empirical model) is best fit for each simulation by referring to what is known as a rule based expert system (Doneker & Jirka, 2007). According to the authors, the CORMIX expert system can handle most existing configurations, except for cases where complicated discharge geometries are evident or where the ambient flow exhibits highly non-uniform conditions including local recirculating flows. In terms of water quality parameters, the system can predict the mixing of conservative and first-order decay rate processes.

CORMIX sub-models

Within CORMIX, three sub-models can be chosen: CORMIX1, which models a single submerged port discharge; CORMIX2, which models a submerged diffuser discharge; and CORMIX3 which models an above surface single port outfall. For the purposes and relevancy of this thesis, only the first two have been implemented. The CORMIX package also offers some post-processing tools, one being the Cornell Buoyant Jet Integral Model (or CorJet). CorJet acts as a secondary model which allows for the prediction of the near-field jet trajectory, dilution and plume geometry (Zhao *et al*., 2011) to provide localized information that is simplified in the original CORMIX run. This tool cannot be used for shallow rivers, as it assumes that the receiving water body is deep and unbounded, or in other words, that there are no boundary interactions present.

Simulation results provide information about jet or plume geometry; dilution and concentration of the chosen constituent (including reaction effects, if existing) along the hydrodynamic centreline; jet or plume flow if it differs from ambient flows; cumulative travel time used to assess the usefulness of the predictors for steady-state simulations; as well as information such as bottom or bank attachment and model restrictions, if necessary (Doneker and Jirka, 2007).

Provided with details of discharge characteristics (effluent details and outfall information) and ambient conditions, CORMIX will run through a series of existing classifications available to it until reaching the most suitable case for the given situation. From here, it will

provide simulation results defined by the chosen case, as well as reasons as to why this case was chosen (Doneker and Jirka, 2007). The model contains a large suite of classifications (Doneker & Jirka, 2007) which, as Jirka, *et al.* (1996) claim is fit for approximately 80% – 95% of existing situations (percentage depends on which of the three modules are used). The classifications have been developed through both theoretical derivations and experimental studies based on flow interactions and calculated physical parameters (Jirka, *et al*. 1996). An example of a decision tree identifying flow classification for multiport diffusers in uniform density ambient layer is provided in Figure 2.3 (Doneker and Jirka, 2007). The flow interactions are based on length scales, which describe the relative influence a particular hydrodynamic processes have on the mixing between the effluent and the ambient flow. Examples of length scales for the CORMIX2 model are provided in Figure 2.4 (Doneker and Jirka, 2007).

In order to describe mixing results along the path of travel, the model will provide descriptions of jet/plume and cross-sectional distributions for spreading with a Gaussian or a top-hat (uniform) profile, as well as signifying whether the mixing is in the near- or far field region. Once again, depending on the situation, CORMIX will determine the outcome of the profile, whose information can be used to plot spatial contours of the plume. Figure 2.5 provides a description of the distributions that may ensue from the simulation. Employing a Gaussian function, the jet/plume width in CORMIX is defined at 37% or 46% from the centreline of the concentration (see Figure 2.5), although in their study, Zhang & Zhu (2011) use 50% from the centreline for jet half-width which they claim is a more commonly used method. For Gaussian 37% half-width (or 1/e) distributions, the concentration C at each transverse location r along the given cross-section is:

$$C = C_C e^{-r^2/b^2} \tag{14}$$

where C_C is the centreline concentration and b is the Gaussian half-width, both of which are provided by the model. For Gaussian 46% half-width distributions, the concentration at each transverse location along the given cross-section is:

$$C = C_C e^{-\pi r^2 / 4b^2} \tag{15}$$

CORMIX has been widely used for diffuser discharges.

The CORMIX2 model ignores individual jet spreading and merging from discharges of the diffuser nodes and instead assumes a long discharge port (often called a line source) with equivalent dynamic processes originating from it (Doneker and Jirka, 2007). The CORMIX manual suggests that if individual jet spreading and merging are important to the study, the user should employ CORMIX1 instead. Zhang & Zhu (2011) show that these tricks do help modelling results, depending on the region of study. The model takes into consideration three different diffuser designs: unidirectional (where net horizontal momentum flux is perpendicular to the diffuser line), staged (where net horizontal momentum flux is parallel to the diffuser line) and alternating (where no net horizontal momentum flux is produced) designs (Doneker & Jirka, 2007). For a more detailed explanation, please refer to Doneker & Jirka (2007).

Some other assumptions made by the CORMIX models, relative to this study are listed below:

- The cross-section of the ambient flow is a uniform, rectangular channel that may or may not be bounded.
- The ambient velocity is uniform throughout the given cross-section.
- The ambient density is uniform throughout the given cross-section.
- All models are steady state models.

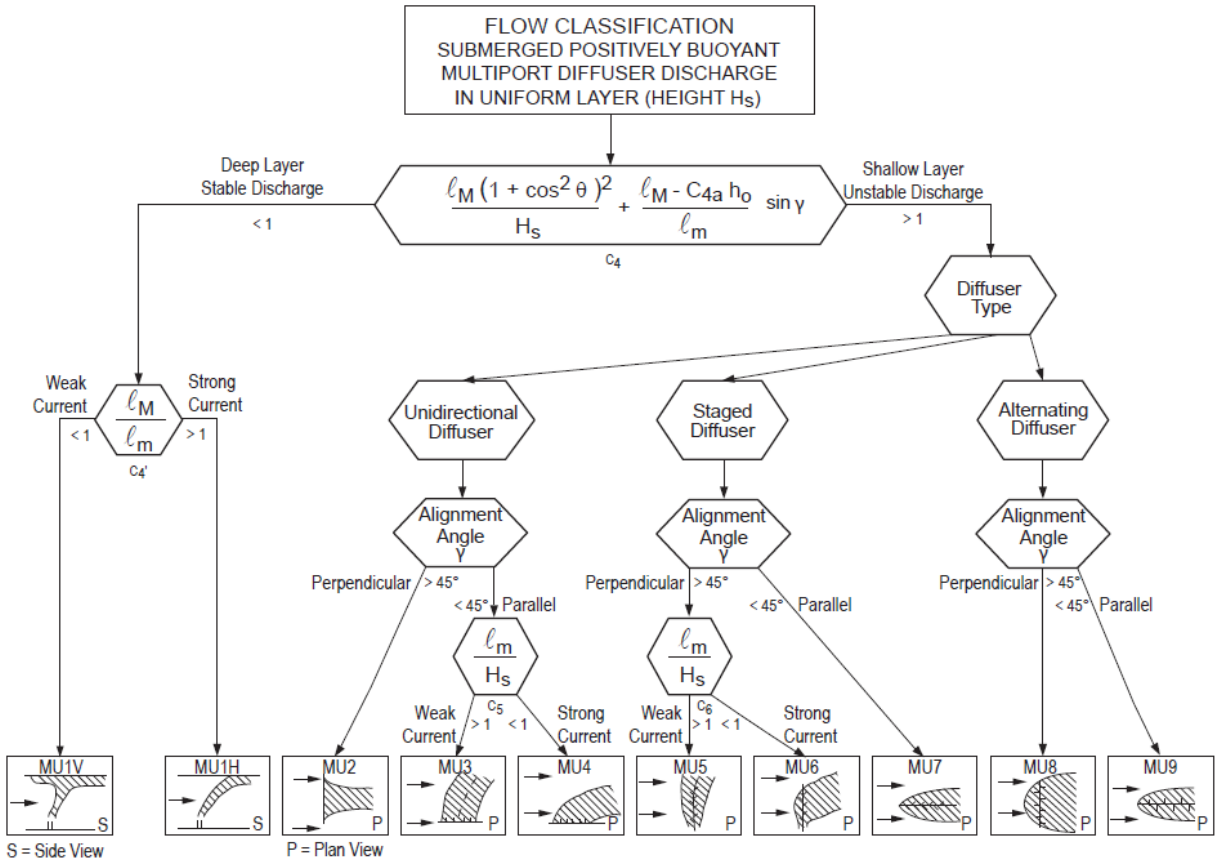

Figure 2.3: Flow classification decision tree for multiport diffusers in uniform density ambient layers, utilized by CORMIX2 (Doneker & Jirka, 2007).

Length Scale	Interpretation
Slot jet/plume transition: $\ell_M = m_o/j_o^{2/3}$	For combined buoyant jet flow, the distance at which the transition from jet to plume behavior takes place in a stagnant uniform ambient.
Slot jet/crossflow: $\ell_m = m_o/u_a^2$	In the presence of a crossflow, the distance of the transverse (i.e. across ambient flow) jet penetration beyond which the jet is strongly deflected (advected) by the cross flow. For a strictly co-flowing discharge ($\theta = 0$, $\sigma = 0$), the length of the region beyond which the flow is simply advected.
Slot jet/stratification: $l_m' = m_o^{1/3}/\varepsilon^{1/3}$	In a stagnant linearly stratified ambient, the distance at which a jet becomes strongly affected by the stratification, leading to terminal layer formation with horizontally spreading flows.
Slot plume/stratification: $l_b' = j_o^{1/3}/\varepsilon^{1/2}$	In a stagnant linearly stratified ambient, the distance at which a plume becomes strongly affected by the stratification, leading to terminal layer formation with horizontally spreading flows.
Crossflow/stratification: $l_a = u_a/\varepsilon^{1/2}$	The vertically upward or downward floatation distance beyond which a plume becomes strongly advected by crossflow.

Notes: $M_o = U_oQ_o$, kinematic momentum flux
$J_o = g'_oQ_o$, kinematic buoyancy flux
$Q_o = U_oA_o$, source discharge volume flux
A_o = port area
u_a = ambient velocity
U_o = port discharge velocity
ε = ambient buoyancy gradient
g'_o = discharge buoyancy = $g(\rho_a - \rho_o)/\rho_a$
n = total number of nozzles
L_D = overall diffuser length

Figure 2.4: Length scales for multiport diffusers utilized by CORMIX2 (Doneker & Jirka, 2007).

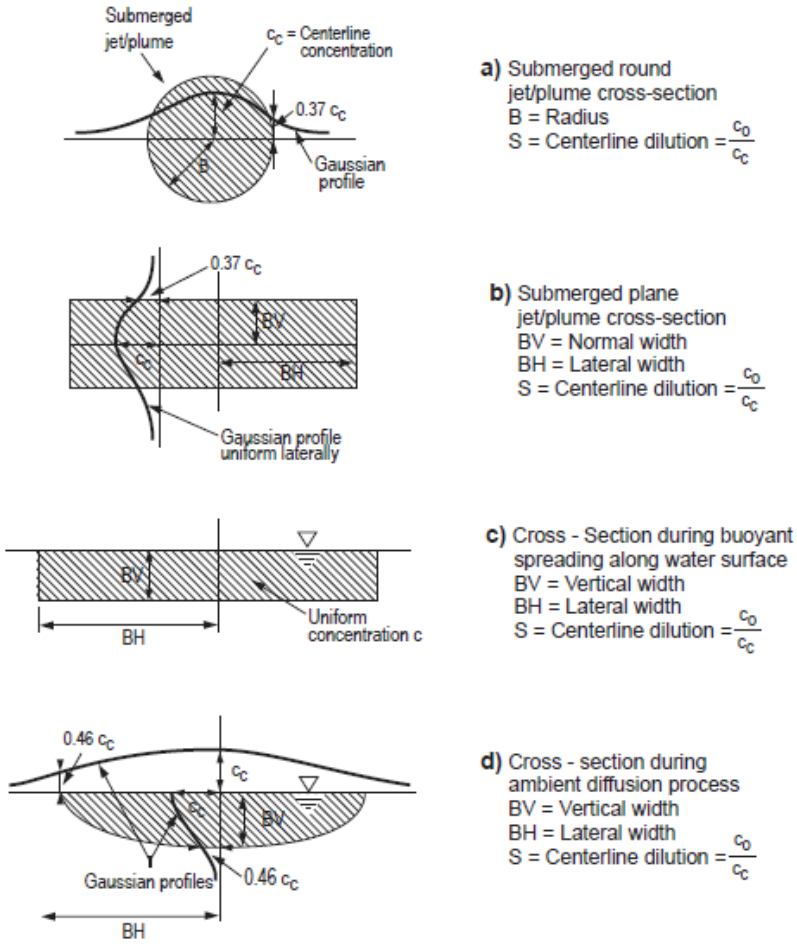

Figure 2.5: Cross-sections of different types of discharge profiles calculated by CORMIX (Doneker & Jirka, 2007).

2.3. Literature Review

The literature review encompasses modelling methods applied in river transport and mixing. In particular, studies of the physical processes of river mixing caused by discharges from diffuser effluents are summarized, applicable modelling efforts are reviewed including CFD modelling and an emphasis is given to the treatment of the FLOW-3D model in this area or studies of similar concern.

2.3.1. Mixing in rivers

River mixing involves two main processes: transportation and transformation. Transportation is primarily a physical vehicle, involving advection and diffusion. Advection

relates to the movement of a fluid governed by the flow characteristics of a river. Diffusion can be subdivided into molecular and turbulent diffusion processes; where molecular diffusion is described as a random process due to the movement of particles from areas of high to areas of low concentration; while turbulent diffusion is a combination of molecular diffusion and turbulent velocity fluctuations. In turbulent flows, Rutherford (1994) notes that, "small-scale turbulent eddies increase local concentration gradients" allowing "molecular diffusion to proceed more rapidly." Dispersion is another term often found in literature relevant to the transportation process in rivers. Rutherford (1994) defines dispersion as "an artifact of averaging", opposed to a "fundamental physical process." Dispersion is used to account for processes that are not modelled directly (Pilechi, *et al.*, 2014), and is governed by the difference in velocity fields within the vertical and transverse profiles. Chanson (2004) describes mixing as lateral spreading (vertical and transverse) due to turbulence and dispersion as longitudinal spreading due to turbulent shear. Transformation involves chemical and biological reactions in the river, such as the reaction between discharging effluents and the surrounding (or ambient) environment. All of these processes are responsible for dilution of a constituent or a group of constituents in flowing water. As rivers flow mainly due to gravity, buoyancy does not play a role in mixing unless there is a density difference between the mixing fluids, such as temperature and salinity differences (Rutherford, 1994).

2.3.2. Ammonia and nitrate in the environment

Nutrient rich effluents, especially those with high concentrations of ammonia, can negatively impact receiving waters by: creating toxic habitats for aquatic wildlife, creating nutrient enriched environments inducing eutrophication, reducing available oxygen due to oxidation of ammonia and creating high levels of nitrate rich water directly impacting human health (Craig & Middelraad, 2003). One of the most common sources of ammonia pollution originate from municipal wastewater treatment plant effluents, which are largely composed of domestic sewage and potentially commercial and industrial waste (Craig & Middelraad, 2003). Using Environment Canada's National Pollution Release Inventory (NPRI), Holeton, *et al*. (2011) observed that large Canadian urban centers discharge

significant amounts of ammonia into receiving surface waters through the discharge of municipal wastewaters.

Owing to the nitrogen cycle, ammonia does not bio-accumulate nor is it persistent. In aqueous solutions ammonia exists as ionized ammonium (NH_4^+) and unionized ammonia (NH_3) according to the following reaction:

$$NH_4^+ \leftrightarrow NH_3 + H^+ \tag{16}$$

Total ammonia refers to the form enveloping both NH_3 and NH_4^+ and from hereon in will be referred to as ammonia.

The distribution between the two species is dependent on temperature and pH. Figure 2.6 defines the distribution between (ionized) ammonium and unionized ammonia in freshwater at a temperature of 21°. As the pH increases, so does the fraction of the unionized ammonia, which is the dominant toxic form of ammonia to aquatic species.

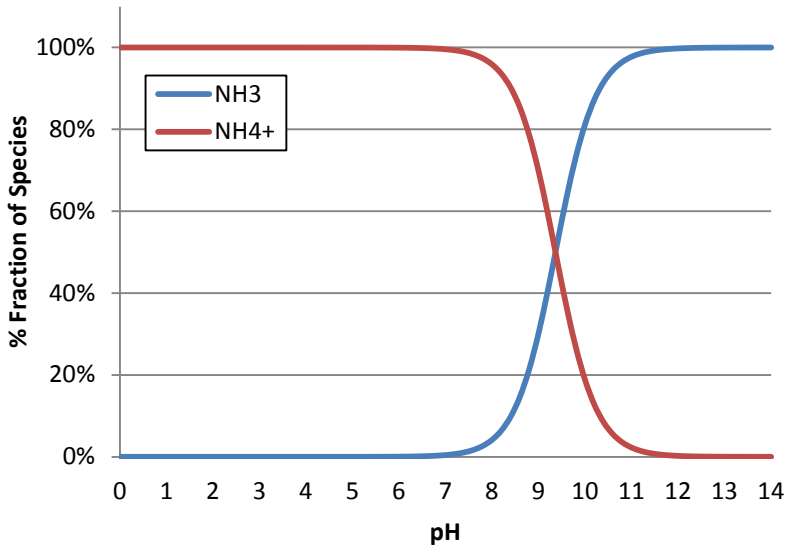

Figure 2.6: Dissociation of unionized ammonia (NH_3) and ammonium (NH_4^+) ions in water at a temperature of 21°C.

Emerson *et al*. (1975) developed the following two equations in order to calculate the fraction of ammonia which was subsequently used to quantify the unionized ammonia concentration from the total:

$$pK_a = 0.0901821 + 2729.92/T \quad (17)$$

where pK_a is the dissociation constant and T is the temperature in units of Kelvin, and

$$f = 1/[10^{pK_a - pH} + 1] \quad (18)$$

where f is the fraction of total unionized ammonia. The fraction value f is used to calculate the unionized ammonia concentration according to the following equation:

$$[NH_3] = f\,[NH_4^+ + NH_3] \quad (19).$$

Although both species of ammonia can cause toxicity, the unionized form is of greatest concern, especially to freshwater fish such as salmonids (Wade, *et al*., 1988). As water becomes more basic, the NH_3 ratio increases exponentially, and with every 10°C increase in temperature, the NH_3 ratio increases tenfold (Craig & Middelraad. 2003). Naturally occurring ammonia in surface freshwater can be found at concentrations below 0.1mg/L. At ambient water temperatures of 20°C and a pH between 7 and 8, naturally occurring unionized ammonia can range between 0.0004 and 0.004 mg/L (EC & HC, 2000). Higher concentrations of unionized ammonia suggest the effects of anthropogenic activity and organic pollution (EC & HC, 2000).

A guideline, established by the Canadian Council of Ministers for the Environment (CCME), limits unionized ammonia concentrations of 0.019mg/L (0.016mg-N/L) in freshwater bodies (CCME, 2010), considered a chronic toxicity limit. In 2012, the Canadian government passed a regulation Canadian Wastewater Systems Effluent Regulation (WSER) to restrict the levels of unionized ammonia discharging from WWTPs (Fisheries Act, 1985). The end-of-pipe regulation states that a maximum concentration of 1.25mg-N/L of unionized ammonia is allowed in the final WWTP effluent at a temperature of 15°C ± 1°C. For special circumstances, when a discharge cannot pass this limit, a temporary permit allows an exceedance of this limit, but only up to a maximum of 0.016mg-N/L of unionized ammonia at any point that is at a 100m radius from the discharge source. All of the values indicated must take pH and temperature into account. Environment Canada (EC) issued a "Guideline for the Release of Ammonia Dissolved in Water Found in Wastewater Effluents" (EC, 2013) as an instrument to aid in release of ammonia concentrations in an effluent. The guideline provides two proposed limits differentiating between chronic and acute toxicity for any WWTPs discharging effluent into ambient waters at a volume of 5,000m^3/day or more based on an annual average. EC's guideline stipulates a chronic toxicity limit for unionized ammonia in surface waters to 0.019 mg/L (0.016mg-N/L), while an acute toxicity limit is dependent on effluent pH. A chronic toxicity limit is based on adverse effects to living organisms repeatedly and continuously exposed to a substance over a long period of time, while an acute toxicity limit is based on a brief exposure or an exposure of a very short period of time. The graph provided (Figure 2.7) indicates an acute toxicity limit considered lethal to fish. If an ammonia measurement falls below the given curve the effluent passes acute toxicity, but if it is above the curve, the effluent's unionized ammonia level is considered lethal. The graph is based on a threshold equation

$$y = 306132466.34 \times (2.7183^{(-2.0437 \times pH)}) \quad (20)$$

where y is the unionized ammonia value and pH is the pH of the effluent. It was developed using results from “Environment Canada's Rainbow Trout Acute Lethality Test RM 9” (EC, 1990).

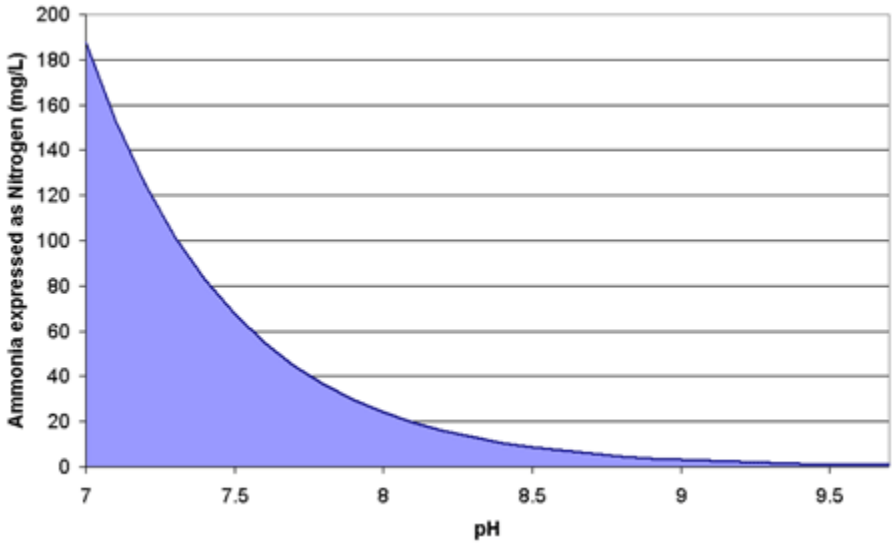

Figure 2.7: Threshold acute concentration for ammonia versus pH (source, EC 1990)

In 2013 USEPA published a document titled “Aquatic life ambient water quality criteria for ammonia – freshwater” (USEPA, 2013) recommending chronic and acute ammonia discharge limits to surface waters. Although the document is very thorough and contains specific recommendations for thresholds aimed at specific organisms the general recommendation rules with caveats are provided in Figure 2.8. Suggested ammonia limits are in units of total ammonia nitrogen (TAN), where both unionized and ionized ammonia are included. To estimate unionized ammonia limits from the given numbers, EPA also recommends using the two equations developed by Emerson *et al*. (1975), see equations (17) and (18).

Ammonia is a non-conservative constituent and one of the components of the nitrogen cycle. In freshwater, ammonia is converted to nitrite (NO_2-) then to nitrate (NO_3-) by nitrifying bacteria.

Nitrates are another source of nitrogen toxicity in the environment and at very high concentrations can be detrimental. One of the most common effects to human health

caused by high concentrations of nitrates is methaemoglobin formation. When exposed, a human body will reduce its oxygen carrying capacity in the blood. This infliction is more commonly known as Blue Baby Syndrome. CCME's guideline (CCME, 2003) to limit the amount of nitrate in the freshwater aquatic environment is 13mg NO_3^-/L (2.935mg NO_3^--N/L). This guideline serves as protection from direct toxic effects, but as nitrate is readily available through the nitrogen cycle (especially in high summer temperatures when more biota is available to oxygenate existing forms of nitrogen) the possibility of eutrophication is quite prevalent. Camargo, *et al*. (2005), recommend that a limit of 2mg NO_3^--N/L be imposed to protect "the most sensitive freshwater species."

2013 Final Aquatic Life Criteria for Ammonia (Magnitude, Frequency, and Duration) (mg TAN/L) pH 7.0, T=20°C	
Acute (1-hour average)	17
Chronic (30-day rolling average)	1.9*
*Not to exceed 2.5 times the CCC as a 4-day average within the 30-days, i.e. 4.8 mg TAN/L at pH 7 and 20°C, more than once in three years on average.	
Criteria frequency: Not to be exceeded more than once in three years on average.	

Figure 2.8: Source USEPA, 2013.

2.3.3. WWTP discharges

Flows from a WWTP vary on a daily and an annual basis, and often exhibit a diurnal cycle. The size of the plant, the types of users served (including or only domestic, commercial, institutional and industrial) and the types of pumping stations will all influence the flow variation. For example, a smaller WWTP will show greater diurnal variation. Storm events will influence flow for combined systems, where surface runoff and groundwater

infiltration will play a role, often pronounced at the beginning of a storm after a dry period (Water Environment Federation [WEF], 2008). Peak daily flows can be anywhere between 50 to 200% of the average flows, depending on the size of the system. If not influenced by a storm event, peaks in flow of a municipal WWTP are often seen in the morning and early evening. Other main variations are caused by industrial discharges to the system, if industrial effluent is greater than 40% of the overall volume (USEPA, 1981).

Effluent concentrations from a WWTP also vary on a daily and annual basis. Just as for flows, diurnal peaks for effluent concentrations are associated with the type and size of facility, as well as the composition of the sewage influent. WEF (2011) reports that total Kjeldahl nitrogen (TKN), which is comprised of organic Nitrogen and ammonia, peaks in the mornings with smaller peaks in the evening in all domestic sewage. Unless the solids retention time in the plant is long the TKN peaks may cause the effluent ammonia peaks to be quite pronounced even if the average concentration of ammonia is low.

Since flows and concentrations vary temporally, it is interesting to note whether a correlation exists between the two. Pocernich & Litke (1997) found that a correlation between effluent discharge and ammonia concentration was, in fact, significant for 75% of the WWTP they surveyed. Out of these, half were direct while the other half were inverse in relationship. This, they assumed, described the differences in plant functions such as retention times before discharge, the composition of the sewage as well as effluent temperature. They also found that approximately 67% of the WWTP they surveyed had a correlation between ammonia and nitrite/nitrate concentration.

2.3.4. Diffuser outflows: understanding the mechanics

Multiport diffusers have been used for sewage discharge in large coastal cities for the last 70 years. Diffusers have since been taken up for smaller operations (e.g. smaller cities, industry, etc.) on rivers to help abide to stringent environmental discharge criteria and limits. Effluent discharges can be conveyed through a single pipe or through a diffuser. In principle, discharge from a diffuser dilutes in the receiving water body faster than the same amount of discharge from a single pipe outlet. However, the rate of dilution is very

dependent on the physical design (e.g. port location and orientation) and location (e.g. depth of submersion, distances from walls) of the diffuser, and on the flow (i.e. coflow or crossflow) and nature (e.g. deep sea, shallow river, etc.) of the receiving environment. This thesis deals with a vertical multiport diffuser, discharging a neutrally or a weakly buoyant fluid into a shallow, moving flow.

A diffuser distributes a plant's outflow through a multiple number of ports. At the discharge point these discharges look like individual jets. The jets eventually merge, but the merging distance depends on local geometry and discharge characteristics (Jirka, 2006). The dynamics of the flow are often controlled by the source momentum due to a forcible discharge (Kim & Seo, 2000). In a shallow, fast-flowing stream, Jirka & Akar (1991) observed complete vertical mixing and a quick transition to lateral ambient mixing.

Dynamic effect of the river current also plays an important role on the effluent discharge from a diffuser. To help describe this Roberts (1979) defined a type of Froude number (F):

$$\mathrm{F} = \frac{u^3}{b} \tag{21}$$

where, u is the ambient (river) current and b is the buoyancy flux per unit diffuser length. In the above equation, if F>>1, the flow is dominated by the ambient current, and if F<<1 the flow is dominated by buoyance. The buoyancy flux is:

$$b = \frac{\Delta\rho}{\rho_a} gq \tag{22}$$

where $\Delta\rho$ is the density difference between the effluent (ρ_e) and ambient or river (ρ_a) density; and q is defined as total effluent discharge divided by the length of the diffuser (Tian & Roberts, 2011).

A jet is defined as a fluid of high intensity discharge which causes turbulent mixing. In a *pure jet* (also known as *momentum jet* or *non-buoyant jet*) only initial momentum flux is responsible for turbulent diffusion, while in a *pure plume* initial buoyancy flux causes turbulent diffusion. These specific instances are rarely the case and in general a *buoyant jet* comprised of both fluxes will cause turbulent mixing (Holley & Jirka, 1986).

At the discharge source, ambient flow encounters sharp discontinuity due to an incoming jet. The forceful flow of the jet causes high shear, which in turn causes eddies. Eddies force the less turbulent ambient flow into the region of high shear, causing the jet to grow as it entrains more ambient fluid. Through this process initial concentration of the jet begins to dilute. If a number of jets are discharged, as from a diffuser, they eventually merge into one another through "spread by turbulent entrainment" (Lee, *et al.*, 1977).

In deep water conditions (where static pressure is assumed negligible and jet momentum is conserved), Cederwall (1971) found that a diffuser discharge may be treated as a line-source. He proposed the width of the source as $b = \pi D^2/4s$, where D is the nozzle diameter and s is the distance between ports, or port spacing. He calculated the mixing efficiency between a row of point-sources and a line-source, which resulted in 0.95 for non-buoyant jets and 0.78 for buoyant plumes. However, Lee, *et al*. (1977) argued, that this theory did not hold in shallow water conditions, because pressure fluctuations cannot be neglected and boundary effects are imposed on jet momentum by the water surface and the bed bottom. To differentiate between point-sources and line-sources Tian *et al.* (2004b) performed experiments in a laboratory for stationary, moving, unstratified and stratified flows (Tian *et al.,* 2004a; Tian *et al.,* 2004b; Daviero & Roberts, 2006; and Tian *et al.,* 2006). The results, they found, depended on the ambient environment and diffuser design. For unstratified, moving waters (of interest to this thesis) Tian *et al.* (2004b) found that the discharge behaviour depended on s/H, where s is port spacing and H is the depth of water at the diffuser site. They found that a line-source was defined by s/H ≤ 0.5 and the

transition between line-source and point-source was defined by $0.5 < s/H \leq 4.5$. The definition for point-plume could not be identified due to a limit in the laboratory setup size. Such differentiation between point-source and line-source is of value to engineers as it aids in design criteria and improved costs for diffuser construction.

To better understand the process of mixing and transport (whether it be by effluent release into a river, a coastal zone or into the air) scientists have broken it down into two to three zones of investigation: near-field and far field, or near-field, mid field and far field. Near-field is dominated by discharge dynamics: jet momentum or plume buoyancy. Here the process of mixing between the discharged source and ambient flow is very quick (Socolofsky & Jirka, 2005), where jets are evident and the momentum and density differences (if existent) are an important consideration. In the mid field (otherwise called the intermediate or transitory field) the jet characteristics essentially disappear. The physical processes are dominated by advection prevalent in the streamwise direction, while dispersion is still noted in the transverse direction. Some studies simplify the research by transitioning directly from the near-field into the far field (Baptist & Ujittewaal, 2005). In the far field, mixing and transport of constituents is dictated by ambient conditions of the receiving environment. In this region, mixing is independent of diffuser or outfall design and therefore outfall design does not directly dictate how a contaminant behaves and impacts the receiving environment. Because of this reason, as well as increased abilities in computing power, three-dimensional modelling of this region has become of interest. In terms of scales, near-field time and distance parameters are generally provided in units of minutes and water depth, respectively; whereas far field time and distance parameters are generally provided in units of hours and kilometers, respectively (Zhao, *et al*., 2011).

Near-field

As the near-field is of interest to this thesis, further discussion of this region ensues.

Lee, *et al*. (1977) examined a diffuser discharging into a coflowing current, where a region of high pressure was defined in front of the diffuser. Their theoretical approximations

showed that the extent of the near-field can be assumed by half of the diffuser length. Tian, *et al*. (2004b) defined the end of the near-field zone where jets and buoyant plumes associated with discharge no longer play a significant role in mixing and the dilution of the pollutant is 10% of its ultimate value. In stratified regions, Roberts, *et al*. (2011b) defined end of the near-field at a point where turbulence collapses "under the influence of stable stratification."

In a study comprised of vertically discharged turbulent buoyant jets in a depth confined channel, Jirka & Harleman (1979) defined stable and unstable discharges. By their definition, a stable discharge occurs when a jet creates a horizontal spread towards the surface and does not come into contact with the initial jet region, while an unstable discharge occurs when the jet re-entrains the original jet region, causing recirculating cells. If the discharge is buoyant, there is less chance for instability, as shown in Figure 2.9. Kuang & Lee (2001) showed through numerical analyses that unstable discharges occur when a high momentum, non-buoyant jet (a pure jet) discharges and creates primary circulating cells, which also cause secondary circulating cells downstream. Downstream of a diffuser, Tian *et al*. (2004b) observed large scale rolling vortices in stationary water and concluded that these serve as the main mechanism for mixing in the horizontal spreading layer. As the ambient current increased the dilution decreased and eventually these large-scale vortices disappeared, making the horizontal spreading negligible. Though this particular theory was not investigated, no evidence of vortices at $F \geq 0.26$ was found.

Tian, *et al*. (2004b) defined "empirical and semi-empirical equations to predict near-field characteristics", which will be tested in this thesis. To approximate the near-field length (x_n) (the distance at which mixing due to the diffuser discharge has essentially ceased and where the dilution has reached 90% of its potential) for $F \gg 1$ and $0.5 < s/H \leq 4.5$, the following equation was suggested:

$$\frac{x_n}{H} = 5.2\mathrm{F}^{1/3} \pm 10\% \qquad (23)$$

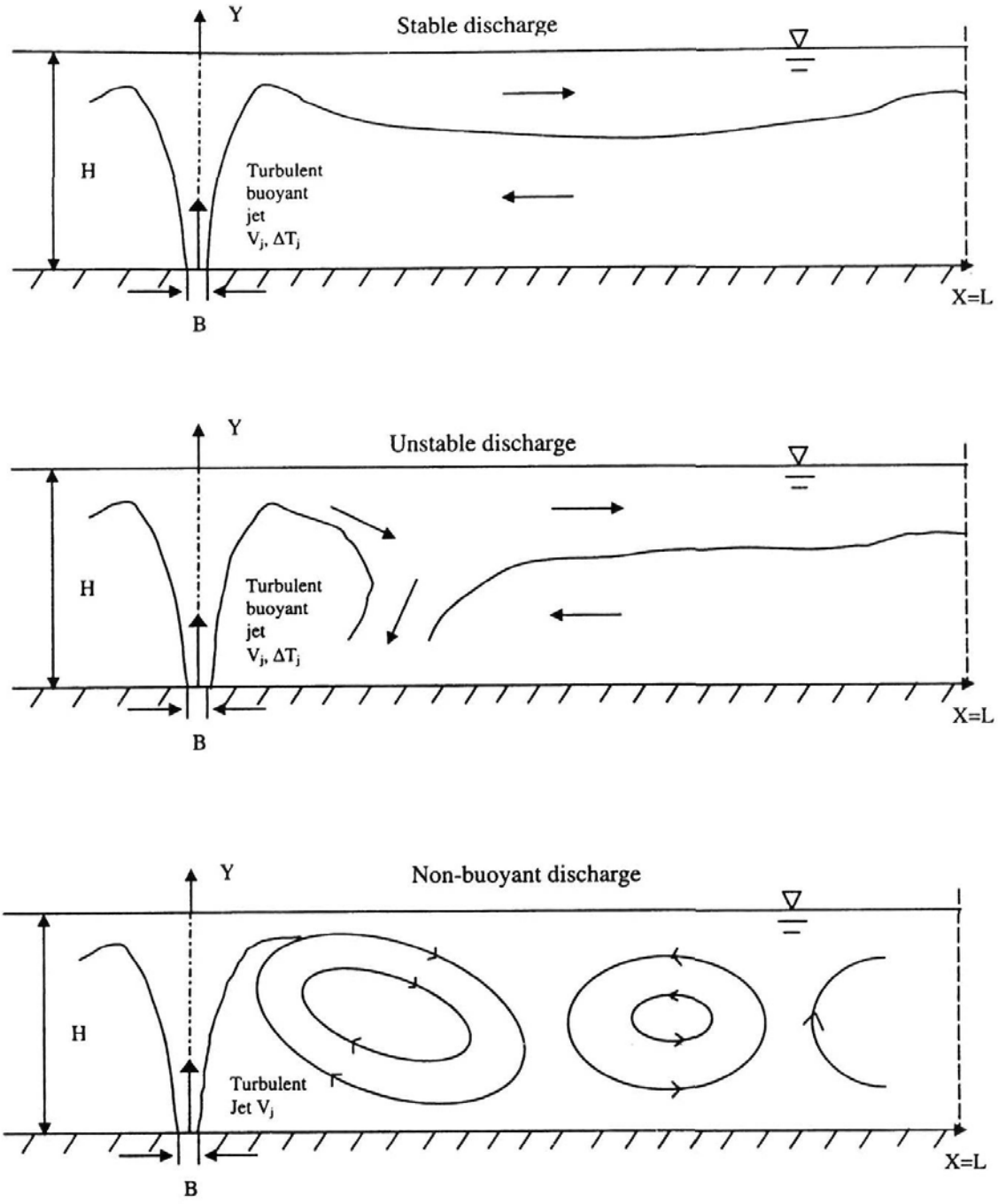

Figure 2.9: Examples of stable and unstable discharges. The top image illustrates a strongly buoyant jet which results in a stable discharge. The middle and bottom images illustrate weakly buoyant and non-buoyant jets, respectively, both resulting in unstable discharges (Kuang & Lee, 2001).

To approximate the dilution (S_n) the following equation was suggested:

$$\frac{S_n q}{H} = 0.55\left(\frac{s}{H}\right)^{-1/2} \pm 20\% \tag{24}$$

An equation developed through earlier studies, relied on an experimentally derived C_2 (Chu, 1979; Wright, 1977; and Lee & Neville-Jones, 1987) for F >> 1 and s/H >> 1:

$$\frac{S_n q}{H} = 2C_2\left(\frac{s}{H}\right)^{-1} \tag{25}$$

To compare the results using empirically driven equations (24) and (25) to the field and model data in this thesis, the following equation is used (Huai, *et al.*, 2010):

$$S_n = \frac{(C_0 - C_a)}{(C_x - C_a)} \tag{26}$$

where C_0 is the initial concentration of the effluent discharged from the diffuser, C_a is the concentration of the ambient environment and C_x is the concentration of the plume at length x from the diffuser.

Plume width

The width (B) of the plume from a point source may be approximated using a term known as the transverse mixing coefficient ε_t, which for "slowly meandering rivers with moderate sidewall irregularities" (Chanson, 2004) is generally calculated to be:

$$\varepsilon_t = Cdu_* \tag{27}$$

where d is the water depth, u_* is the average shear velocity and C is an empirical constant. Rutherford (1994) suggested that for meandering streams, the C in the transverse mixing coefficient can fall anywhere between 0.3 and 0.9, while for very strongly curved channels it is equal to anywhere between 1 and 3.

Thus using ε_t as described above, the following equation approximates the width of the plume from a point source from a distance x and mean velocity u of the ambient current (Chanson, 2004):

$$B = 4\sqrt{2\varepsilon_t x/u} \tag{28}$$

Near-field breakdown

Since the near-field zone displays the most physical complexities, scientists have further broken down this zone of study. The categorization is dependent on discharge dynamics, ambient environment and discharge buoyancy. For example, for a plane, buoyant jet that is discharged into stationary, shallow water, Jirka & Harleman (1979) divided the near-field into three regions: buoyant jet, surface impingement and internal hydraulic jump. In a study examining a vertical, non-buoyant jet in stationary, shallow water Kuang *et al*. (2001) demonstrated that the discharging field can be broken down into four different zones as seen in Figure 2.10. The zones were categorized by measured data and distinct differences in the flow. Modelling studies followed based on these field results (Aziz & Khan, 2011; Chen *et al*., 2006).

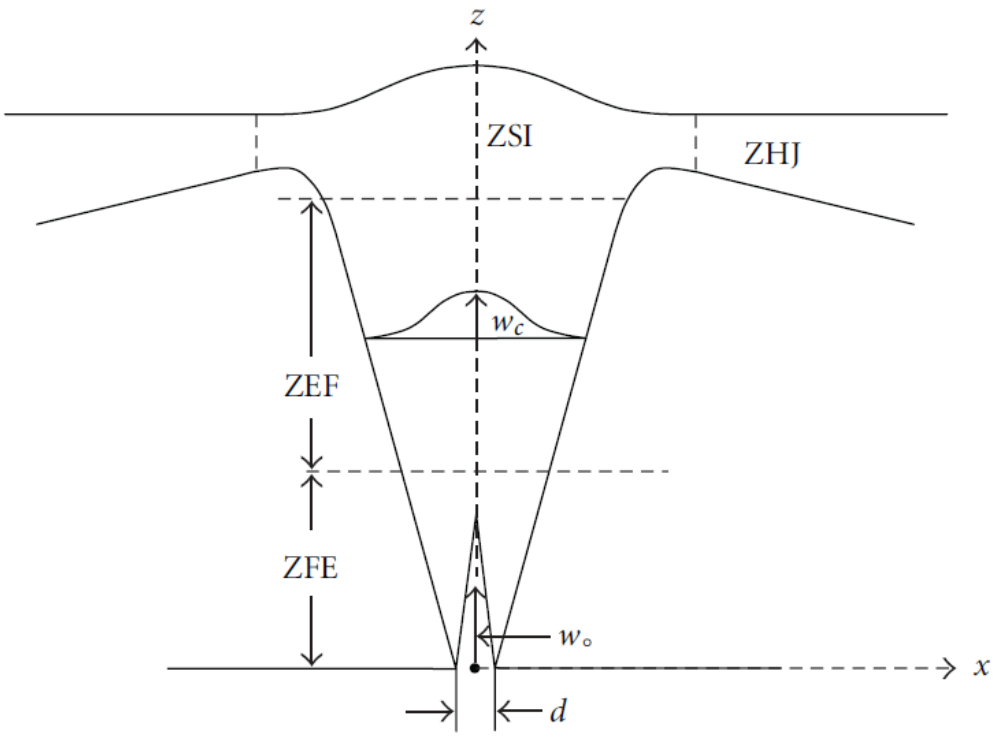

Figure 2.10: A breakdown of a vertically discharged confined jet into four zones: *zone of flow establishment* (ZFE), *zone of established flow* (ZEF), *zone of surface impingement* (ZSI) and *zone of horizontal jet* (ZHJ). Image from Aziz & Khan (2011) originally reported by Kuang *et al.* (2001).

For discharges from multiple jets in shallow, flowing waters, the most recent categorization was done by Zhang & Zhu (2011) who categorized the near-field into four zones (Figure 2.11). The first zone, known as the *free jet zone*, is the initial integration of the discharge and ambient flows where external boundaries have no influence. In the second zone, the *jet surface impingement zone*, the formerly free jet is now imposed on by the free water surface. Here, spread of the plume seems to be stable in the vertical direction (thickness of the plume increases at the same speed as in the free jet zone), but because of the free surface, the jet in the transverse direction spreads out. As the water surface impinges on the vertical spread, the spread is transferred to the transverse direction at which point the rate of spread quickly increases. The third zone, the *merging zone*, is where passive dispersion is observed. Due to much of the energy having been dissipated in the jet surface impingement zone, the dispersion in this section mimics the ambient river flow. Thereafter, the authors identify a *vertical mixing* zone. Here, it is assumed that the vertical mixing has fully developed or in other words the vertical column is fully mixed. As seen in the

illustration of Figure 2.11, this diffuser discharges at an angle from the free surface and bed bottom boundaries.

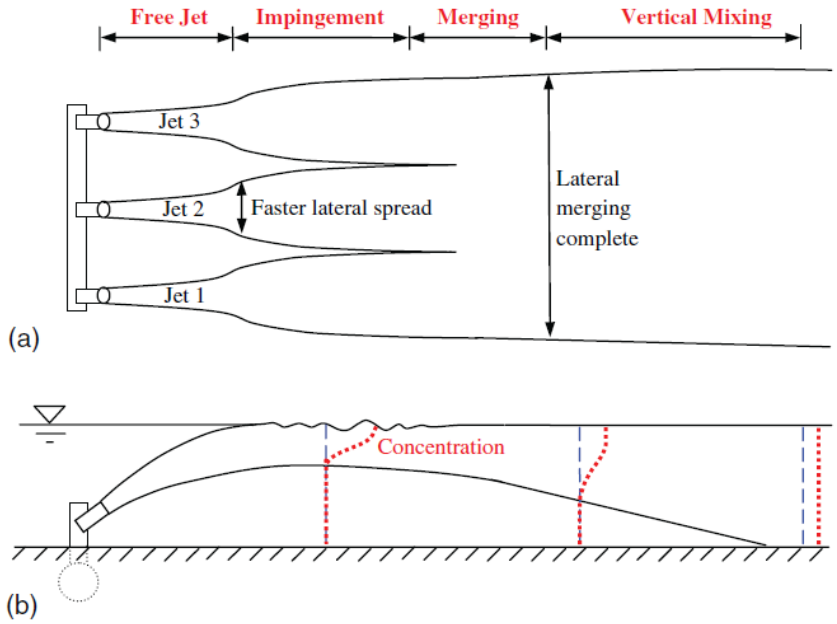

Figure 2.11: Breakdown of diffuser discharge in the near-field into four different zones (Zhang & Zhu, 2011).

2.3.5. Collection of field data

To study multiport discharges in open water, most recent studies have undergone a similar method of data collection (Roberts, *et al.*, 2011a; Zhang & Zhu, 2011; Pilechi, *et al.*, 2014). Rhodamine WT (a fluorescent dye) is injected into a plant's effluent in order to be used as a tracer to measure the fluorescence and therefore the dilution of the discharge in ambient waters. It is measured using a Rhodamine fluorometer which instantaneously measures the concentration of the dye at each measurement location. All studies showed that both near and far fields can be measured effectively this way. However, studies have not been undertaken (to the author's knowledge) using existing effluent contaminants as the tracer.

2.3.6. Modelling of diffuser discharges

CFD models for river studies are available in one-, two- or three-dimensional (1D, 2D and 3D, respectively) analyses. Choosing the number of dimensions depends on the problem and the details required to solving a problem. 1D models describe the flow in the

streamwise direction and typically calculate the energy loss of a system. 2D models describe the flow in the streamwise and transverse directions, where a depth-averaged flow is assumed. 3D models add the vertical velocity component to a simulation. At this point, complicated processes such as turbulence intensity and air entrainment can be modelled (Toombes & Chanson, 2011). 3D modelling can be computationally costly, but is required if horizontal and particularly vertical variations in flow are of interest to understanding a system's behaviour (USACE, 2001). Due to current computational limitations, 3D modelling is generally confined to local scales.

A large number of scientific contributions have been made with respect to modelling the processes of effluent mixing with a receiving water body. Some of these contributions have used CFD modelling techniques to simulate outfall discharges of single ports (Zhang & Adams, 1999; Kuang & Lee, 2001, 2006; Park, *et* al., 2007; Huai, *et al*., 2008; Lowe, *et al*., 2009; Aziz & Khan, 2011; Lai & Lee, 2012) and diffusers (Kim & Seo, 2000; Kim & Cho, 2006; Li & Hodgins, 2010; Yannopoulos, 2010; Lee, 2012; Li, *et al*., 2012; Ali & Fieldhouse, 2014; ; Xue, *et al.*, 2014). Only a very small number of studies (to the author's knowledge) have been applied to modelling a multiport diffuser in a riverine setting (Tang, *et al*., 2008; Zhang & Zhu, 2011). Typically, CFD modelling is focused on thermal discharges from a multiport diffuser along a coastal shoreline boundary (Kim & Seo, 2000; Ali & Fieldhouse, 2014). Those researchers that do apply CFD models often develop their own models (Kim & Seo, 2000; Tang, *et al*., 2008). Blumberg *et al*. (1996) found that separate far field and near-field models are necessary to model appropriately the process of mixing. Near-field models are more appropriately suited to simulate the jet discharge dynamics and envelop the outfall design with the use of a fine mesh, while far field models more properly simulate hydrostatic conditions and capture a large area with a coarse mesh. More recent studies have further shown that a CFD model can be used to simulate near-field processes (Park, *et* al., 2007; Tang, *et al*., 2008), while others applied it to the intermediate and far field processes (Choi & Lee, 2007; Stamou & Nikiforakis, 2013).

Before modelling between mixing of discharge with the ambient environment can take place, characteristics of the receiving environment (i.e. unconfined vs. bounded flow) and

the type of discharges (i.e. high vs. low buoyancy) must be identified (Harleman & Jirka, 1974).

Modelling diffusers in rivers

As already mentioned, very few studies have been published specifically targeted to modelling of diffuser discharges into a river. The authors of one such study (Tang, *et al.*, 2008) developed their own CFD model, using a steady RANS simulation with a buoyancy corrected mixing length turbulence model on an overset grid. The overset grid method dissects a complex domain or mesh into a number of simpler sub-meshes, where each sub-mesh conforms to the feature it is encompassing while still obtaining a structured mesh. In this way, the features of a diffuser are completely captured. The model was designed to be computationally inexpensive in order to quickly perform simulations of near-field discharges from outfall pipes and diffusers. The model was validated via several means: by comparison to published experimental results by Violet (1980) and He *et al.* (2002); by comparison to other CFD models (which used k-ε and LES turbulence closure schemes) for the same experimental results; by comparison to commonly used semi-empirical models CORMIX and Visual Plumes; and by field measurements (AADS, 2004) for a diffuser discharge on the Columbia River. The results were comparable to the experimental data, as well as to the more complex CFD modelling results. The model results deteriorated with increasing Froude numbers, but this was expected, as a simple eddy viscosity model was used. The model also yielded similar results to those of semi-empirical models, illustrating that first principles are able to provide similar findings to those based on empirical studies and laboratory calibration. Finally, the model showed "reasonable agreement" (Tang, *et al.*, 2008) with measured velocities from the field. Overall, the study illustrated that the model acted as a good engineering tool in terms of understanding the general behaviour of discharges from a complex diffuser design; most importantly, this study provided an illustration of the effect neighbouring ports and their jet interactions have with one another and the ambient flow. However, note that the centreline velocities and temperature from each port were validated, whereas the width or the spread of effluent away from the centreline was not captured in this study.

A second study (Zhang & Zhu, 2011) detailing diffuser discharges in a river was based on semi-empirical and analytical modelling. The authors studied a diffuser used in oil sands operations on the Athabasca River. River2D was used to model the hydrodynamics of the river, while CORMIX1 (superimposed to give the effect of a multiport diffuser) and CORMIX2 were used to study the near-field mixing of effluent and ambient flow. The authors found that both models provided a poor simulation of the field findings, but CORMIX1 with superposition outperformed CORMIX2, even though the latter was developed for diffuser discharge. Depending on the mixing zone (see Figure 2.11), the authors provided different suggestions for modelling. They recommended using CORMIX1 with superposition in the free jet zone (where the jet trajectory and minimum dilution are of interest). CORMIX2 was recommended only in reaches after the vertical mixing zone has fully developed. To compensate for the deficiencies in CORMIX modelling, the authors developed analytical models for use in the merging and vertical mixing zones, which require the calculation of diffusion coefficients. If field data are not available to calculate diffusion coefficients, the authors recommended the use of CORMIX1 with superposition in the merging zone. For the jet impingement zone, the authors suggested that a 3D CFD model be developed.

Turbulence closure models

Investigations in the use of turbulence closure models for river studies show that the RNG k-ε models provide a reasonable tool for river engineering. Abad *et al*. (2008) used it to study (within FLOW 3D) flow patterns in a meandering river with bendway weirs. The resulting model was good at simulating the flow in the study reach, the areas of recirculation and the shear velocity patterns near the bed. Li, *et al.* (2012) described the standard k-ε model as "robust, economical and reasonably accurate", but they warned that the model does not perform well when imposed with "larger pressure gradients, large streamline curvature and high swirling component." For these types of problems, they recommended the RNG k-ε model. Simulating a sinuous river reach Rodriguez, *et al*. (2004) showed that the RNG k-ε model resembled the measured velocity field with satisfying results. Others implied that the RNG k-ε turbulence closure provides reliable results when used in river studies as it adequately simulates turbulence "near walls and in flows with

rapid distortions" (Abad, *et al*. 2008). However, the RNG *k*-*ε* model has not shown good results for simulating transverse and vertical velocities (Abad, *et al.*, 2008), nor secondary velocities (Rodriguez, *et al.*, 2004). Both authors agreed that the magnitude of transverse, vertical and secondary velocities is hard to predict compared to the magnitude of streamwise velocities. Also, because of the isotropic nature of the *k*-*ε* models, they are bad at evaluating the turbulence anisotropy found in regions such as the shear layer near walls (Rodriguez, *et al.*, 2004; Abad, *et al.*, 2008).

Some studies have used the RNG *k*-*ε* model to setup other larger models. For instance, Park *et al*. (2007) used it to determine far field boundary conditions by simulating the near-field mixing of freshwater discharge in a deep marine environment where buoyancy differences are large.

Kocaman *et al*. (2010) demonstrated that FLOW-3D can be used as a "supplementary tool" to river engineering designs. They simulated river hydraulics for bridge design. The authors used all available turbulence closure schemes available in the model (five in total – Prandtl's mixing length, one-equation turbulence energy, *k*-*ε*, RNG *k*-*ε* and LES) and found that for up to 60m downstream of the bridge structure the results were very similar.

In a study (Aziz & Khan, 2011) of a vertically discharged jet from a single port in a shallow pool, the standard *k*-*ε* model represented the turbulence closure better than the RNG *k*-*ε*, though the latter predicted the centreline vertical velocity better.

To study merging jets, Li, *et al*. (2012) examined up to four jets in cross-flow whose discharges were parallel to the water surface. They used both the standard *k*-*ε* model and the RNG k-ε models, but found that the realizable *k*-*ε* model (another type of *k*-*ε* model) performed best compared to experimental results of velocity and concentration fields.

Recently, Kheirkhah Gildeh, *et al.* (2015) examined an inclined jet in stationary water, using the RNG *k*-*ε*, realizable *k*-*ε*, non-linear *k*-*ε*, Launder-Reece-Rodi (LRR) and Lauder-Gibson models. The LRR and the realizable *k*-*ε* models had shown most accurate results, though the LRR was computationally more expensive.

CORMIX

Although CORMIX has been used for a number of outfall designs, recent studies criticized the use of this model. Baptist & Ujittewaal (2005) warned that CORMIX has limitations especially when two outfalls affect one another in complex bathymetries and low flow conditions. Etemad-Shahidi & Azimi (2007) found that CORMIX (CORMIX2 in particular) overestimated the dilution rate in their study by an average of 21.5%. Park, *et al*. (2007) cautioned that models such as CORMIX cause discontinuities in initial mixing rates due to steady-state assumptions. Roberts, *et al.* (2011b) caution that the CORMIX underestimates the dilution for stationary and low flows, but provides better results for higher flows.

2.4. Conclusion

As is evident from the presented literature review, the mixing processes between an effluent discharge and its receiving environment are quite complex and thus present many difficulties in modelling. The mixing in the near-field is highly dependent on the outfall design, on the effluent characteristics and the receiving environment. Majority of the studies identifying diffuser discharge behaviours have relied on the development of empirical approximations defined by laboratory settings and some field studies. Generally the field studies have focused on coastal regions. Lately, with the improvement of computing power, more emphasis has been made towards CFD modelling of diffuser discharges, but much can still be learned in this field.

3. Methods

3.1. Collection and Processing of Bathymetry and Current Profiles

3.1.1. Description of the field campaign and setup

To define the bathymetry and the current profile of the study reach, a spatial survey of the river reach was performed. The spatial survey was conducted on August 22, 2011 and water quality samples were collected on August 23, 2011. A SonTek M9 Acoustic Doppler Profiler (ADP) was used to collect georeferenced depth and current velocity measurements simultaneously. The ADP was mounted on a small pontoon boat (**Error! Not a valid bookmark self-reference.**a); housing an antenna and a GPS receiver, which received error corrections via radio link from a base GPS unit on land (**Error! Not a valid bookmark self-reference.**b). The ADP transducer was mounted at a depth of 0.09m and the antenna at a height of 0.51m from the water surface. The base GPS unit was setup on the south shore of the river reach such that the ADP was never more than 1.5km from the base GPS unit and well within communication range. Use of the base GPS unit allowed real time kinematic (RTK) GPS measurements, providing a position accuracy of ±3cm in the horizontal plane. All position data were converted using Universal Transverse Mercator (UTM) NAD 83 projection, providing easting and northing coordinate points. The study reach is situated in UTM north Zone 18, which is the projection (coordinate system) used throughout this thesis. The magnetic declination for the city of Ottawa during the spatial survey was -13.6°.

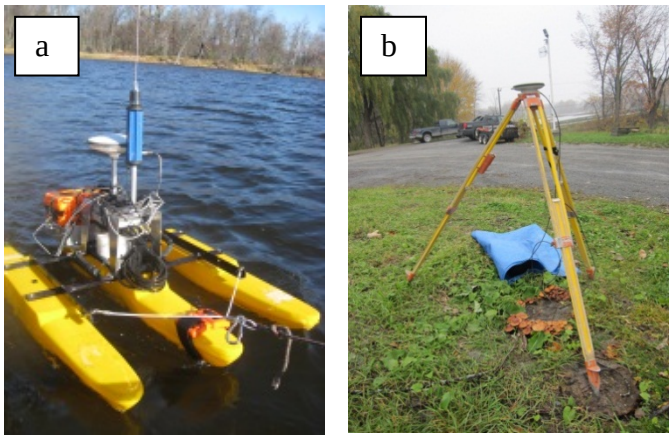

Figure 3.1: Photograph of a) a small pontoon boat carrying an ADP, GPS antenna and receiver, instruments which communicate to b) the land based GPS in order to use RTK-GPS.

The ADP was towed beside a 4.57m aluminum boat at an average speed of 1m/s. Data were collected along approximately 30 bank to bank transects covering a 1.2km river section (Figure 3.2). The separation distance between transects ranged from 5m near the diffuser to 100m along the river banks.

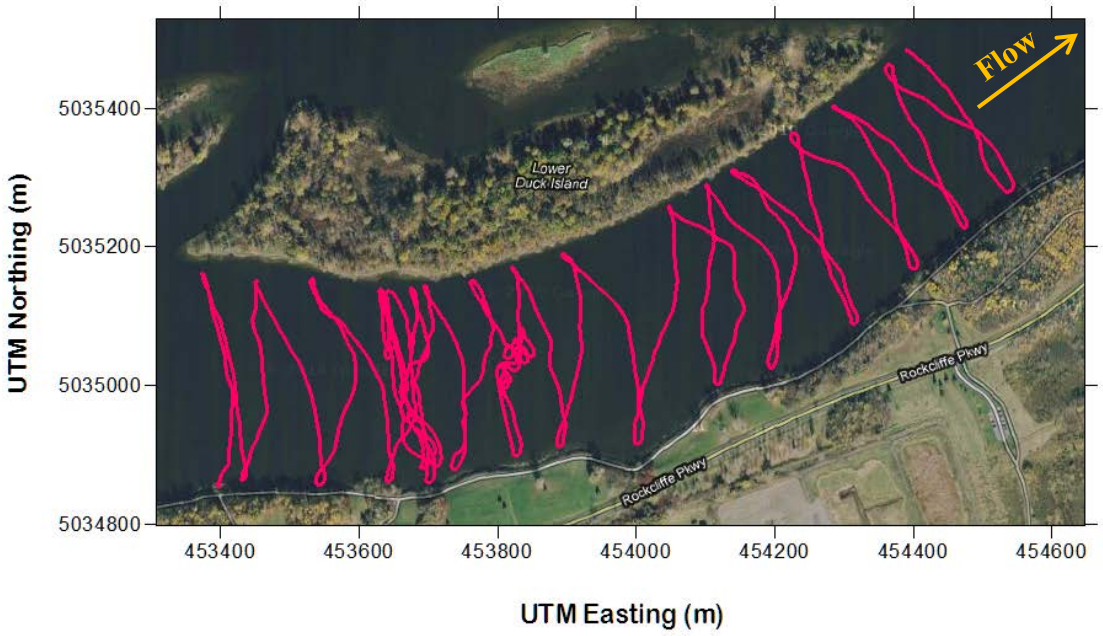

Figure 3.2: Diagonal transect path (pink line) of the spatial survey on the study reach on the Ottawa River. The coordinates are in UTM-18, x-axis representing the easting and y-axis representing the northing coordinates.

3.1.2. ADP data collection

Data from the spatial survey provided depth and elevation measurements along the path of the boat (Figure 3.2) using an ADP. An ADP is equipped with an echo sounder emitting a 0.5MHz vertical acoustic beam. Echo sounding is a technique by which flow depth is measured based on the speed of sound through water and the time required to receive an acoustic pulse backscattered from the channel bed. The instrument collects data in raw form, which were consequently transferred to MATLAB and converted to appropriate units by a code courtesy of Dr. Rennie.

To collect current data, the M9 uses four transducers. Each transducer emits an acoustic beam to measure the Doppler shift in the reflected signal and thus measure the radial velocity. It works on the principle that the suspended matter in the water column reflecting the beam moves at the same velocity in all three directions as the water that it is located in. The sound signals are termed pings. Backscatter from each ping from each beam is range gated to estimate along-beam radial velocities in individual bins along the beam axis. Beam velocities from bins at the same elevation are coordinate transformed to estimate a three-dimensional Cartesian velocity. The bins are processed over the depth of the water column providing a velocity profile. Three acoustic beams are required to resolve a Cartesian three dimensional water velocity. The fourth beam allows for estimation of error in the measured velocity, known as the Error Velocity, which can be due to Doppler noise and/or velocity heterogeneity between beams. For more information on ADCP theory and operation, refer to Simpson (2001).

The M9 contains two sets of transducers, one set of four emitting a 3.0MHz sound signal and another set of four emitting a 1.0MHz sound signal (Figure 3.3). The 1.0MHz transducers typically measure velocities in depths between 2 and 30m and contain bins that are 20cm high; whereas the 3.0MHz transducers are usually employed in depths less than about 2m, and allow for bins that are 10cm high. The instrument decides instantaneously which transducers to use based on depth. During the spatial survey, despite depths reaching up to 5m, the 1.0MHz transducer was seldom used. This was due to relatively low velocities, which also allowed for finer resolution of data. Only 39 of 13531 pings or 0.3% of the data were collected with the 1.0MHz transducer.

Just like depth measurements, velocity measurements were collected in raw form and subsequently processed in MATLAB, including calculation of depth averaged water velocities (Rennie & Church, 2010).

Figure 3.3: The photo above is of a SonTek M9 Acoustic Doppler Profiler base containing an echo sounder and transducers. The large yellow dot in the center of the base is the echo sounder. The yellow and black dots following the perimeter of the instrument are the 1.0MHz and 3.0MHz transducers, respectively.

Generally, ADP compass readings contain an inherent error that changes with direction in travel, which can in some cases influence results. After calibration, the M9 compass has been shown to have a RMS error of 2.9° (Marsden, 2012). Through data processing, it was discovered that indeed a compass error occurred during the field campaign, which also accumulated with time and distance. Since no moving bed was observed, bottom tracking as reference velocity was used to process velocity data. It is worth noting that compass errors will not influence velocity magnitudes if bottom track is used for the reference velocity (Wagner & Mueller, 2011). Errors in velocity direction can occur due to compass error, but this did not appear to be the case in the present study.

3.1.3. Estimation of the diffuser location and port heights

Some uncertainty existed with respect to the exact location of the ROPEC municipal wastewater diffuser. The City of Ottawa (Brian Bezaire, personal communication) provided a single point for the diffuser location (453658E, 5035005N), but could not verify whether it represented the mid- or end-point of the diffuser. Originally, the assumption was that the point represented the mid-point of the diffuser. After surveying the region by boat and noting the jet impingement from port discharges, it was best estimated that the point represented the end-point of the diffuser. Therefore, note that the diffuser position (as will be shown throughout the remainder of this paper) is an estimated location.

The height of the ports above the river bed varies depending on the bathymetry at each port. For simplicity, the height of each port is set to an equivalent depth from the water surface in the modelling setup.

3.1.4. Creation of bathymetry and velocity maps

In order to estimate the depth profile and bottom contours throughout the study reach and to create a 2D map of bathymetry, a spherical Kriging interpolation in Surfer (version 8, by Golden Software) was used to interpolate between the transect lines. Kriging uses a weighted moving average to spatially correlate data points of known values to spatial points of unknown values. A variogram model was developed by determining all of the correlations between data points and plotting the correlations versus distance as shown in Figure 3.4. Using this model, the range (maximum distance between data points that have a significant correlation) and sill (highest difference between data points that fall within the range) were visually estimated. Based on Figure 3.4, the range was set to 240m and the sill was set to equal the variance of the data (0.86 m^2). Anisotropy (similarity in one direction is greater than in the other) was assumed since the river gradually becomes shallower approaching the banks.

Two maps (or meshes) with different resolutions were created. A fine (5mx5m) mesh was created to encompass the area around the diffuser, where transects were approximately 5m apart. It was used as a topographic profile for simulations in FLOW-3D in order to capture interesting and possibly necessary details in the diffuser region. A coarse (25mx25m) mesh was created to encompass transects spaced as far as 100m apart (at points near the river banks). This mesh was used to interpolate observed three-dimensional velocity data collected by the ADP in TECPLOT 360™ (2011, Release 2). Using the finer mesh, the kriging interpolation in TECPLOT created too much noise to create a meaningful picture of the measured velocity field.

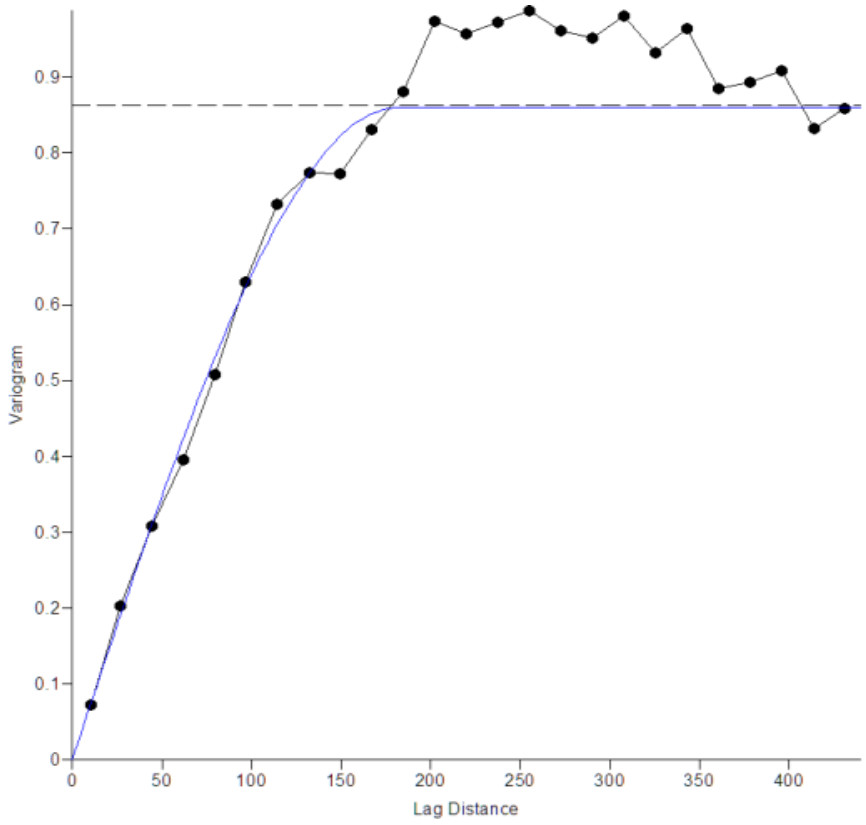

Figure 3.4: Variogram model used to create a contour map of the bathymetry in the study reach. The x- and y-axis show the range (otherwise known as the lag distance) and the sill, respectively, where both axes are in meters.

Depth averaged velocity was processed using the "measured portion of the water column" and ignoring the unmeasured top portion and the bottom 6% which can induce data errors due to the side-lobe effects (Rennie & Churchill, 2010); and further interpolated in SURFER using spherical Kriging in two directions: easting and northing. A mesh of 25mx25m cells was used for the interpolation. All ADP data include random error to due to both Doppler noise (beam velocity errors) and velocity heterogeneity between beams (Cartesian velocity errors). In order to account for these errors in the interpolation, the model variograms included a nugget effect (Daneshfar, 2011). The larger the value of the nugget effect, the less confidence is placed on measured data and more reliability is placed on the trend of the data. In this way, outliers have less significance on the result. A nugget effect was found in the Kriging model for both easting and northing depth-averaged velocities. Table 3.1 provides the values (range, sill and nugget) used for Kriging of depth-averaged velocity. To interpolate, anisotropy was assumed since velocity is impacted as the river gradually

becomes shallower approaching the banks. An equivalent mesh size of 25x25m for both easting and northing velocities were selected.

Table 3.1: Values used for Kriging of depth-averaged velocity in both easting and northing directions.

Parameter	Easting velocity	Northing velocity
Sill	0.007m	0.003m
Range	75m	75m
Nugget	0.007m	0.005m
Anisotropy Ratio	2.3	2.3
Anisotropy Angle	20°	20°

Easting and northing velocity interpolations were combined to create a vector map. A contour map of the depth-averaged velocity was created by calculating the velocity magnitude ($v_{magnitude}$) for each grid point using the following equation:

$$v_{magnitude} = \sqrt{{v_e}^2 + {v_n}^2}, \quad (29)$$

where v_e and v_n are the measured easting and northing velocities, respectively.

The individual bin three-dimensional velocities were also evaluated. Measured easting and northing velocities at and downstream of the river bend do not represent streamwise and transverse velocities well, as at this point the river is no longer flowing directly east. Therefore, easting and northing velocities had to be reprocessed to a correct grid rotation. Angles of difference between easting and the actual perpendicular cross-section of the channel were measured along the bend. These angles were used to create appropriate streamwise and transverse velocities using the following grid rotation:

$$\begin{pmatrix} v_u \\ v_v \end{pmatrix} = \begin{pmatrix} cos\theta & -sin\theta \\ sin\theta & cos\theta \end{pmatrix} \begin{pmatrix} v_e \\ v_n \end{pmatrix}, \qquad (30)$$

where v_u and v_v are the streamwise and transverse velocities, respectively; and θ is the angle of the perpendicular cross-section of the river bend to the easting axis.

The reprocessed 3D velocity data were subsequently interpolated throughout the flow field using the Kriging function in Tecplot 360™. First, a 25x25m bathymetric mesh (created in Surfer) was used to create a 3D prism of the river channel, where the water surface was set to an elevation of 40 m and the vertical axis set to 10 sigma levels (where cell heights change with changes in depth to maintain 10 equivalent cell heights within a column). To interpolate the velocity, the range was set to 0.3, which in Tecplot 360™ is a fraction of a diagonal line in a box encompassing the data points. The zero value (nugget effect) was set to 0.05, which assumes that source points have small uncertainty and noise and thus the interpolation does not weigh solely on source points, but (by a small fraction) on the average of the dataset (Tecplot, Inc., 2011). An eight point octant search was used to estimate each local interpolated value.

3.2. Collection of Water Samples

A preliminary water quality survey was completed (during the spatial survey, day 1) using API® Freshwater/Saltwater Ammonia colorimetric test kits for aquariums and ponds to provide a preliminary illustration of the spread of ammonia in the study reach. The capacity of the test kit ranges from 0 to 8mg/L of total ammonia (NH_3/ NH_4^+), from hereon in referred to as ammonia. The test provided an immediate but rough estimate of the length and width of the plume, as well as a rough estimate of concentration levels at and downstream of the diffuser. The precision of the test kit is not adequate to infer total ammonia concentrations from the samples and it was not used for modelling purposes. Surface water was scooped in a cup, from which 5mL were transferred into a test tube, mixed with an ammonia reagent and allowed 5 minutes for colouration. A high quality hand-held Magellan Thales ProMark3 GPS with WAAS correction was used to record spatial

coordinates of each measurement. In total, 16 water samples were collected (one sample upstream of the diffuser, one directly above the diffuser, two samples immediately downstream – within the region of visually observed jet impingement, two immediately downstream and north of the diffuser, five approximately 150m downstream and five samples at the end of the survey reach approximately 1km downstream) and their results recorded.

On day 2, the Sontek M9 ADP was used again to collect current (river velocity) data and provide accurate spatial positions of water sampling sites. The ADP was always 3.7m (12 feet) away from the sampling site, on the opposite side of the survey boat in order to avoid any disturbances water sampling might incur in the ADP readings. On this day, the GPS antenna height was at 57.2cm from the water line while the receiver was attached to the boat, changing the configuration of **Error! Not a valid bookmark self-reference.**a) due to some technical difficulties encountered with the electronics. These changes did not have effects on final data.

3.2.1. Sampling location

Water sampling locations on day 2 are shown in Figure 3.5. A total of seven transects were sampled: a single point upstream of the diffuser to capture ambient conditions, a transect consisting of five sample points in line with the diffuser to capture conditions at the effluent discharge, transects consisting of three sample points at 5m, 18m, and 30m downstream of the diffuser, a transect of four sample points at 70m, and a single point 200m downstream of the diffuser. This resulted in a total of 20 sample sites. From herein, this area will be referred to as the sampled reach (constrained to 200m downstream of the diffuser) in contrast to the study reach encompassing a distance of 1.2km.

Water sampling locations were determined by several factors:

- First, samples had to capture mixing both near the diffuser and downstream. It was of interest to study the mixing behavior in the area near the diffuser where high turbulent activity was observed with a naked eye; as well as the mixing behavior

downstream where passive advection is assumed to be taking place. As a result sampling was focused within the first 200m of the plume.

- Second, capturing the complete width of the plume was of interest. A preliminary simulation using CORMIX2 model provided an approximate plume width of 60m for the first 25m downstream of the diffuser; and a width of 80m, from 70m to 150m downstream of the diffuser.
- Third, vertical mixing of the plume with ambient flow was of interest. Therefore, samples at various depths were taken at each site. For sites near the diffuser (transects at 0 to 30m downstream of the diffuser) 4 depths were sampled: near the surface (0.5m from the surface), approximately 1/3 and 2/3 of the site depth and near the bed-bottom (0.5m from the bottom). At sites further downstream from the diffuser (transects at 70 and 200m downstream) 3 depths were sampled: near the surface (0.5m from the surface), at mid-depth and near the bed-bottom (0.5m from the bottom). Depths were approximated using the M9 depth measurements at each site.

For comparison purposes, ambient conditions were recorded at a single site upstream of the diffuser at four different depths, as at sites near the diffuser.

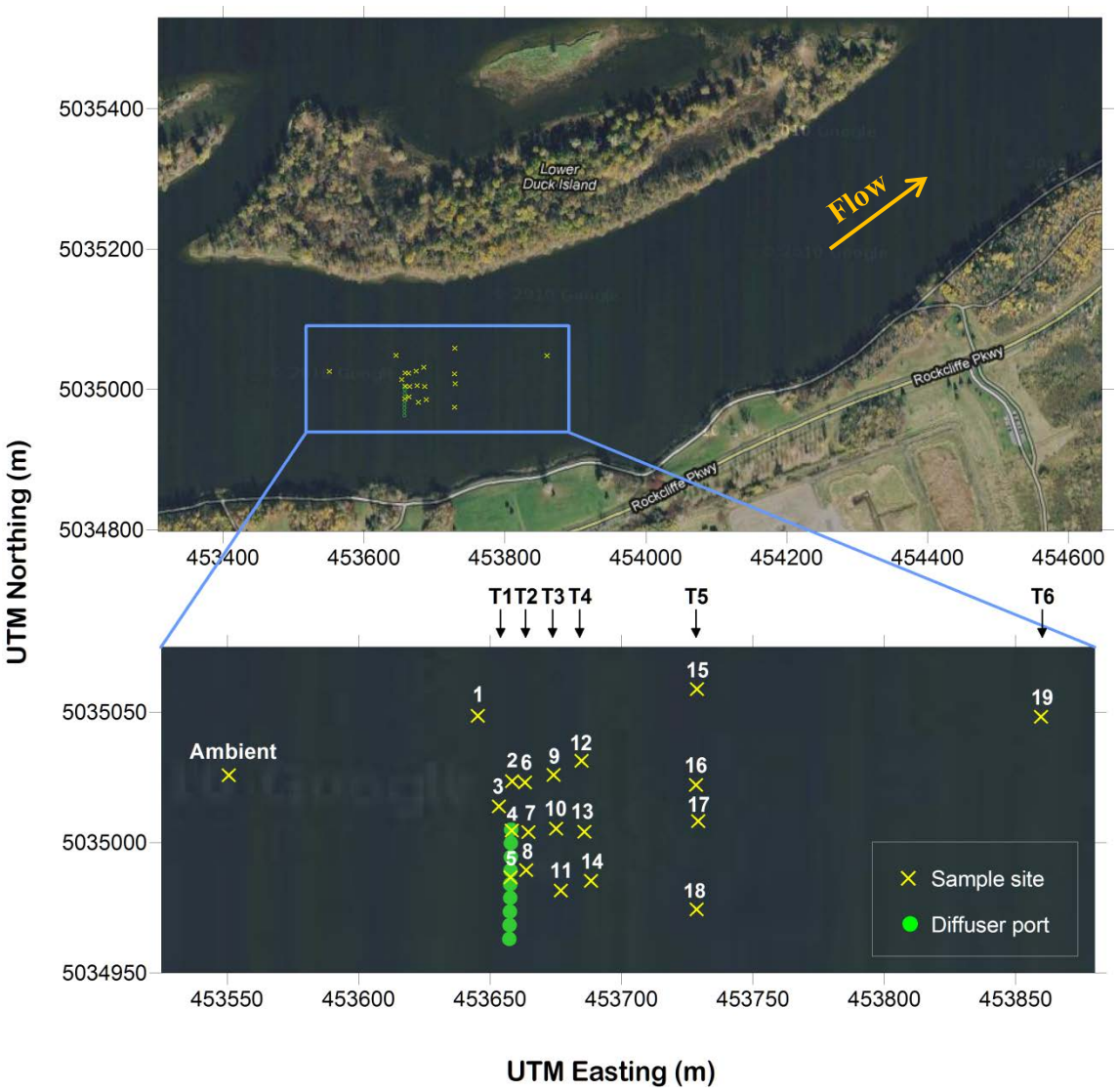

Figure 3.5: The top image shows a full view of the sampled reach and provides the sampling area in the context of the study reach. The bottom image is a close-up view of the sampling area, where each sampling site is labeled by number. The diffuser location is estimated as discussed in Section 3.1.3.

3.2.2. Period of water sample collection

According to four years of annually averaged hourly flow, ROPEC's discharge rate (Ranya Sherif, personal communication) reaches a minimum at approximately 7:00 hours, increases between 9:00 and 13:00 hours, and is constant from 13:00 to 19:00 hours (Figure 3.6). Thus, water samples were collected between 13:00 and 19:00 hours in order to capture a period of most constant discharge.

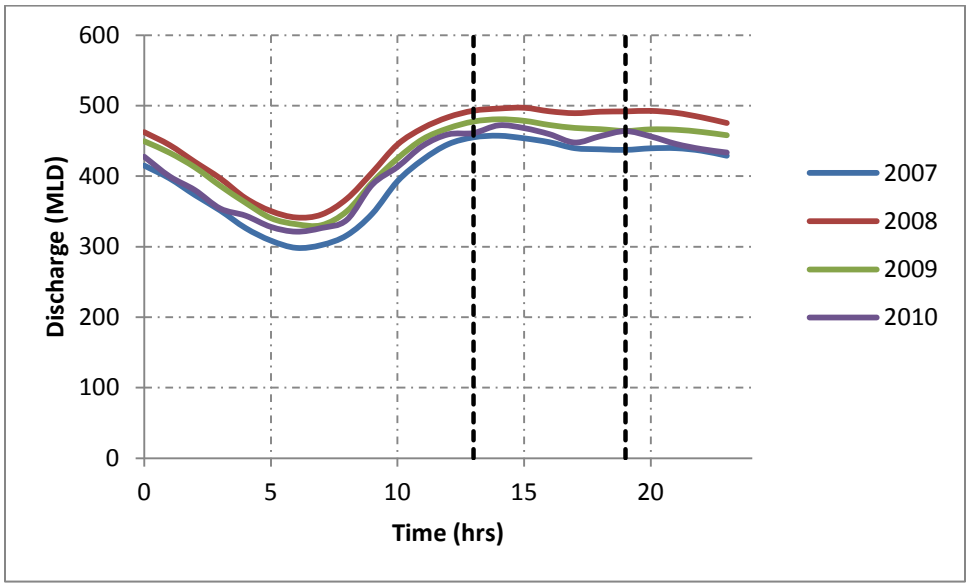

Figure 3.6: ROPEC diurnal between 2007 and 2010. The discharge is provided in units of million litres per day in a 24 hour period, averaged over the year. The dashed, vertical lines indicate the start and end hours of the water sampling for this project. Data provided by ROPEC (Ranya Sherif, personal communication).

Water samples were collected with a 2L beta sampler (i.e., Van Dorn sampler) from a 25' pontoon boat. A 6lb weight was attached to the beta sampler to ensure the minimum possible angle of carry by the river current (this was also ensured by measuring the angle of the rope, where the rope angle was never more than 6° from the vertical). Coordinate points for the pre-selected sample sites were entered into a hand-held Magellan Thales ProMark3 GPS with WAAS correction. The boat was anchored as close as possible to a desired location. Due to the river currents and wind, the boat moved while collecting multiple water samples at each site. For that reason, the location of each water sample was recorded using the RTK-GPS. Water samples from each depth were brought to the surface and stored in a glass sample bottle. Samples were kept on ice in coolers during field

sampling and transferred to a 4°C refrigerator for storage. In total, 92 water samples were collected.

3.2.3. Ambient temperature

River temperature was measured with a simple mercury-in-glass thermometer during the spatial survey of day 1. The thermometer was calibrated a day prior to setting out into the field. It consistently measured a river surface temperature of 21°C, a value which was used for determining unionized ammonia and in the models. These values were compared to the ADP temperature measurements on both days, which equaled 24°C. The difference between the glass thermometer and ADP temperature measurements does not have a significant effect on ammonia speciation.

3.3. Chemical Analysis

3.3.1. Laboratory analysis

Chemical analysis of river water samples was performed in the Environmental Laboratory of the Department of Civil Engineering at University of Ottawa. Ammonia, nitrite and nitrate concentrations of each sample were measured. Measured ammonia concentrations were equal to the sum of the ammonium ion (NH_4^+) and unionized ammonia (NH_3) concentrations (as discussed in Section 2.3.2). Ammonia was measured 3 days after sample collection. Nitrite and nitrate were measured within 48 and 54 hours of sample collection, respectively. As per the specified storage procedure (APHA, 2005), all samples were stored at 4°C between sampling and laboratory measurements. Prior to measurement, required volumes of samples were brought to room temperature.

Nitrogen constituents were measured using standard methods 4500-NH_3 C for ammonia (APHA 1995), 4500 NO_2- B for nitrite and 4500 NO_3- B for nitrate (APHA, 2005). Table 3.2 provides a summary of the reagents used, the volume of each reagent and sample used, the type of spectrophotometer employed for testing and the wavelength of light required for each test (APHA 1995, 2005). Approximately, 10mL of water sample was brought to room temperature prior to analysis of nitrogen constituents. HACH DR2700 and HACH DR5000 spectrophotometers were used to read absorbance, as indicated in Table 3.2.

Table 3.2: Summary of chemical methods for determination of ammonia, nitrite, and nitrate.

	Ammonia	Nitrite	Nitrate
Reagent	Nessler	Colour reagent[1]	HCl
Volume of Reagent	0.4mL	0.4mL	0.2mL
Volume of Sample	10mL	10mL	10mL
Spectrophotometer	HACH DR2700	HACH DR2700	HACH DR5000
Wavelength	425nm	543nm	220nm + 275nm[2]
Standard Method	4500 NH_3 C. Nesslerization Method[3]	4500 NO_2^- B. Colorimetric Method[4]	4500 NO_3^- B. Ultraviolet Spectrophotometric Screening Method[4]

[1] Sulphanilamide and N-(1-napthyl)-ethylenediamine dihydrochloride.

[2] 220nm used for nitrate reading and 275nm for interference caused by dissolved organic matter.

[3] APHA (1995)

[4] APHA (2005)

For this thesis, all analyses were performed following trace-clean procedures, meaning all glassware was washed and rinsed three times using Milli-Q water between sample measurements.

Seven sets of triplicates were collected from the Ottawa River at various depths and locations. Triplicate sampling included collecting 3 bottles of sample, and was used to determine the overall variance of the sample collection and measurement (i.e. variance of the collection procedure in the field and of the lab technique).

To calculate the accuracy between triplicates, standard error of the mean (SDE) for each constituent was calculated:

$$SDE = \frac{average(st.dev.(set\ of\ triplicates))}{\sqrt{3}}, \qquad (31)$$

Another method to determine the amount of error in the laboratory measurement technique is to measure blanks and standards. Blanks are used to zero the instruments and measure the drift in instrument during analysis and thus provide accuracy of the measurements, while standards are used to verify the precision of the instrument at the time of analysis. Blanks were made up of Milli-Q water and the appropriate reagent (as provided in Table 3.2), whereas the standards contained a known concentration of the analyte. One sample blank and one sample standard were analyzed every 20 samples. Error values were defined by calculating root-mean-square errors (RMSE) and mean errors for precision and accuracy, respectively. Both errors were calculated for each blank and standard.

RMSE is calculated by the following equation:

$$RMSE = \sqrt{\frac{\sum value^2}{number\ of\ values}} \quad (32)$$

where *value* for a blank sample equals the measured value of a blank, while *value* for a control sample equals the difference between the expected and measured values of the standard.

The mean error for a blank is a simple average of all the tested blanks. For a control sample, it is the average of the differences between each measured standard and the standard value it was created at.

Using the calibration curves, *limits of detection* (LOD) were calculated. LOD provides the minimum level at which the analyte's concentration can be detected given the type of method, instrument and sample (ICH, 2005) used. Refer to ICH (2005) for calculations.

3.3.2. Statistical analysis

A t-test was used to test for significant differences in the depth averaged concentration of ammonia, nitrite, and nitrate between each sample site and the ambient upstream concentration. The Bonferroni correction was used to adjust the P-value for multiple comparisons. Due to only a single water sample at each depth further statistical comparisons between depths or across sample sites at a single depth were not possible.

3.3.3. Unionized ammonia

Unionized ammonia was calculated using the method of Emerson et al. (1975), see Section 2.3.2. Average river temperature of 21°C was used to calculate the concentration of unionized ammonia in the river. The VWR™ SympHony™ Meter version SB80PD was used to measure pH levels of all water samples. Samples were brought to room temperature (which by chance was also 21°C) before measurement.

Two-dimensional interpolations of unionized ammonia data were generated at near surface depth (0.5m from water surface) and near bed-bottom depth (0.5m from the bed-bottom). It should be emphasized that interpolations at near surface depth share the same elevation level of 39.5m. However, interpolations near bed-bottom do not share the same elevation levels, but are rather exactly as stated, 0.5m from the river bed bottom.

The Kriging function in Tecplot 360™ was used for the interpolation of the data. To avoid a misleading interpolation of the measured data (where an interpolation will force upstream interpolations of high concentrations at the diffuser), the interpolation was split into two areas: one representing samples upstream of the diffuser and the other representing samples at and downstream of the diffuser. The rectangular zones were limited by the spatial coordinates of the samples and some extrapolation was inherent. Kriging was determined using a 30% data range, assuming no drift, and an octant for the point selection with eight points. For both near-surface and near-bed interpolations, a total of 61 cells in the x-direction (split between 21 cells for the upstream and 40 cells for the downstream direction) and 17 cells in the y-direction comprised the interpolation mesh, whose cell sizes equaled 5x5m. Extrapolated area (outside of the sample points) was blanked. Figure

3.7 provides an aerial image of the study reach with a mask of the blanked interpolated region as well as location of the sampling sites.

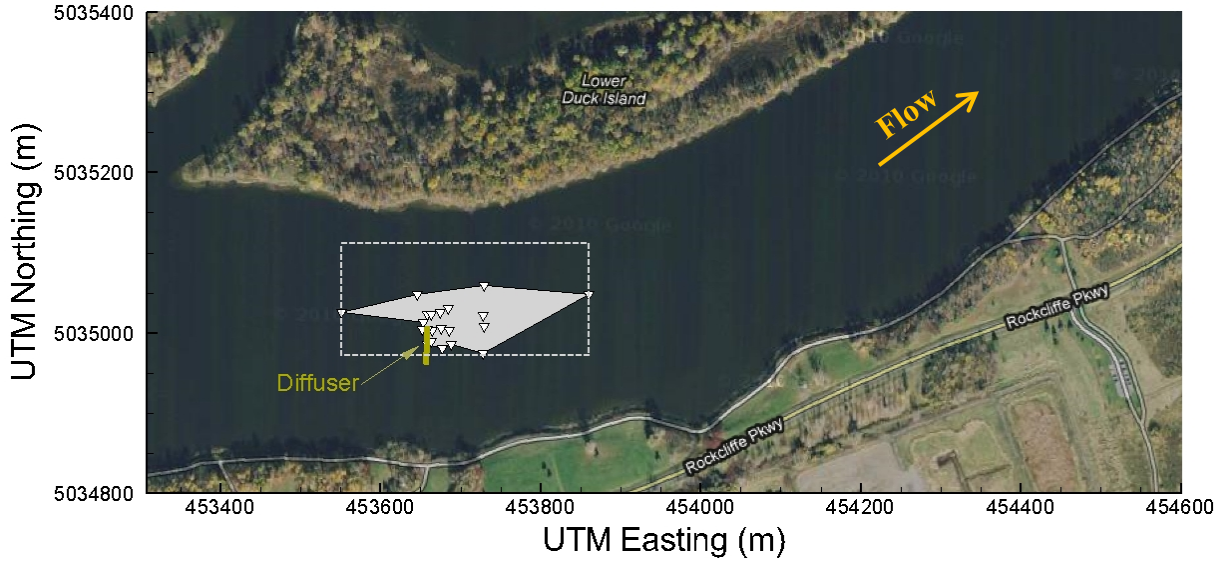

Figure 3.7: Aerial image of the river reach with a superimposed mask of the interpolated area (grey), sampling sites (▽) and diffuser (gold line).

3.4. Application of FLOW-3D

The following section provides full details of the methods used to simulate in FLOW-3D for this thesis.

3.4.1. Computational domain and model setup

First, the flow domain was defined to encompass the majority of the river reach surveyed during the field campaign. A topographic file for FLOW-3D was created using interpolated bathymetry in Surfer (Section 3.1.4). This initial flow domain was used to run the model until steady state was reached. Second, the mesh was modified to a smaller computational domain and the model was rerun as a restart simulation. This final flow domain was created in order to increase the resolution of the area of interest without significantly increasing computational time and to simulate only the area of interest (area where the plume was situated). A single mesh was used after simulations with embedded and multi-

block meshes using both coarse and fine meshes were found to be heavy on computational time.

The vertical axis of the computational domain was set equal to 6m, which acted as the height of the water surface. The lowest point on the topographic map, at a bed height of 0.4m, corresponded to the deepest survey point having a depth of 5.6m from the water surface. Initial domain size was 650m x 450m x 6m in the x-, y-, z-directions (streamflow, transverse and vertical axes, respectively) with rectangular grid spacing of $\Delta x = \Delta y = 1m$ and $\Delta z = 0.5m$. This yielded approximately 1.7 million active cells. The final domain was reduced down to 220m x 150m x 6m in the x-, y-, z-directions with all three cell sides equalling 0.5m, yielding approximately 1.3 million active cells. The model was allowed to reach steady state before analysis.

Pressure was approximated using an implicit scheme with the successive over-relaxation (SOR) method (Section 2.2.3). Momentum advection was approximated explicitly using first-order accuracy. An explicit scheme was also used to approximate viscous stress and heat-transfer terms. The computational time-step was dynamically controlled using only stability as a criterion. Initially, convergence and stability were both used, but this option yielded similar results with a significantly longer computational time. For turbulence closure, the k-ε and RNG k-ε methods were applied allowing the maximum turbulent mixing length to be dynamically computed. The LES method was also applied, although it resulted in steady-state. It is important to note that LES is spatially filtered (similar to time-averaging as in RANS equations, but over space) and thus should not result in steady-state if the resolution is small enough to resolve eddies. In this thesis, the mesh was not fine enough to resolve the unsteady eddies, but the computational cost for a finer mesh was too costly to consider.

The diffuser was created by inserting 9 solid cylinders at estimated coordinate points of the port locations. To mimic the diffuser during the field sampling campaign, each cylinder was assigned a diameter of 0.9m and a height of 3m from the base of the mesh. This height ensured that effluent discharge would always be 3m below the water surface, where the port tips were estimated to be. At the top of each cylinder (or port), a two-dimensional

mass momentum source was created with an equivalent diameter (0.9m). Each source delivered a discharge of 0.447m^3/s, with a temperature of 22°C and a concentration of 26.57ppm, as deduced from ROPEC information (Appendix). By applying a flow discharge from the mass momentum source, no pressure details were required. Any energy losses incurred by the pipe on the fluid were ignored for simplicity.

Bed roughness in FLOW-3D is applied by providing a surface roughness to the bathymetry (the reader is referred to FLOW-3D for further details); $n_{manning}$ was given a value typically used for a fine sand river substrate (0.03), (Franzini et al., 1997).

3.4.2. Boundary and initial conditions

A constant velocity of 0.2m/s in the streamwise direction, with uniform pressure and a fluid elevation of 6m were defined for the upstream boundary condition. A temperature of 21°C and an ammonia concentration of 0.381ppm were assigned for the inflowing river water. The transverse and vertical velocities were assumed insignificant at the upstream boundary (far from the diffuser) and therefore ignored.

During model setup, a rectangular basin without topography was initially created to provide a necessary length of distance in order that a fully developed velocity profile is reached before a diffuser is introduced. This distance was found to be within the first 120m of the model mesh in the x-direction (Easting). To provide some room for further development with uneven topography (bathymetry of the river bed) a 240m margin was provided before the diffuser was inserted into the mesh. Thus, enough space was allowed for the flow to develop by the time it reached the diffuser.

An assumption was made that the bathymetry used in the model (and created from data collected during the field campaign as described in Section 3.1.4) created a similar velocity profile at the diffuser as seen in the field. The downstream boundary condition was assigned the outflow boundary option. Here, the fluid was allowed to leave the boundary, but was not allowed to enter it. A rigid wall condition was set to the right, left and bottom boundaries, which actually did not play a significant role, since the bathymetry for all three acted as an obstacle and therefore used the FAVOR function. No-slip wall conditions were

imposed. Although, the VOF method is available in FLOW-3D, a rigid lid was imposed on the top boundary (water surface). Initially, a free-surface scheme was applied to the top boundary, which required extremely small time-steps to avoid instabilities. However, with too low of a vertical resolution the method resulted in unstable results.

For the final simulation, where the mesh area was smaller with a finer mesh, the upstream, downstream and two side boundaries were assigned the grid overlay boundary. This way, solutions calculated in the preceding model were used as initial and part of the boundary conditions for this model. The top and bottom boundaries were assigned the rigid lid and rigid wall conditions, respectively, as in the initial simulation.

3.4.3. Sensitivity analyses

Sensitivity analysis provides insight to modelling uncertainties. The most common method for numerical modelling is to test for sensitivities in the mesh size and time-step size. For open channel flows, the roughness parameter is used (which is also used for calibration). The sensitivity analyses of these parameters are briefly discussed, with respect to work undergone for this thesis. Also, because the effluent discharge rate and ammonia concentration were uncertain, the sensitivity to these values were performed as discussed below.

Grid and time-step size

Computational costs are highly dependent on simulation grid and time-step size. The grid's cell size limit for simulations in this thesis was 0.5m. A finer mesh was not possible as greater computer resources were required. However, if they were available, it would be preferable to increase the mesh resolution until changes are no longer noticed. The time-step size was controlled based on the stability criterion. Initially, both stability and convergence criteria were used, but differences in results between the two methods were insignificant. However, with the stability (only) criterion, much computational cost was saved.

Channel roughness

Channel roughness sensitivity was performed by changing Manning's roughness coefficient $n_{Manning}$. Three values were compared, encompassing the minimum and maximum limits of the given river bed (fine-sand). These were $n_{Manning}$ = 0.025, 0.030 and 0.035. The resulting ammonia concentrations were compared for significance.

Effluent discharge and ammonia concentration

Effluent discharge used in the model was 0.447m^3/s. Since the discharge of the effluent was variable throughout the field campaign, the maximum and minimum flows provided by ROPEC during the time of the campaign were used for sensitivity analysis: 0.427m^3/s and 0.456m^3/s, respectively. It has been shown that the ammonia concentration values of the effluent also fluctuated with time. Since a sparse amount of data was available, an average value of 26.57ppm was used. For sensitivity analysis, the minimum and maximum recorded concentrations (within the two week period within which the field campaign was nested) were used: 21mg-N/L and 29mg-N/L. An assessment comparing effluent discharge rates and ammonia concentrations at ROPEC did not show any correlation. Thus, sensitivity analyses for these two parameters were performed combining the minimum and maximum values. The combinations resulted in: high concentration – high discharge, low concentration – high discharge and low concentration – low discharge; creating three different cases to be examined. Ammonia concentrations were compared for significance. The case of high concentration – low discharge was not considered due to lack of computational resources. However, the important cases of most input (high concentration and discharge) and least input (low concentration and discharge) have been captured.

3.4.4. Creation of modelled results in Tecplot

Simulated data were imported into Tecplot 360™ with a *FLOW-3D Loader tool* available in the visualization software. These data did not require any manipulation (such as interpolation) to plot. Velocity and ammonia modelled results (of the course mesh models, where $\Delta x = \Delta y = 1$m and $\Delta z = 0.5$m) for all three turbulence models (k-ε, RNG k-ε and LES) are compared to field data and provided as explained in Section 3.6.

3.5. Application of CORMIX

CORMIX1 and CORMIX2 require very similar information to parameterize the model. The method of running the model differs only in inputs with respect to the geometry of the outflow pipe. While CORMIX2 requires full details of the diffuser, CORMIX1 requires only details of a single diffuser port. In order to present the CORMIX1 simulation as a diffuser, results from each port are superimposed at points of convergence between neighbouring plumes (Zhang & Zhu, 2011). However, this is only applicable in areas where passive ambient diffusion and advection take place. In areas where jet or plume momentum exists, the superposition is not a simple addition. Thus, the CORMIX1 sub-module was not utilized.

Average depth of the study reach and the average depth of the river in the diffuser area were 3.4m and 4.5m, respectively, as determined by the spatial field survey. The study reach was bounded, with a slight meander and a cross-sectional width of 300m, which corresponded to the river width where the diffuser was situated. The ambient velocity was assumed steady at 0.2m/s with a typical roughness for such a river of 0.03 (Franzini et al., 1997) for Manning's n. To correspond to the FLOW-3D simulations, imposed on by a rigid lid, the wind velocity was set to 0m/s. Temperatures of the river and the effluent were set to 21°C and 22°C, respectively. CORMIX itself determines whether any buoyancy effects exist.

Port diameter was assigned vertical geometry with a diameter of 0.9m. Port height was limited to 1.5m. CORMIX was developed to model deeply submerged or slightly submerged discharges, limiting the port height to less than 1/3 or greater than 2/3 of the water depth, respectively. Since the port height was approximated to be outside those limits, a 1/3 height was chosen rather than the latter, as it resembled closer the conditions observed in the field.

The diffuser placement was assigned to 112m north of the right (south) bank, having a length of 42m. The ports were identified as well rounded (having a contraction ratio of 1) and unidirectional.

Ammonia concentrations were modelled as a conservative constituent, as will be discussed in Section 4.4.2. The applied concentration of ammonia in CORMIX was 26.19mg-N/L as NH_3/NH_4^+ which is the difference between ROPEC's mean ammonia concentration calculated for the day (26.57mg-N/L) and the mean measured ambient river ammonia concentration (0.38mg-N/L). The ambient flow in CORMIX is assumed to have 0 concentrations of pollutants. The average effluent flow rate was assigned 4.02m^3/s, which was determined as the average rate from ROPEC during the field sampling campaign.

Sensitivity analyses in CORMIX were equivalent to FLOW-3D for applicable parameters: channel roughness, effluent discharge rate and effluent ammonia concentrations. Section 3.4.3 provides a description of the methods used. Please refer to it for details.

3.6. Comparison of Measured and Simulated Data

Measured and simulated data were compared in several ways. Velocity was compared by qualitative means (Section 4.3.2). Ammonia concentration was compared qualitatively (Section 4.5.1) and quantitatively (Section 4.5.2) using scatter plots. Sensitivity analyses were compared using ammonia concentration through scatter plots (Section 4.5.2). All methods are described below. Measured data were also compared to empirical methods by calculating the near-field dilution and the plume width (Section 4.5.3).

3.6.1. Comparison of velocity results

Velocity results were compared visually using contour maps at various depths and intersections along the river channel, between measured and modelled results. Slices from horizontal (x-y or Easting-Northing) and vertical (y-z or Northing-Elevation) planes were extracted from the prism grid to study streamwise and transverse velocity magnitudes. Horizontal slices were extracted at elevations of 39.5m (0.5m below the water surface) and 37m (at height of diffuser ports and approximately, mid-depth of the flow). Vertical slices were extracted at Easting coordinates of 453580m (78m upstream of the diffuser), 453658m (at the diffuser), 453688m (30m downstream of the diffuser), 453728m (70m downstream of the diffuser) and 453858m (200m downstream of the diffuser). Vertical transects were selected to study the flow behaviour: upstream of the diffuser where

ambient conditions exist; at and near downstream of the diffuser where mixing between diffuser discharge and river flow may prevail; and, further downstream of the diffuser to study whether the diffuser discharge has any further influence on the ambient flow. The upstream vertical slice and the last two downstream slices were selected due to their proximity to the boat path, to ensure for minimal error. The extent of horizontal maps and the location of vertical transects are illustrated in Figure 3.8, where the boat path is also shown.

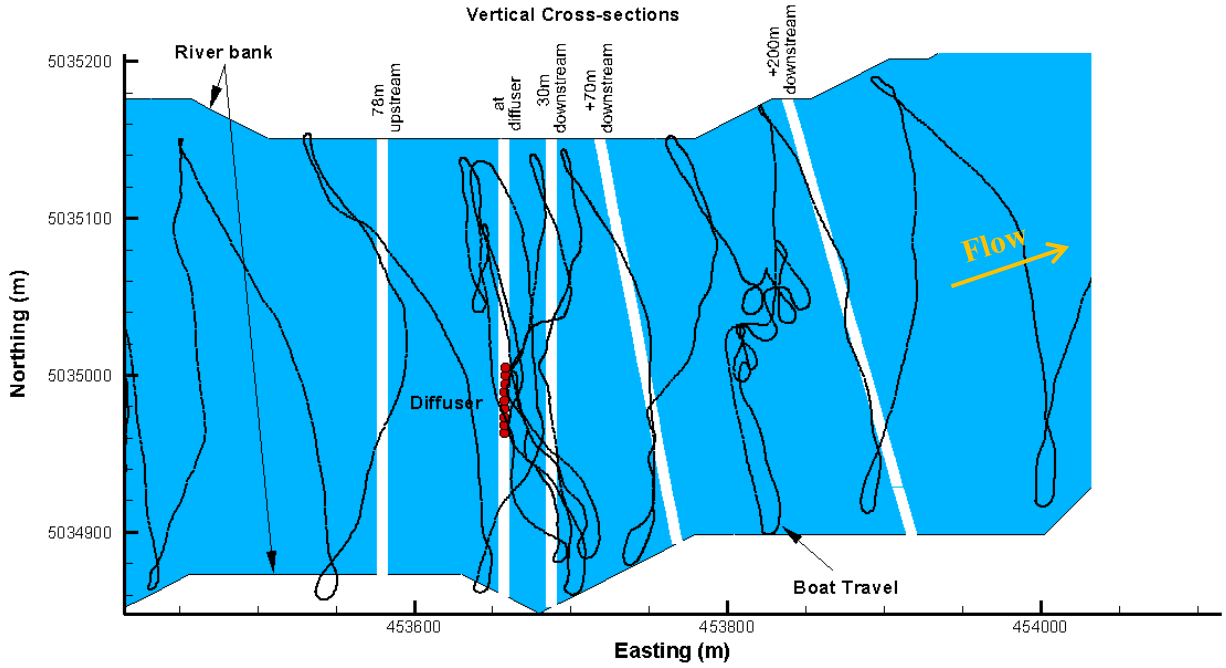

Figure 3.8: The extent of horizontal transects and positions (white lines) of vertical transects to visually describe the measured and modeled velocity fields of Section 4.3. The vertical transects are identified by their distance from the diffuser (red circles). The boat travel is shown by a black polyline.

3.6.2. Comparison of ammonia concentration results

Contour results for ammonia concentrations were only provided for the *k-ε* model (since visually, the results were very similar between all three models) for both the coarse and fine mesh models. Measured results were superimposed as points (since the number of measured samples is too low to warrant for any interpolation methods) on top of the model results. An equivalent colour scale for simulated and measured data was used. Plan view and vertical cross-sectional planes were extracted from the model to analyze

ammonia concentrations (Figure 3.9). For plan view, elevations of 39.5m (0.5m below the water surface) and 37m (at height of diffuser ports and approximately, mid-depth of the flow) were analyzed. For vertical cross-sections the following locations were analyzed, all perpendicular to the river banks: 453658m (at the diffuser), 453633m (5m downstream), 453676m (18m downstream), 453688m (30m downstream), and 453858m (200m downstream). A vertical cross-section at 453728m (70m downstream of the diffuser) was extracted perpendicular to the diffuser in order to capture all of the measured data in one graph.

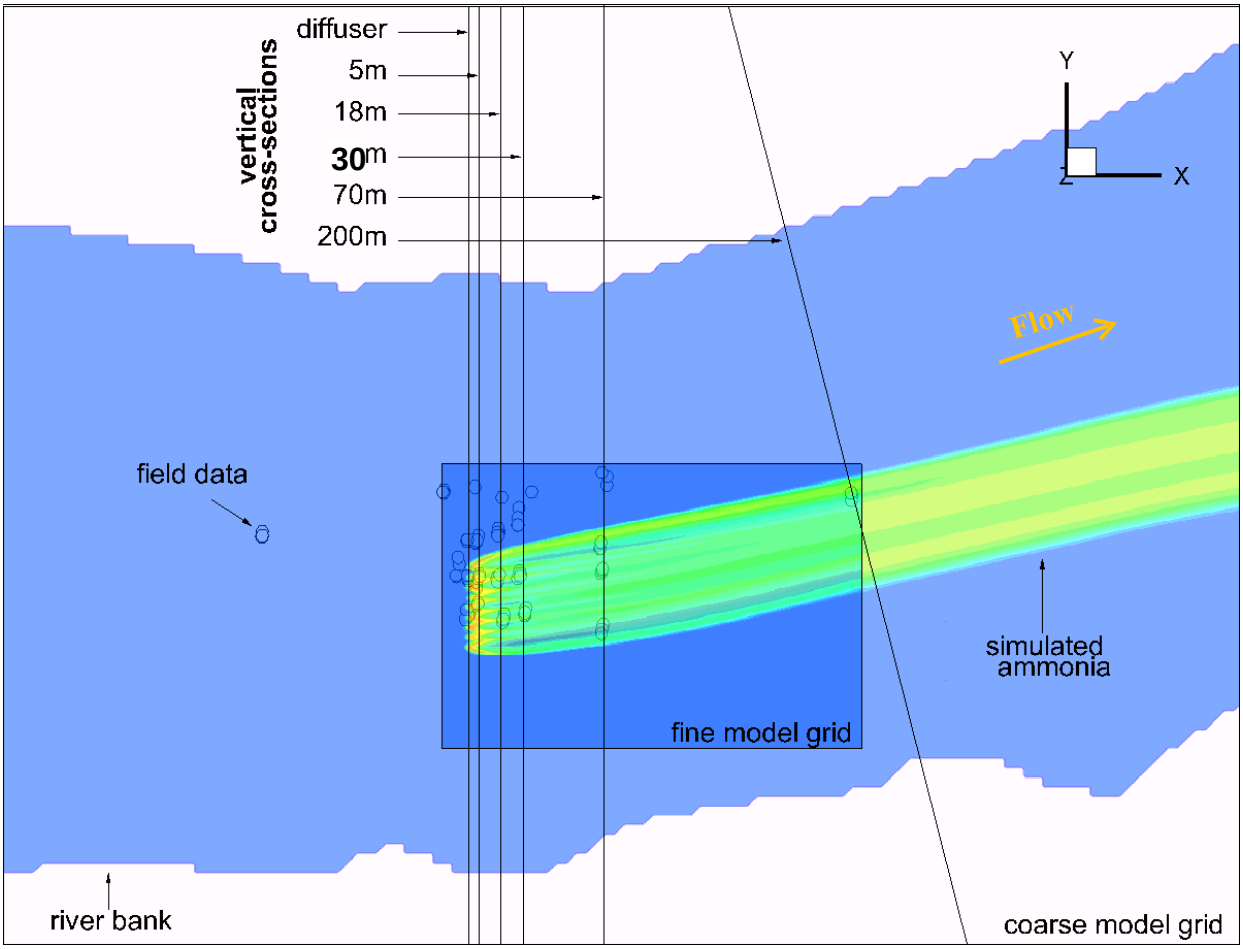

Figure 3.9: Extent of FLOW-3D coarse and fine models. The overall image shows the extent of the coarse mesh which was used for all three *k-ε*, RNG *k-ε* and LES models and all sensitivity simulations. The smaller rectangle shows the extent of the fine mesh used for the *k-ε* and RNG *k-ε* models. Also shown are all of the field data (hollow circles) samples as well as the positions of the vertical cross-sections (black lines).

Scatter plots of field and simulation ammonia concentration results are provided in a $C_{measured}$ vs. $C_{simulated}$ graphs. All five modelling situations are represented: *k-ε*, RNG *k-ε* and

LES as well as CORMIX2 simulations. The r^2 results comparing linear fit between measured data and modelled results are provided in a table.

Dilution concentrations were compared using empirical approximations of equations (24) and (25) to an approximation using measured or modelled data, equation (26). For equation (26) the near-field length was approximated using equation (23). For C_x, the mean about all of the measured data within the approximate near-field length was calculated. Concentrations from the matching locations were extracted from the model to calculate model dilution.

Plume widths were approximated using a point-source equation (28) by applying an imaginary point source upstream of the diffuser until a width of 42m – diffuser length – was reached. Values of 0.6 and 0.9 were used for the constant, C. To calculate ε_t for the Ottawa River in the study reach, an average shear velocity (u_*) of 0.016m/s was found by averaging the shear velocity calculated using ADP results.

3.6.3. Predicted ammonia toxicity

Unionized ammonia portion of ammonia can be of risk to aquatic wildlife at concentrations above 0.016mg-N/L. Thus, it was of interest to show the resulting unionized ammonia simulation by the CFD model, especially if the modelling results showed satisfactory results. The k-ε turbulence closure model with the coarse mesh was used to show the ammonia toxicity results (Section 4.5.4); since all three turbulence closure models were very similar, while the fine mesh showed some questionable results. Measured points were superimposed on top of the simulated contours. To convert from (total) ammonia to unionized ammonia portion for the modelled results, equations (17) and (18), as developed by Emerson, et al. (1975), were used with a pH and temperature of 7.84 and 21°C, respectively. The given pH was the average value from all of the measured samples at a temperature of 21°C.

4. Results & Discussion

This section discusses the data and results acquired from the field campaign, laboratory analysis and numerical modelling. A map of the interpolated bathymetry is presented, which was subsequently used to interpolate velocity field data in a 3D prism, as well as for topography of the river bed inside the FLOW-3D mesh for simulations. Depth averaged velocity vectors and magnitude are shown to provide a snapshot of generic flow behaviour. To present how well the model simulates 3D flow behaviour measured in the field, streamwise, transverse and vertical velocity maps are compared. These data are provided in plan view over two depths and vertical cross-sections over five transects. N-constituent concentrations collected during the field campaign are presented, to illustrate the behaviour of the effluent from the WWTP. Simulated ammonia concentration results are compared to measured data points. The graphs are provided in plan view at two depths and vertical cross-sections over six transects. Finally, calculated and simulated unionized ammonia are presented and discussed.

4.1. Visual Observations & Assumptions

While on the water, during the field campaign, jets from the diffuser were visible by their impingement on the surface of the river (see Figure 4.1). Thus, the position of the diffuser (and each of the nine ports) could be inferred from the boat. Each jet created wide boils, but interaction between each jet was not evident.

Figure 4.1: A photo taken near the vicinity of the ROPEC diffuser, where boils created by the discharged jets are visible.

For this thesis, upstream sources of ammonia were assumed to be negligible. Measurement of ammonia at a single site upstream of the diffuser confirmed minimal ambient concentrations. Approximately 0.4mm of rain was recorded during field day 1 and only trace amounts during field day 2 (EC, 2012).

4.2. Bathymetry

Bathymetry of the studied river reach was calculated by interpolating elevation data measured by the ADP (Section 3.1.4). The produced maps are shown in Figure 4.2, along with resulting standard deviations. Two separate interpolations of elevation data were performed to create bathymetry maps. The low resolution (25x25m) map (Figure 4.2A) does not hug the shoreline very well because of the coarseness of the interpolation. However, the resolution was chosen to encompass transects which were furthest apart (approximately 100m at points near the river banks). The high resolution (5x5m) map (Figure 4.2B) follows the shoreline well, but provides too fine of a resolution for available data outside of the boxed in region (Figure 4.2D – hatched purple box). The boxed in region represents transects spaced closely together, approximately 5m apart.

The river reach has a slight bend to channel left flowing north-east downstream of the diffuser. The thalweg (the deepest line along the river channel) is found near the right (or south) bank (Figure 4.2A and B). The north side of the channel is shallower than the south side, at some instances having an elevation 2m higher than its southern counterpart. The deepest section of the reach is found immediately downstream of the channel bend. The diffuser is situated near if not in the thalweg at approximately 453658m easting. Here, a dense region of contour lines is indicated in maps of Figure 4.2. Upon close inspection, the maps reveal that bed elevation just upstream of the diffuser is slightly raised while slightly deepened immediately downstream of the diffuser. The diffuser's main pipe was buried into a trench below the river bed and covered with riprap. Thus, a slight elevation in the river bed is expected. The thalweg is fairly narrow both upstream of the diffuser and 700m downstream of it. However in the region immediately downstream of the diffuser, the thalweg is quite wide suggesting that the diffuser discharge may have some influence on the bathymetry.

Surface water elevation was 40.0m the day of the survey. The deepest measured point of the river reach was at an elevation of 34.4m (a depth of 5.6m); while the mean measured elevation was 36.6m (a depth of 3.4m). The elevation of the river bed where the diffuser is situated was measured at an elevation of approximately 35.5m (a depth of 4.5m).

Kriging standard deviations (SD) were calculated (for bathymetry at both resolutions) to evaluate the reliability of the interpolation process (Rennie & Church, 2010). Kriging SD maps (Figure 4.2C and D) illustrate the significance of the measured points to the interpolation, in other words they provide a snapshot of the spatial distribution of variance. Low values of kriging SD suggest the measured data were spatially correlated and sufficiently dense to provide good information for reliable local interpolation, whereas high values approaching the standard deviation of the measured data suggest interpolated values are relatively unreliable. The survey path is evident in Figure 4.2D, where a kriging SD of zero (dark) signifies observed data points. In the region of concern (within the first 200m downstream of the diffuser) the highest value of the kriging SD is 0.35m, whereas the SD of the measured data was 0.98m. The kriging estimations were best in the region around the diffuser, as expected, where fairly dense boat paths exist and where transects were approximately 5m apart. Elsewhere in the study reach transects were further apart (up to 100m in some cases), causing some interpolated regions to have a larger area of uncertainty than others.

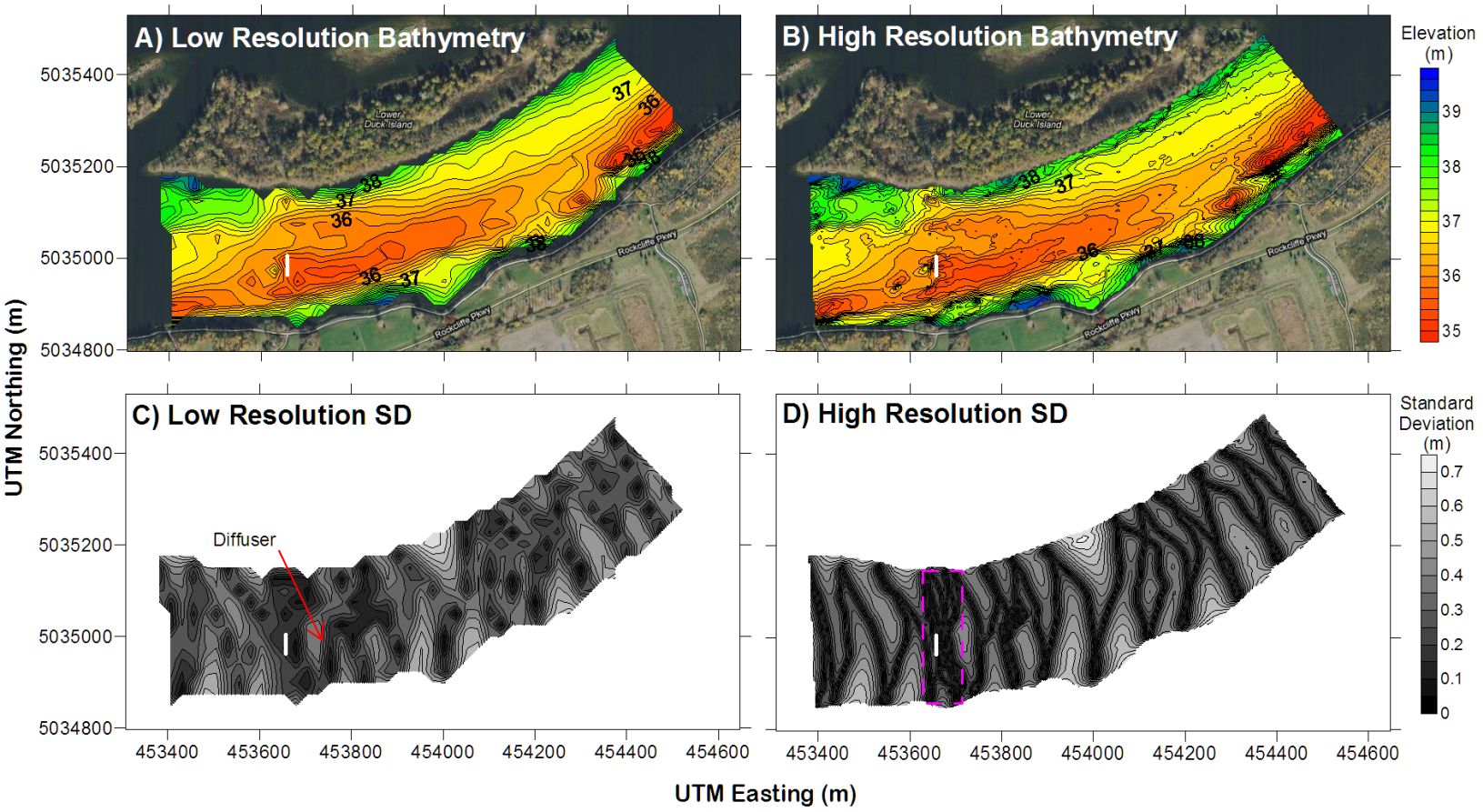

Figure 4.2: Interpolated bathymetry (A & B) of the studied river reach and resulting kriging standard deviations (C & D). Bathymetric maps (A & B) are superimposed over a Google satellite image to illustrate the extent of the coverage over the area. Low (A & C) and high (B & D) resolution images represent 25x25m and 5x5m interpolations, respectively. Bathymetry is shown by elevation contours, where the red contours denote deepest depths, as well as the path of the thalweg. Water surface elevation during the field campaign was measured at 40.0m across the whole reach. A boxed in region (hatched purple box) on Map D) indicates the limits of acceptable interpolation for the high resolution maps (B & D). The map coordinates are in UTM-18. The diffuser is depicted by a white line on all four maps.

4.3. Velocity

Maps of the flow field are presented in this section from both the field campaign and from the model simulations. Depth averaged velocity maps using data from the field were developed to illustrate the general behaviour of the flow in the study reach and are shown in Section 4.3.1. 3D velocity maps comparing measured and modelled results were developed in the horizontal plane at two different depths and in the vertical cross-section at 5 different locations and presented in Section 4.3.2.

4.3.1. Depth averaged velocity

Spatial distribution of the depth averaged velocities, derived by interpolating spatially recorded data (Section 3.1.4) is presented in Figure 4.3 in plan view. The figure provides three maps: A) depth averaged velocity vectors superimposed on top of the bathymetry map, B) velocity magnitude and C) kriging standard deviation for the velocity interpolations provided in map B).

Figure 4.3A) illustrates that the velocity upstream of the diffuser was distributed evenly across the channel, decreasing toward the channel banks where the elevation of the river bed is higher. At the diffuser, the flow split on either side of the diffuser, and a low velocity area is observed immediately downstream of the diffuser. A high velocity region is observed to the left of the diffuser.

The velocity magnitude contours in Figure 4.3B) provide a clearer picture (despite the minor scalloping effect caused by the interpolation) of the difference between high and low velocities downstream of the diffuser. Higher velocities are expected along the thalweg, which does start occuring approximately 400m downstream of the diffuser. Here, high velocity contours found near the center of the channel start tending towards the right bank as the flow nears the end of the study reach.

The kriging SD contours of velocity magnitude are presented in Figure 4.3C), which demonstrates low SD in regions (dark) where survey transects were closely spaced together. Near shore interpolation resulted in high SDs where transects were spaced as far

as 100m apart (light regions). The SD (kriging SD) of the depth averaged velocity in the U and V direction were 0.100m/s (0.062m/s) and 0.102m/s (0.066m/s), respectively.

Upstream of the diffuser, the mean, depth averaged, streamwise velocity was 0.20m/s. This value was used for initial conditions of the FLOW-3D and CORMIX models.

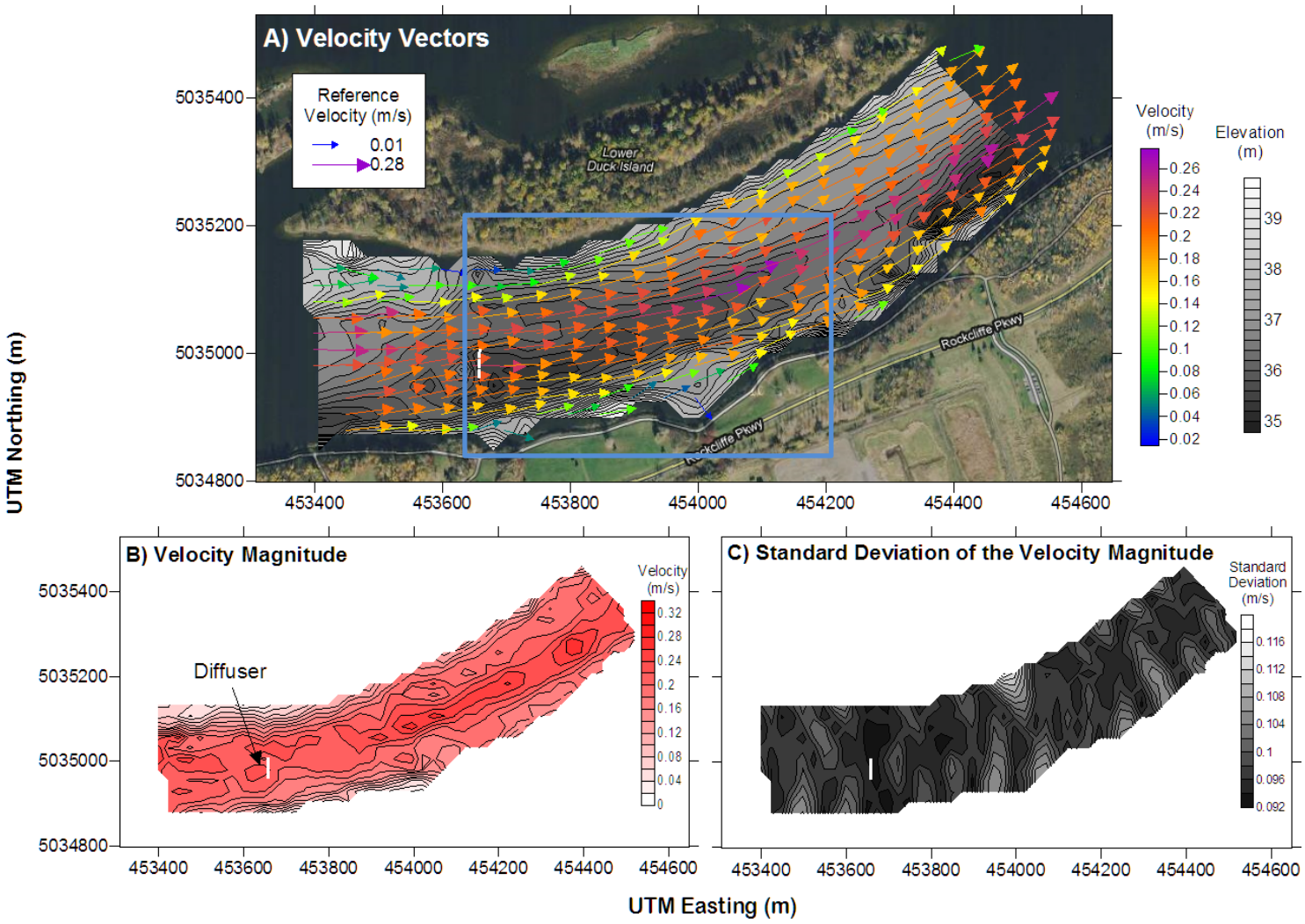

Figure 4.3: Map A) shows depth averaged velocity vectors superimposed on river bathymetry (also found in Figure 4.2A). A Google satellite image is used to visually orient the velocity field. The blue square illustrates the extent of FLOW-3D modelling of the study reach. Map B) shows the magnitude of the depth averaged velocity. Map C) shows the spatial distribution of the velocity magnitude kriging standard deviation. The map coordinates are in UTM-18. The diffuser is depicted by a white line on all three maps.

Approach velocity in the streamwise direction (Figure 4.4 and 4.4) measured in the field was variable, while the simulated velocity field was overall even. This was mainly because initial velocity within the FLOW-3D models was set to a constant value (0.2m/s) over the entire upstream boundary. Similar to the depth averaged velocity calculated using measured results (Figure 4.3), the model results (Figure 4.4 and 4.4) also suggest that the ambient flow field at the diffuser separated and was pushed to either side of the diffuser. The diffuser jets acted like a flow obstruction, causing the ambient flow to split around the diffuser with a wake flow immediately downstream. The model results also demonstrate that as the bulk flow split around the diffuser, a relatively quiescent region emerged immediately downstream of the diffuser. Since jet interaction with the ambient flow is not evident, this quiescent region suggests that ammonia was not mixing well with the ambient flow. The quiescent regions simulated by the k-ε and LES models are up to 140m and 230m long (Figure 4.4), respectively. The effects were observed at both elevations (near surface and mid-depth). The relatively quiescent wake region is clearly visible in the vertical cross-sections (Figure 4.5) of the models, as well. In contrast, a quiescent region is difficult to discern using results from the measured data. Thus, the model results suggest that the diffuser has a much stronger effect on the ambient flow than the measured results illustrate. The models also demonstrated a high velocity region of both transverse and vertical velocities (Figure 4.7: G, L, Q and Figure 4.9: G, L, Q) at the diffuser. However, this high velocity region was not apparent at the 30m transect in any of the models. Finally, the numerical model may have led to some oscillatory results at the diffuser, which is often attributed to meshes with a resolution that is too coarse and aspect ratio too high. This effect may explain the oscillation in Figure 4.9: G, L and Q, where the mesh resolution was 1m in the transverse axis and 0.5m in the vertical axis. However, because a Finite Volume Method was used, the overall mass and momentum balance remained conserved.

Although the 3D velocity results measured in the field exhibit a similar flow separation at the diffuser, a zone of high velocity core is evident to the right of the diffuser while a significant zone of low streamwise velocity is exhibited in the region immediately to the left

of the diffuser. The quiescent region in the models is not observed in the measured data. Downstream of the diffuser (at approximately 30m and beyond) the measured data contours are too patchy to discern properly the flow behaviour in both plan view and vertical cross-sections provided.

Zones of high velocity core differ between measured and model results. Approximately 200m downstream of the diffuser (453860m Easting), measured results show zones of high velocity core moving from the center of the channel towards the left, away from the thalweg (as seen in Figure 4.2). The model results however, illustrate that these high velocity regions continue along the thalweg, closer to the right bank of the river. The LES model exhibits streamwise velocities up to 0.04m/s higher than those of the k-ε models.

The discrepancy between modelled and simulated flows may have been due to the bathymetry provided in the model. The best available interpolation provided a resolution of 5x5m, which may not have been fine enough to pick up the fine details around the diffuser. As already mentioned the diffuser manifold was housed in a trench dug into the river bed and covered by riprap. The riprap would have caused a sudden increase (or a swelling) in the river bed which may have acted like an underwater dyke causing local anomalies in the flow.

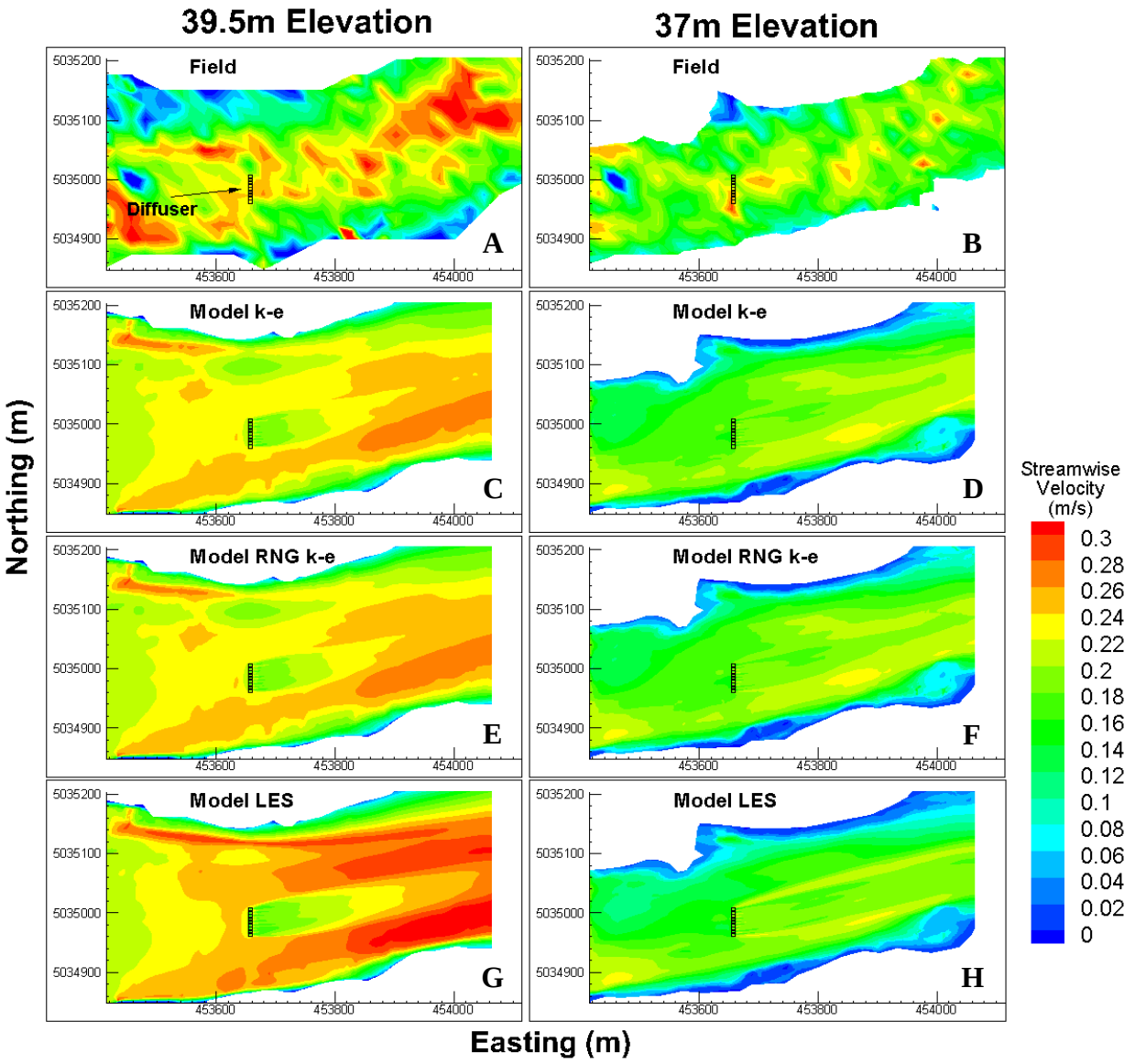

Figure 4.4: Streamwise velocities in plan view for interpolated measured results and FLOW-3D *k-ε*, RNG *k-ε* and LES model data at two different elevations. The same colour scale is used for all maps. The map coordinates are in UTM-18. The diffuser is depicted by a black line on all maps.

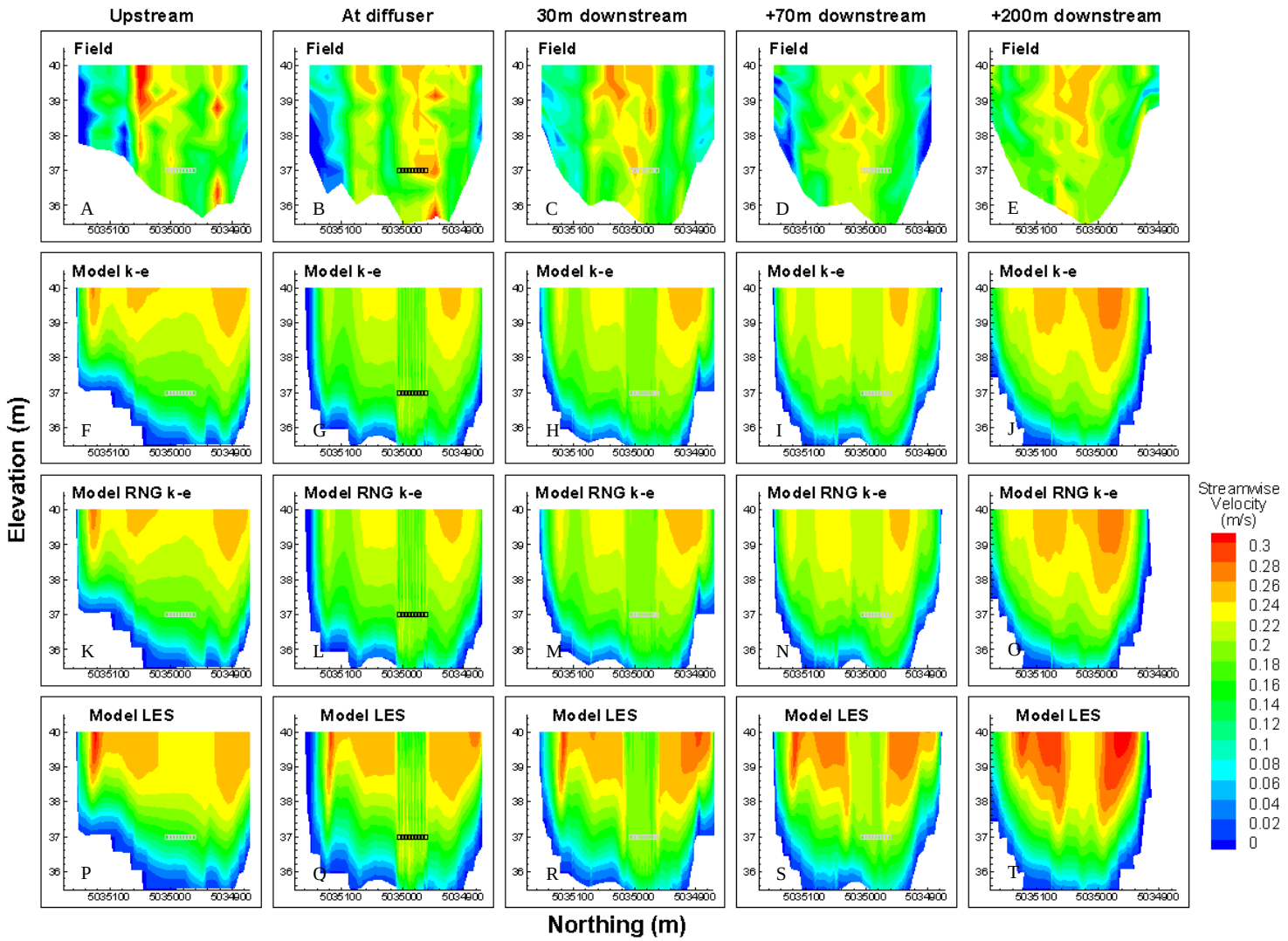

Figure 4.5: Vertical cross-sections of streamwise velocities – upstream, at and downstream of the diffuser – are illustrated for interpolated measured results and FLOW-3D *k-ε*, RNG *k-ε* and LES models. The same colour scale is used for all maps. X-axes are in UTM-18 coordinates, where values are in descending order to present results from left to right bank (as if looking downstream into each vertical cross-section). Y-axes represent the elevation. Width-to-depth ratio (x:y axes) is 1:0.0175. The diffuser is depicted by black squares for cross-sections at the diffuser (2nd column) and by grey squares elsewhere.

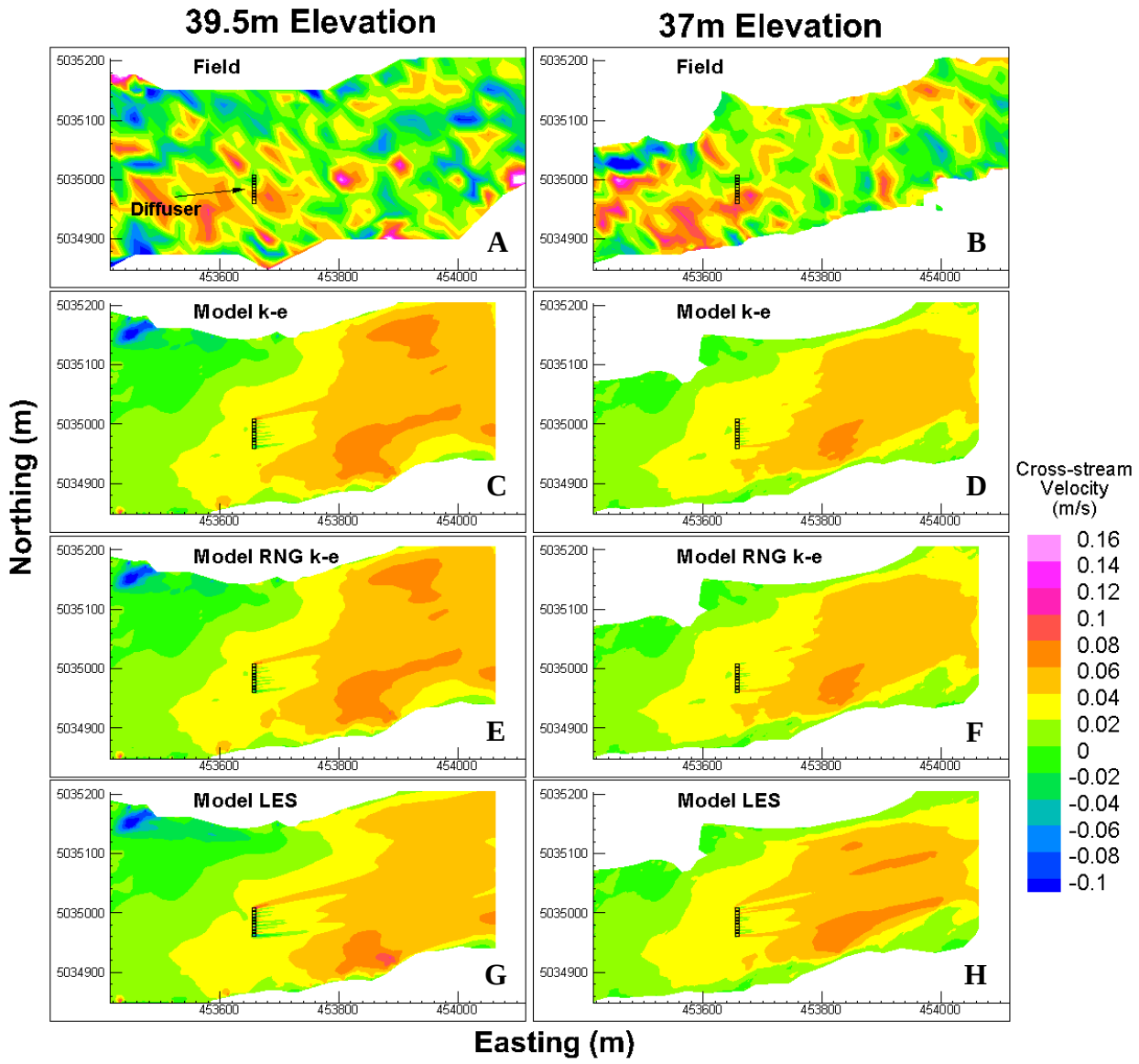

Figure 4.6: Cross-stream (transverse) velocities in plan view for interpolated measured results and FLOW-3D *k-ε*, RNG *k-ε* and LES model data at two different elevations. The same colour scale is used for all maps. The map coordinates are in UTM-18. The diffuser is depicted by a black line on all maps.

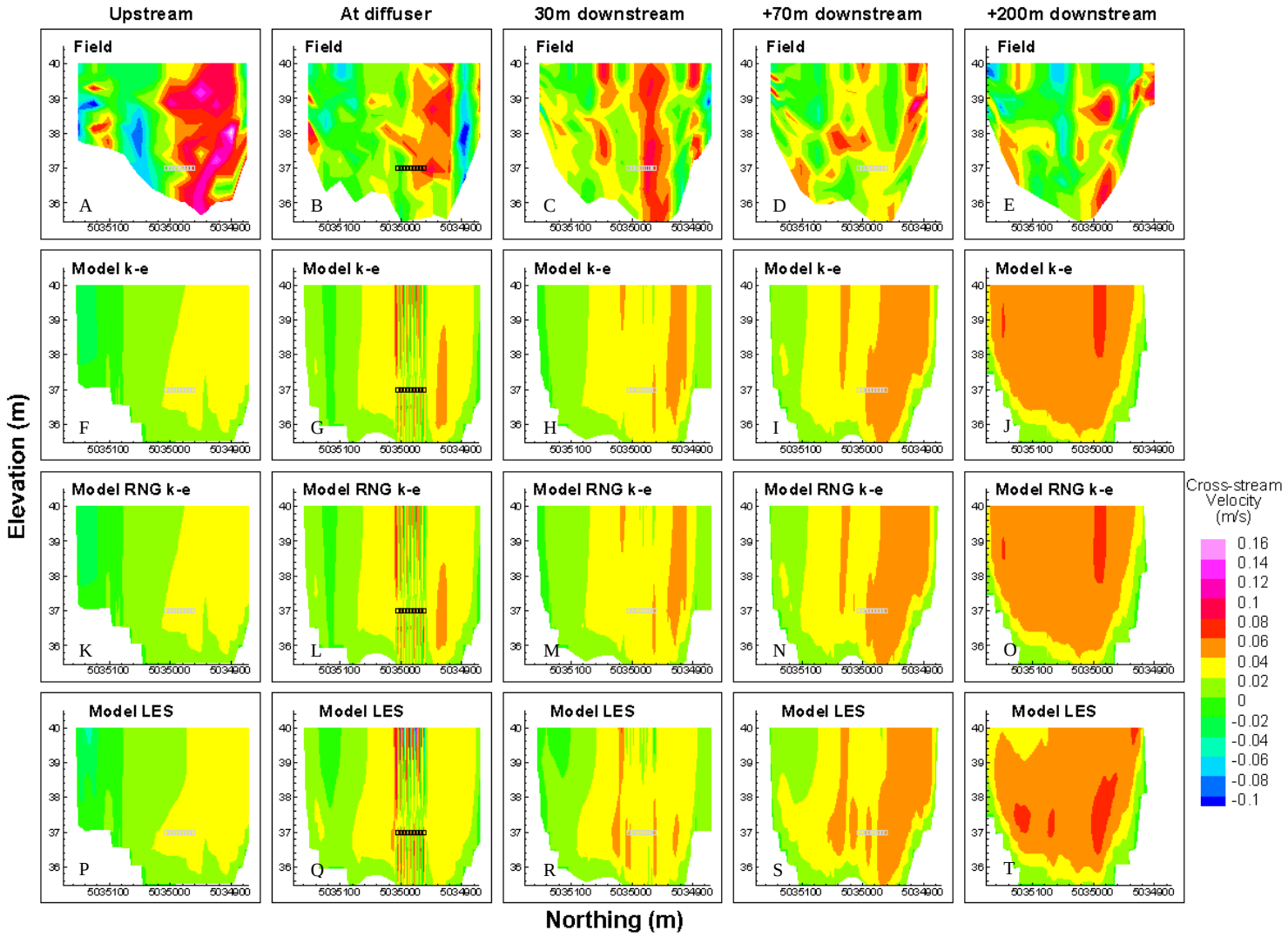

Figure 4.7: Vertical cross-sections of cross-stream (transverse) velocities – upstream, at and downstream of the diffuser – are illustrated for interpolated measured results and FLOW-3D *k-ε*, RNG *k-ε* and LES models. The same colour scale is used for all maps. X-axes are in UTM-18 coordinates, where values are in descending order to present results from left to right bank (as if looking downstream into each vertical cross-section). Y-axes represent the elevation. Width-to-depth ratio (x:y axes) is 1:0.0175. The diffuser is depicted by black squares for cross-sections at the diffuser (2nd column) and by grey squares elsewhere.

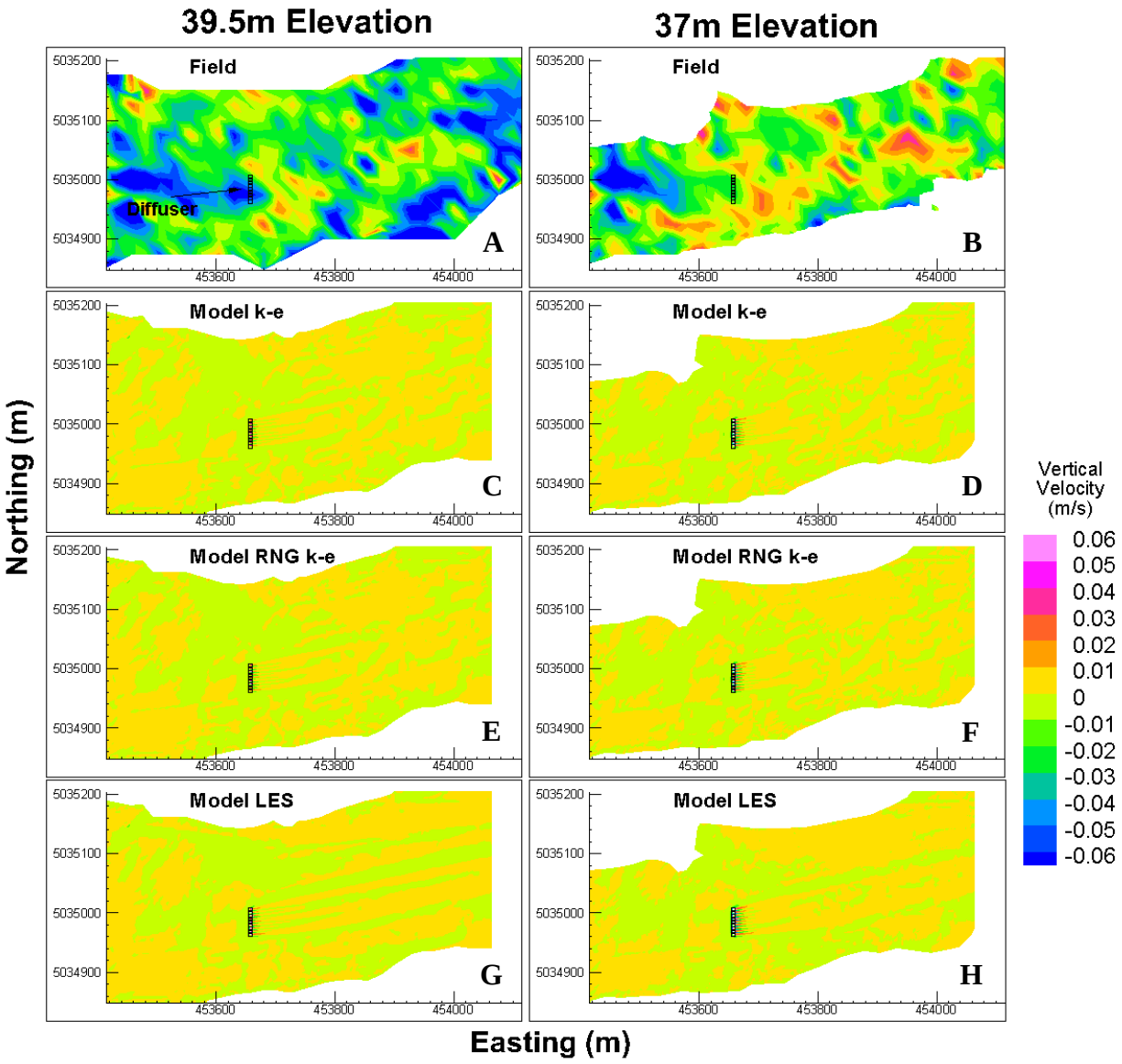

Figure 4.8: Vertical velocities in plan view for interpolated measured results and FLOW-3D *k-ε*, RNG *k-ε* and LES model data at two different elevations. The same colour scale is used for all maps. The map coordinates are in UTM-18. The diffuser is depicted by a black line on all maps.

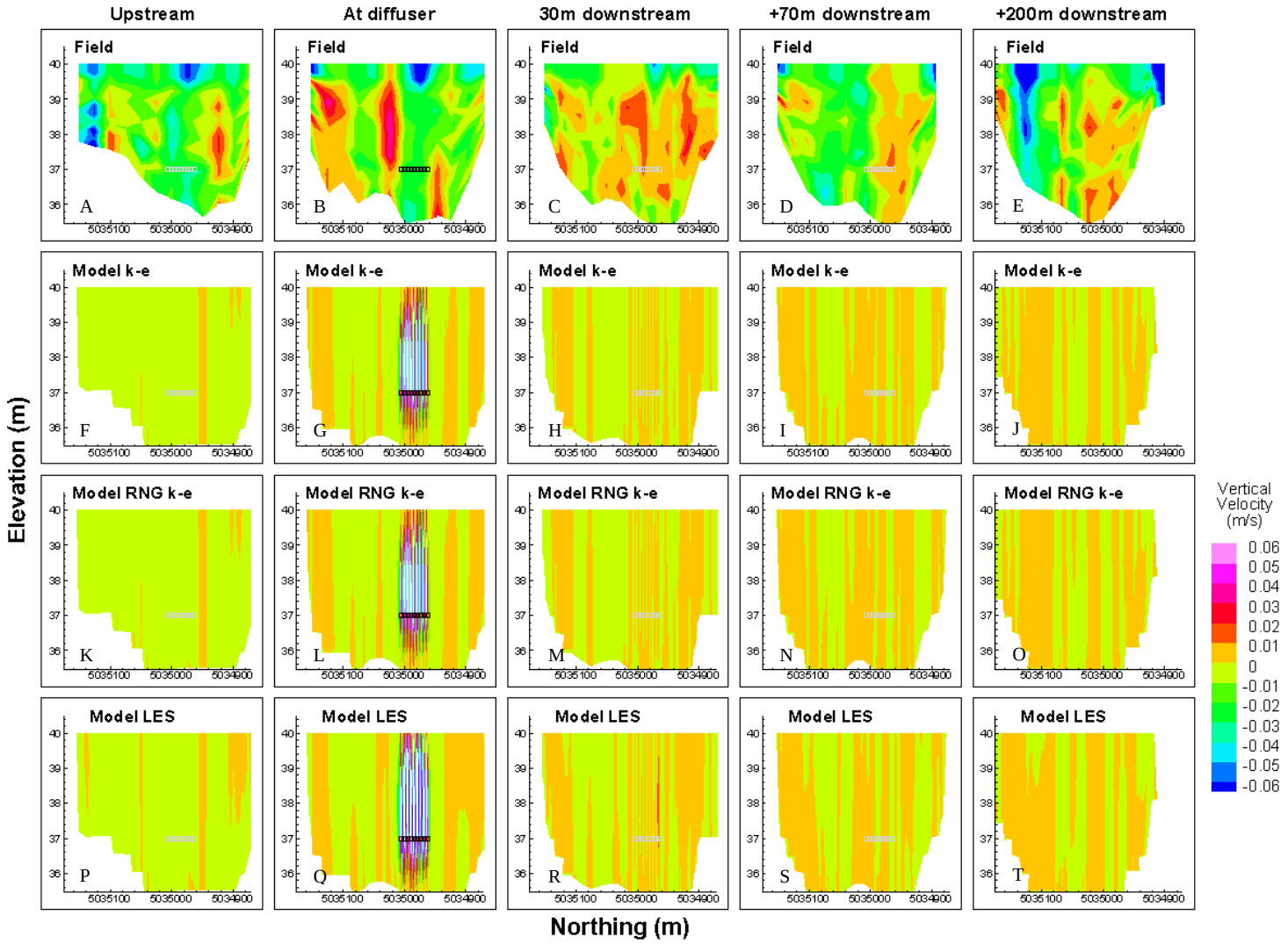

Figure 4.9: Vertical cross-sections of vertical velocities – upstream, at and downstream of the diffuser – are illustrated for interpolated measured results and FLOW-3D *k-ε*, RNG *k-ε* and LES models. The same colour scale is used for all maps. X-axes are in UTM-18 coordinates, where values are in descending order to present results from left to right bank (as if looking downstream into each vertical cross-section). Y-axes represent the elevation. Width-to-depth ratio (x:y axes) is 1:0.0175. The diffuser is depicted by black squares for cross-sections at the diffuser (2nd column) and by grey squares elsewhere.

4.4. Ammonia Measurement of the Ottawa River

Surface water concentrations of total ammonia were tested using a colorimetric test kit on Day 1 of the field campaign. The results of the test are presented in Section 4.4.1. On Day 2 of the field campaign, water samples were collected which were subsequently tested in the laboratory using standard methods of water analyses. Triplicates of seven water samples were measured in the laboratory to estimate analytical error. Relevant errors and the limit of detection are calculated and concentration of ammonia is presented along the extent of the river. These results are presented in section 4.4.2.

4.4.1. Ammonia colorimetric test kit results

Sixteen surface water samples were collected on Day 1 with an ammonia test kit measuring the total ammonia concentration of each sample. The results are shown in Figure 4.10. A sample collected immediately downstream of the diffuser exhibited the test limit for ammonia (8mg/L), while a sample collected upstream of the diffuser – near the surface impingement caused by a diffuser jet – exhibited zero detectable ammonia concentrations. This suggests upstream dispersion from the discharge does not occur. As will be shown later (Section 4.5.3) the ROPEC diffuser is in a jet-dominated (or jet momentum) region, as dictated by $F > 1$ (see equation (21) and Section 4.5.3 for more details). All of the samples (samples 3 to 6) taken in the first 50m downstream of the diffuser showed detectable levels of ammonia. By these results, the effluent width could not be estimated. Further downstream (samples 8 to 11) the results suggest that an effluent plume still persists and that it is bending with the river, where high concentrations are in the center and low concentrations are at or near the river bank. Measurements as far as 1km downstream illustrate that ammonia is still detectable in the middle of the channel. Here, the effluent is still detected at and near the thalweg, whereas any measurements outside the thalweg did not exhibit detectable ammonia.

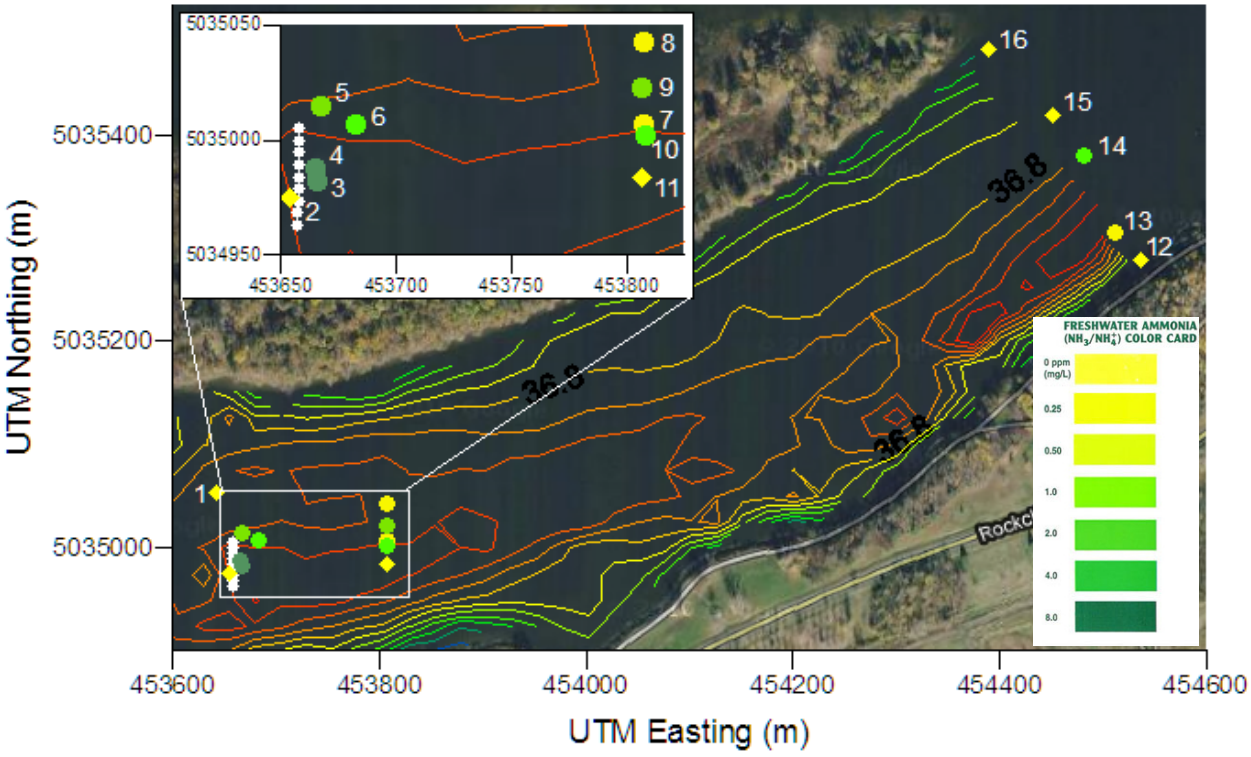

Figure 4.10: Surface water results of total ammonia concentration using a colorimetric test kit. Bathymetry of Figure 4.2A is used to provide perspective of the river topography. A close-up image of test results near the diffuser is provided in the top left corner of the figure. Water sampling sites are represented with a diamond (◆) for zero ammonia concentrations and with a dot (●) if ammonia concentrations were detected. Each sample site is numbered. Resulting colours correspond to the ammonia kit colour chart, which is included in the bottom right corner of the figure. A Google satellite image is used as the base. The maps are in UTM-18 coordinates. The diffuser is depicted by a white line.

4.4.2. N-constituent results

Ammonia, nitrite and nitrate concentrations were measured in the laboratory according to the methods described in Section 3.3.1. Laboratory measurement accuracy and precision were determined using blanks and standards. The results are presented as RMSE and mean error in Table 4.1. The precision and accuracy of the analytical methods are acceptable for the objectives of the research. The limit of detection (LOD) is also presented in Table 4.1.

Table 4.1: Precision, accuracy and the limits of detection. Accuracy and precision are both presented using RMSE and mean error calculations. The limit of detection (LOD) provides the minimum value at which the analyte is traceable for this thesis.

		Concentration		
		Ammonia	Nitrite	Nitrate
Accuracy (mg-N/L)	RMSE	.03	.001	.00
	Mean error	.02	.001	.00
Precision	RMSE	4%	7%	27%
	Mean error	3%	7%	14%
LOD (mg-N/L)		.09	.015	.17

The calibration curves of all three constituents showed r^2 values of 0.98 or higher.

Values of ammonia, nitrite and nitrate concentrations for all of the sampling sites and results of their statistical comparison with ambient concentrations are provided in Table 4.2. The table provides an overview of the effluent's path or direction, partial lateral extents and evidence of vertical mixing. The boat position varied between the sampling of water at different depths at the same location. To put this difference into perspective, Table 4.2 provides the maximum horizontal movement during sampling at depth at each location (under Spatial Variation).

Based on seven triplicate samples analytical error for ammonia was ±0.04mg-N/L (±0.0003 mg-N/L for nitrite and ±0.008 mg-N/L for nitrate). Mean ambient ammonia (measured approximately 100m upstream of the diffuser) was 0.38±0.06mg-N/L. Five sample sites showed statistically significant higher average values than ambient for ammonia and nitrite (Table 4.2). A further seven sample sites had a depth averaged concentration of ammonia 4 to 12 times greater than ambient; however, due to high variability in ammonia concentration between depths at these sites, non-of the observed differences were significant.

A graphical representation of ammonia, nitrite and nitrate concentrations at all depths – corresponding to transect and site locations shown in Figure 3.5 – are presented in Figure 4.11.

For all sampling locations ammonia and nitrite values displayed similar trends in concentration with changes in depth. Unless otherwise stated, the following description relates to both measured ammonia and nitrite concentrations. The sample with the highest measured ammonia (nitrite) concentration was found at T1S5 (directly above the center of the diffuser) with a value of 13.63mg-N/L (0.104mg-N/L). T2S7 and T2S8 (5m downstream from the diffuser) also exhibited high concentrations. These three sites also exhibited a large range of concentrations between depths (demonstrated by high standard deviation values in Table 4.2 and illustrated in Figure 4.11) with, highest concentrations observed near the water surface. Site T3S11 exhibited high values of ammonia (nitrite) over the water column with a mean of 5.02±1.20mg-N/L (0.041±0.011mg-N/L). Sites further downstream of the diffuser (T3S10, T4S13, T4S14, T5S16 and T5S17) continued to show elevated concentrations at all depths. The majority of these sites were downstream of the diffuser along the expectant path of the effluent, where concentrations are still expected to be measurable (see Figure 3.5). Site T5S18 was unique in that it exhibited an elevated concentration relative to ambient near the river bed, but near surface it exhibited low concentrations of ammonia (and nitrite). At the most downstream site (T6S19), approximately 200m from the diffuser, elevated concentrations relative to ambient were observed at all depths except near surface. Results indicate that ammonia (and nitrite) concentrations were highest near surface in the first 18m downstream of the diffuser (see transects T1, T2 and T3), but as the effluent progresses further downstream the concentrations mix vertically as demonstrated by reduced differences between depths within sample sites (transect T4) to the point of showing evidence of full vertical mixing at transect T5. Sample sites T1S1, T1S2, T2S6, T3S9, T4S12 and T5S15 demonstrated low concentrations and low standard deviations, and the average concentration of ammonia, nitrite and nitrate across all depths was not significantly different from ambient (Table 4.2). All of these sites were located north of the diffuser and results indicate they were outside the zone of influence of the effluent plume.

Measured results indicate that the effluent plume was advected by the river and as the effluent propagated further from the diffuser vertical mixing was taking place. Although sampling locations were insufficient to fully characterize the width and depth of the effluent plume the measured results do provide a basis for evaluating model outcomes. Specifically, to be representative of field conditions, model results are expected to show limited vertical mixing over the first 20 meters and full vertical mixing at a distance of 70 meters from the diffuser. In his analysis of river mixing, Rutherford (1994) proposes that full vertical mixing is expected at a distance of 50 times the depth of the river from the point of discharge, which would equal to approximately 200m downstream of the diffuser in this case. Rutherford (1994) also proposes that lateral mixing is expected at a distance of 100 to 300 times the width of the river, however, the lateral spread and mixing of the plume was not possible to delineate based on the measured results.

Finally, measured results indicate the model would need to predict elevated concentrations of ammonia relative to ambient at a distance of 200 meters from the diffuser.

Table 4.2: Ammonia, nitrite and nitrate results from field samples. The number of depth measurements at each site is provided. Minimum, maximum and mean concentrations and the corresponding standard deviation (SD) are presented. The largest spatial variation with respect to sampling position between depths is provided. Values that fall below the LOD are italicized. Values above the LOD are emboldened.

		Ammonia (mg-N/L)				Nitrite (mg-N/L)				Nitrate (mg-N/L)				
SITE	**# of depths**	**Min**	**Max**	**Mean**	**SD**	**Min**	**Max**	**Mean**	**SD**	**Min**	**Max**	**Mean**	**SD**	**Spatial Variation (m)**
Ambient	4	**.36**	**.40**	**.38**	**.02**	*.004*	*.005*	*.005*	*.001*	*.01*	*.05*	*.02*	*.02*	2.5
T1S1	3	**.31**	**.37**	**.35**	**.04**	*.004*	*.004*	*.004*	*.000*	*.01*	*.02*	*.01*	*.00*	1.4
T1S2	4	**.39**	**.44**	**.40**	**.02**	*.005*	*.005*	*.005*	*.000*	*.01*	*.02*	*.01*	*.01*	1.0
T1S3	4	**.37**	**.55**	**.45**	**.09**	*.003*	*.005*	*.004*	*.001*	*.02*	*.05*	*.03*	*.01*	9.7
T1S4	4	**.37**	**5.82**	**2.97**	**2.52**	*.004*	**.041**	*.021*	*.018*	*.00*	*.03*	*.02*	*.01*	3.1
T1S5	4	**.43**	**13.63**	**4.79**	**6.22**	*.004*	**.104**	*.037*	*.047*	*.00*	*.06*	*.02*	*.02*	5.4
T2S6	4	**.37**	**.42**	**.40**	**.02**	*.004*	*.005*	*.005*	*.000*	*.00*	*.02*	*.01*	*.01*	4.5
T2S7	4	**.63**	**7.92**	**3.24**	**3.22**	*.011*	**.054**	*.023*	*.021*	*.01*	*.04*	*.02*	*.01*	5.0
T2S8	4	**.68**	**7.29**	**3.12**	**3.08**	*.005*	.057	*.024*	*.024*	*.00*	*.04*	*.02*	*.01*	9.2
T3S9	4	**.38**	**.44**	**.41**	**.02**	*.004*	*.004*	*.004*	*.000*	*.01*	*.02*	*.01*	*.01*	3.8
T3S10	4	**1.41**	**4.60**	**3.20**	**1.45**	*.008*	**.033**	*.022*	*.011*	*.00*	*.02*	*.01*	*.01*	4.2
T3S11	4	**3.77**	**6.21**	**5.02***	**1.20**	**.030**	**.052**	**.041***	**.011**	*.03*	*.08*	*.05*	*.02*	3.9
T4S12	4	**.36**	**.39**	**.38**	**.01**	*.003*	*.005*	*.004*	*.001*	*.00*	*.02*	*.01*	*.01*	8.9
T4S13	4	**2.39**	**3.96**	**3.32***	**.76**	**.015**	**.030**	**.024***	**.007**	*.00*	*.06*	*.02*	*.02*	4.3
T4S14	4	**3.58**	**5.12**	**4.24***	**.74**	**.030**	**.045**	**.035***	**.007**	*.04*	*.08*	*.06*	*.01*	4.0
T5S15	3	**.39**	**.43**	**.41**	**.02**	*.004*	*.004*	*.004*	*.000*	*.04*	*.10*	*.06*	*.03*	7.2
T5S16	3	**3.94**	**4.65**	**4.24***	**.37**	**.041**	**.049**	**.045***	**.004**	*.04*	*.09*	*.06*	*.03*	3.6
T5S17	3	**3.48**	**3.92**	**3.69***	**.22**	**.034**	**.038**	**.036***	**.002**	*.05*	*.05*	*.05*	*.00*	2.8
T5S18	3	**.50**	**3.29**	**1.55**	**1.51**	*.005*	**.036**	*.016*	*.018*	*.03*	*.13*	*.07*	*.05*	4.9
T6S19	3	**.93**	**4.33**	**2.84**	**1.74**	*.007*	**.047**	*.029*	*.021*	*.01*	*.02*	*.02*	*.01*	4.3

* Indicates significant difference from mean ambient concentration based on the t-test at the P<0.05 level with Bonferroni correction for 19 tests (P<0.0026)

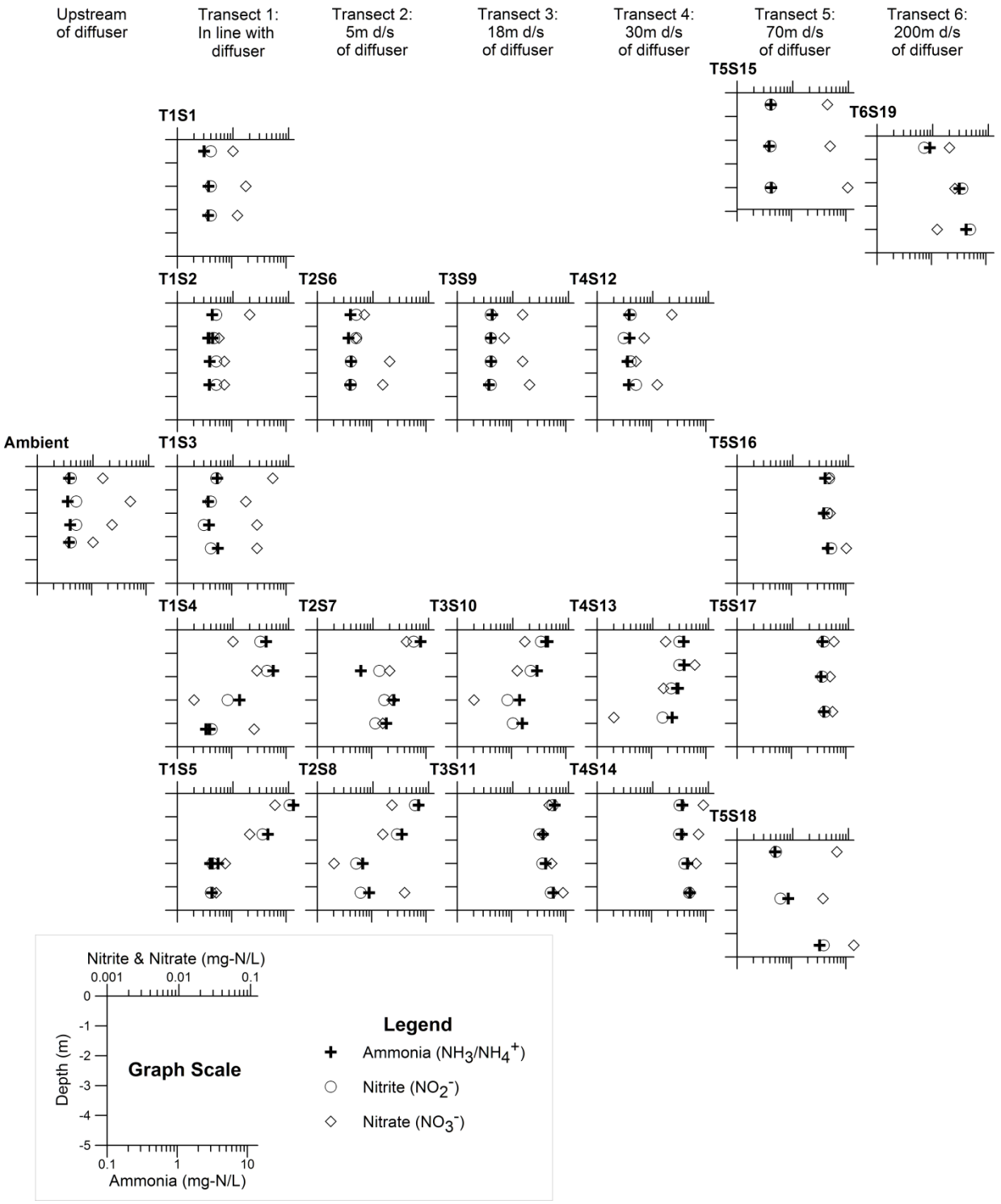

Figure 4.11: Ammonia and nitrite concentrations with respect to depth. The graphs are positioned to approximate the positions of sampling sites from the field campaign. The bottom x-axis represents ammonia concentrations; the top x-axis represents nitrite concentrations where available; and the y-axis represents the depth. The x-axes are in logarithmic scales. The graphs are arranged to closely resemble the spatial location of each sampling site.

Nitrification within the sampled reach

Ammonia in freshwater is converted to nitrite then to nitrate by nitrifying bacteria. Nitrate may be assimilated as a nitrogen nutrient by existing biota; however this pathway of consumption does not often demonstrate large quantities of nitrate removal. Nitrate may also be consumed through anoxic respiration of indigenous bacteria to the benthic zone of the river; with this pathway of removal being significant when low oxygen concentrations exist at the benthic zone (Wetzel, 1983). The most significant nitrification rates have been observed in lakes, estuaries, wastewater treatment plants and in slow moving waters (EC & HC, 2000). That is not to say though, that fast moving rivers do not show tendencies of nitrification.

In order to use ammonia as a conservative tracer for effluent plume mixing – for the purpose of comparing measured and modelled concentrations – it was necessary to determine if the rates of nitrification within the sampled reach were sufficient to affect ammonia concentrations. Specifically, if significant amounts of ammonia were being converted to nitrate over the reach then models would have to take into account nitrification and incorporate kinetics.

Nitrifying bacteria attach to particulate matter, such as sediment and other flowing debris (Brion, *et al*., 2000). In rivers and lakes, studies have shown that the amount of nitrifiers in the sediment and benthic zones can be orders of magnitude higher than in the water column, causing much greater nitrification rates in the former (Pauer & Auer, 2009). In rivers, transformation of nutrients largely depends on contact of biota in the river bed, between the sediment-water interface (Wetzel, 1983). With higher sediment and water exchanges, higher nitrification rates haves been exhibited (Admiraal & Botermans, 1989). Cooper (1983) showed that gravel-bed rivers exhibited higher nitrification rates than sand-bed rivers. Brion *et al*. (2000) showed that nitrification rates were slow even at low-flow (summer) conditions for large rivers receiving large volumes of effluent discharge. The Ottawa River is oligotrophic, with a large volume of water that is fast moving. It has a low suspended sediment load not providing much opportunity for nitrification. Within the

study reach, the river substrate is composed of 100% fine sand with no obvious vegetation, rocks or logs in the mid-channel (WEPP, 2007).

None of the water samples showed nitrate values above the calculated LOD (see Table 4.2). As well, nitrate concentrations did not demonstrate significant change from ambient at any sites (Table 4.2).

A kinetic rate of conversion typical of a river such as the study reach equals 0.25/day or 4 days (Pauer & Auer, 2009). The velocity of the river within the sampled reach (200m) equaled between 0.16 and 0.22m/s (Figure 4.3), whereby nitrification would have to take place within 15 to 20s in order to be measured at the 200m downstream reach.

Thus, the results indicate that nitrification reaction kinetics did not take place in the sampled reach of the river. Ammonia was therefore treated as a conservative constituent.

4.4.3. Ammonia toxicity

The Canadian Wastewater Systems Effluent Regulation (WSER) (Fisheries Act, 1985) limits end of pipe unionized ammonia discharges. The regulation also stipulates that if unionized ammonia discharges are higher than the allowed limit (1.25mg-N/L at a temperature of 15°C), unionized ammonia cannot exceed a value of 0.016mg-N/L beyond a 100m radius of the pipe. The highest ammonia concentration discharging from ROPEC during the week of the field campaign was measured at 29mg-N/L (Appendix, Figure A.3), as discussed in the Appendix. At a temperature of 21°C and a pH of 7.84, the resulting unionized ammonia speciation is 0.83mg-N/L, and is below the regulated concentration. Since the end-of-pipe ammonia regulations for ROPEC were adhered to, it is of interest to examine ammonia concentrations beyond the discharge site, especially that beyond the 100m radius of the diffuser.

Unionized ammonia concentrations were calculated based on Emerson, et al. (1975) as described in Section 3.3.3. Figure 4.12 displays the unionized ammonia profiles similar to ammonia, nitrite and nitrate profiles shown in Figure 4.11. Vertical red lines indicate a value of 0.016mg-N/L. Out of a total of 78 water quality samples taken the unionized

ammonia exceeded the red line value 43 times. However, of all the sample sites tested, only T6S19 was located outside of the 100m radius from the diffuser. This site surpassed the 0.016mg-N/L limit across the entire water column, exceeding the chronic toxicity limit for ammonia. Measured unionized ammonia concentrations at sites T5S16 and T5S17 also suggest that the 0.016mg-N/L limit may be exceeded further downstream just outside the 100m radius.

Differences in unionized ammonia contours between near surface and near bed-bottom are shown in Figure 4.13. Unionized ammonia concentrations were elevated out to the edge of the 200m sampled reach. The black dashed circle represents a 100m radius from the center of the diffuser, illustrating the approximate boundary of the WSER provisional limit.

The WSER clearly does not take mixing abilities of the ambient environment into account as we have just shown that even though the end-of-pipe regulation has been met by ROPEC, the unionized ammonia well beyond a 100m radius downstream of the diffuser surpassed the chronic toxicity limit of 0.016mg-N/L, as shown, by Figure 4.12 and Figure 4.13.

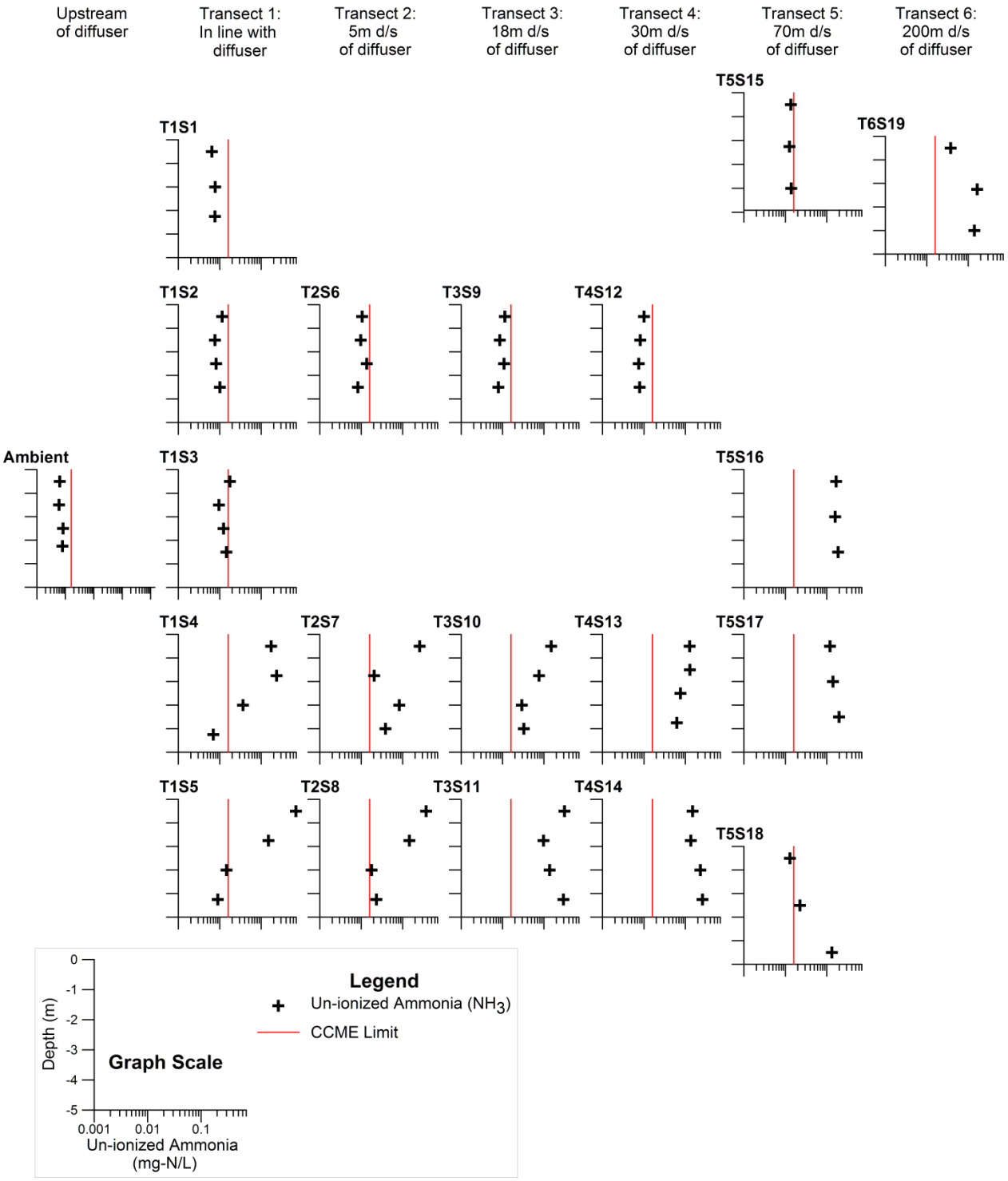

Figure 4.12: Unionized ammonia concentrations based on equations by Emerson *et al.* (1975). Like Figure 4.11 the graphs are positioned to approximate the sampling sites in plan view. A red vertical line is drawn on each graph at 0.016mg-N/L to indicate the CCME guideline limit.

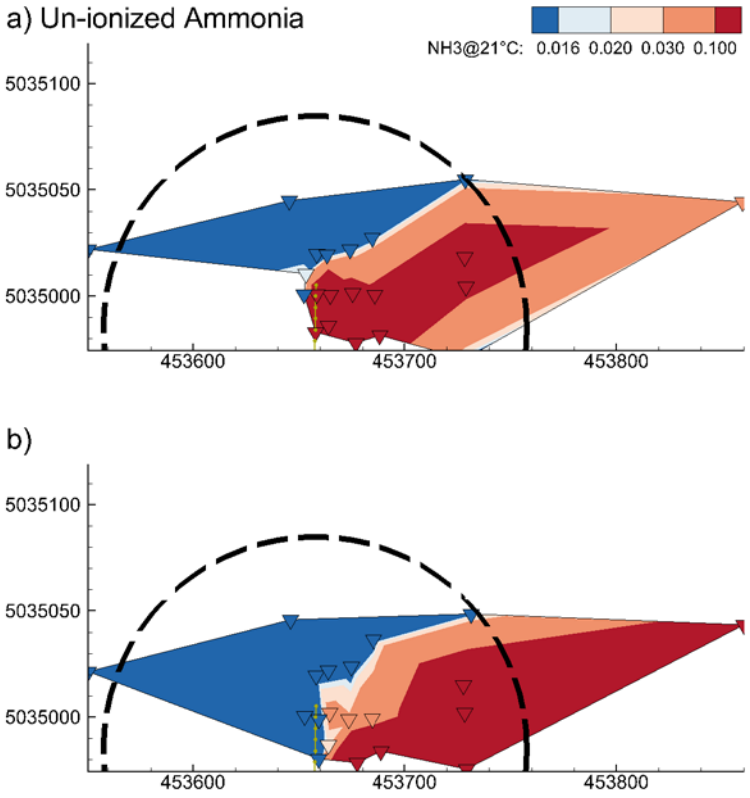

Figure 4.13: Interpolation results for unionized ammonia at a) 0.5m from the surface and b) 0.5 from the bed bottom. The diffuser is represented by gold hatch-marks. A 100m radius indicating the limiting zone beyond which NH_3 limit cannot exceed 0.016mg-N/L was drawn with a dashed arc. For spatial reference, see Figure 3.7. The colour scale shows contours of regions that: meet, slightly exceed, are more than double than, and excessively surpass the WSER. Note, however, that the colour gradation (orange) between low and high concentrations at the edges of the effluent may not be real, as the interpolation cannot show abrupt changes between zero and high concentrations.

4.4.4. Estimates of ROPEC's discharge and concentration

ROPEC collects end-of-pipe discharge data every minute, while ammonia concentration data are calculated once every two days. Since steady-state modelling was conducted in this thesis, average flows and concentrations were required. Thus, ROPEC's time series data were analyzed and a full description is available in the Appendix. Note that ROPEC did not collect ammonia composite data on the day of this study's water sampling day (as shown in Figure A.2).

An average discharge rate of 4.022m^3/s (0.447m^3/s per port) and an average ammonia concentration of 26.57mg-N/L were used for simulations.

4.5. Ammonia Results from Simulations

Water quality samples were collected from the river at various locations beside and downstream of the diffuser at various depths (as explained in Section 3.2). The results (discussed in Section 4.4) were compared to the results of FLOW-3D simulations. Due to a small number of samples collected, the comparison of measured and modelled ammonia data are presented in this section using:

- a visual comparison, where measured data are superimposed as point data on contours of the *k-ε* model; and
- a graphical comparison via scatter plots of measured data versus modelled results for the FLOW-3D *k-ε*, RNG *k-ε* and LES and CORMIX2 models.

The RNG *k-ε* and LES models were not compared as their visual results were very similar to the *k-ε* model. FLOW-3D simulations were modelled using two different meshes: a coarse mesh model (from here on referred to as CM model) with a mesh resolution of x:y:z = 1:1:0.5m, and a fine mesh model (from here on referred to as FM model) with a mesh resolution of x:y:z = 0.5:0.5:0.5m.

Finally, empirical models calculating near-field length, dilution and plume width were compared to available measured and modelled data.

4.5.1. Visual comparison

Visual comparisons of modelled and measured ammonia concentrations are provided in plan view (Figure 4.14) and vertical cross-sections (Figure 4.15 and Figure 4.16). The former are used to demonstrate ammonia movement along the river channel, while the latter are used to demonstrate ammonia movement over the river depth (similar to velocity results in Section 4.3.2). In plan view, the results are presented near the water surface (39.5m elevation) and at an approximate mid-depth (37m elevation). The measured data (points) shown in Figure 4.14 represent approximately 30% of the total (27/79 points in the CM and 25/79 in the FM models). Vertical cross-sections are shown at 0m (the diffuser), 5m, 18m, 30m, 70m and 200m downstream of the diffuser (Figure 4.15 and Figure 4.16)corresponding to transects of the field campaign (see Figure 4.11). Measured data shown in Figure 4.15 and Figure 4.16 represent approximately 65% of the total collected (54/79 points in the CM and 51/79 points in the FM models). For a complete description of the graph setup please refer to Section 3.6.2.

Overall, the measured and modelled data corresponded well spatially, with some exceptions as discussed further.

Both measured and modelled data indicated that ammonia concentrations decreased quickly within the first 18m of the diffuser. This indicated that the majority of the mixing occurred between the discharging jet and ambient flow near the onset of the diffuser discharge. Further downstream, the dilution was quite low with evidence of ammonia as far downstream as 200m. Over the whole reach, both models indicated greatest ammonia concentrations near the water surface, though beyond the 70m transect vertical and lateral mixing was evident. Similarly, measured data indicated highest ammonia concentrations near the water surface until the 70m transect, where two sites indicated full or nearly-full vertical and lateral mixing. Compared to model results, measured data indicated better mixing both vertically and laterally, at these downstream locations. Note that other than at the diffuser discharge, the near surface ammonia concentrations were overestimated by the models compared to measured data. Near-bed ammonia concentrations were continuously underestimated by both models upstream of the 30m transects. Downstream

of the 30m transect, the CM model continued to underestimate the near-bed ammonia concentrations, whereas the FM model illustrated similar concentrations to that measured in the field.

At the diffuser, the model did not simulate the very high (red) concentrations measured in the field (Figure 4.14A and B, and Figure 4.15A and B) near the water surface. However, in this region, results of the ammonia colorimetric testing kit reached the upper end of the testing limiting (see Section 4.4.1) at the water surface. Also, at this vertical cross-section, both model meshes were too coarse to properly capture individual ports and their discharges, but were fine enough to illustrate that jet merging between separate discharges did not occur at the onset. The size of modelled ammonia contours varied in this region, depending on port location, because the given cross-section was not set perpendicular to the diffuser. By the 5m cross-section (Figure 4.15C and D), the models indicated evidence of jet merging. At the 18m cross-section (Figure 4.15F) the FM model indicated jet separation, which is most likely due to numerical diffusion in the model and not an actual occurrence in the field. This was reflected further downstream as well, where one would expect that the individual port discharges be merged.

Model results demonstrated that the discharging effluent was very narrow, following the river's path and slight meander to the North-East. To the left of the diffuser, the modelled and measured data were in agreement to the location of the effluent extent. However, the field campaign failed to capture the ambient region to the right of the diffuser resulting in difficulties in determining the full width of the effluent (see Section 4.4.2).

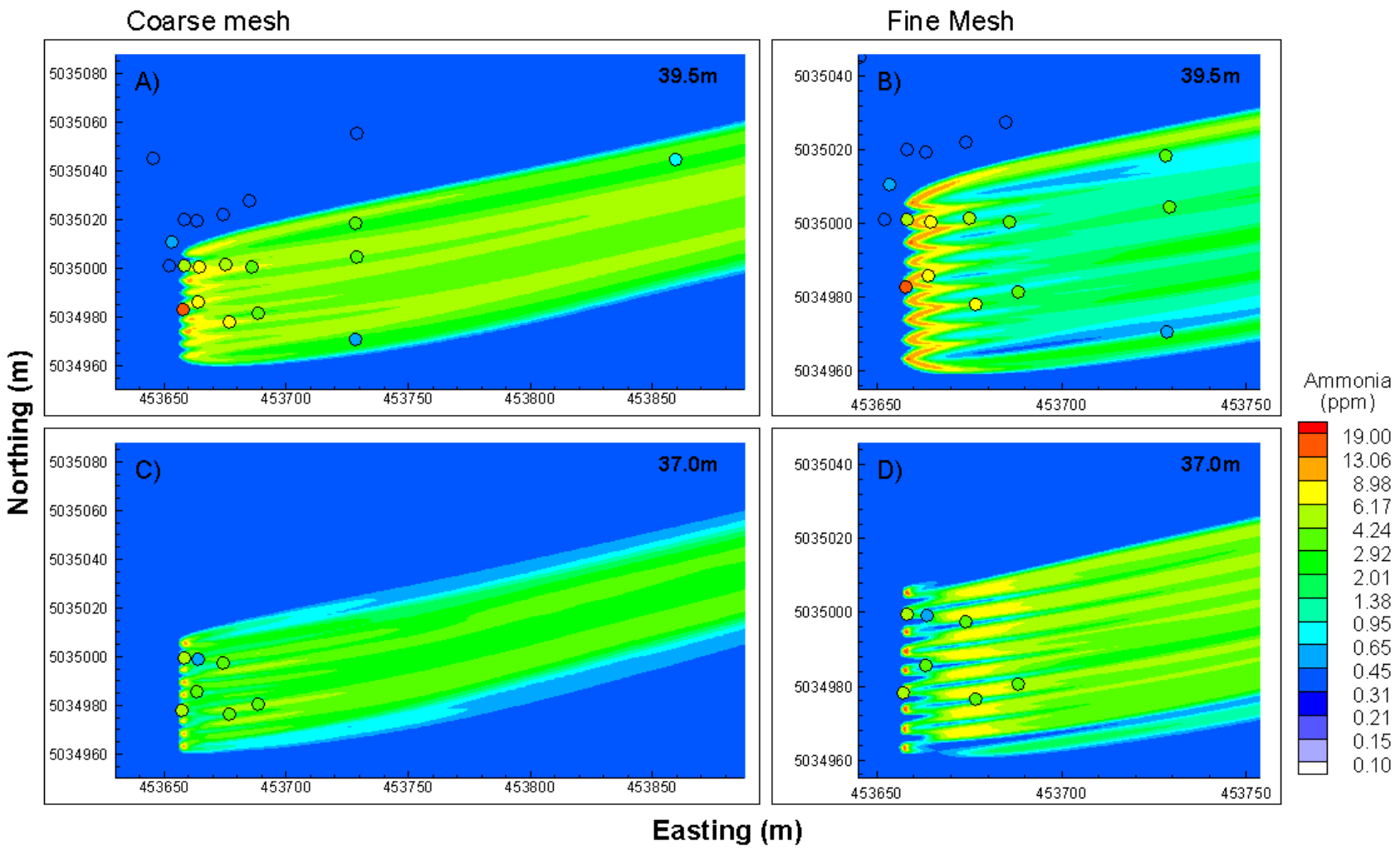

Figure 4.14: Horizontal plane of ammonia at two different elevations. Points represent measured data and contours represent FLOW3D *k-ε* model data. Images are provided for CM (A and C) and FM (B and D) models. The colour scale was chosen to show the ammonia gradient in the plume. The diffuser location is obvious from the high ammonia concentrations (red/orange) on each image.

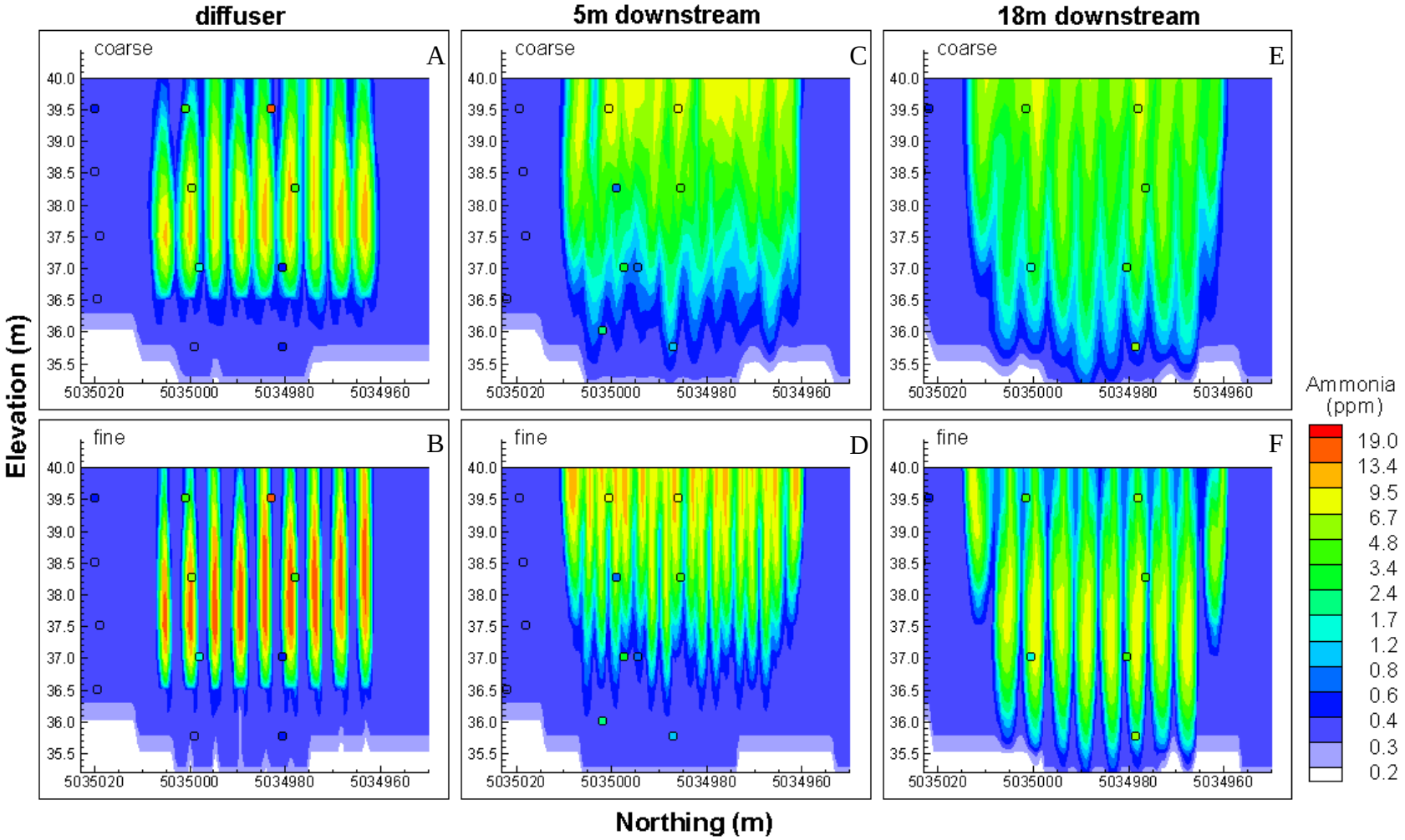

Figure 4.15: Vertical cross-sections of ammonia at and near the diffuser. Points represent measured data and contours represent FLOW3D *k-ε* model data. Images are provided for CM (graphs on top) and FM (bottom graphs) models. The colour scale was chosen arbitrarily to provide a meaningful picture of the ammonia gradient in the plume. The colour scales between Figures 4.14 and 4.15 are equivalent. The diffuser location is not provided as its positioning is identified by the highest concentration contours of all four images.

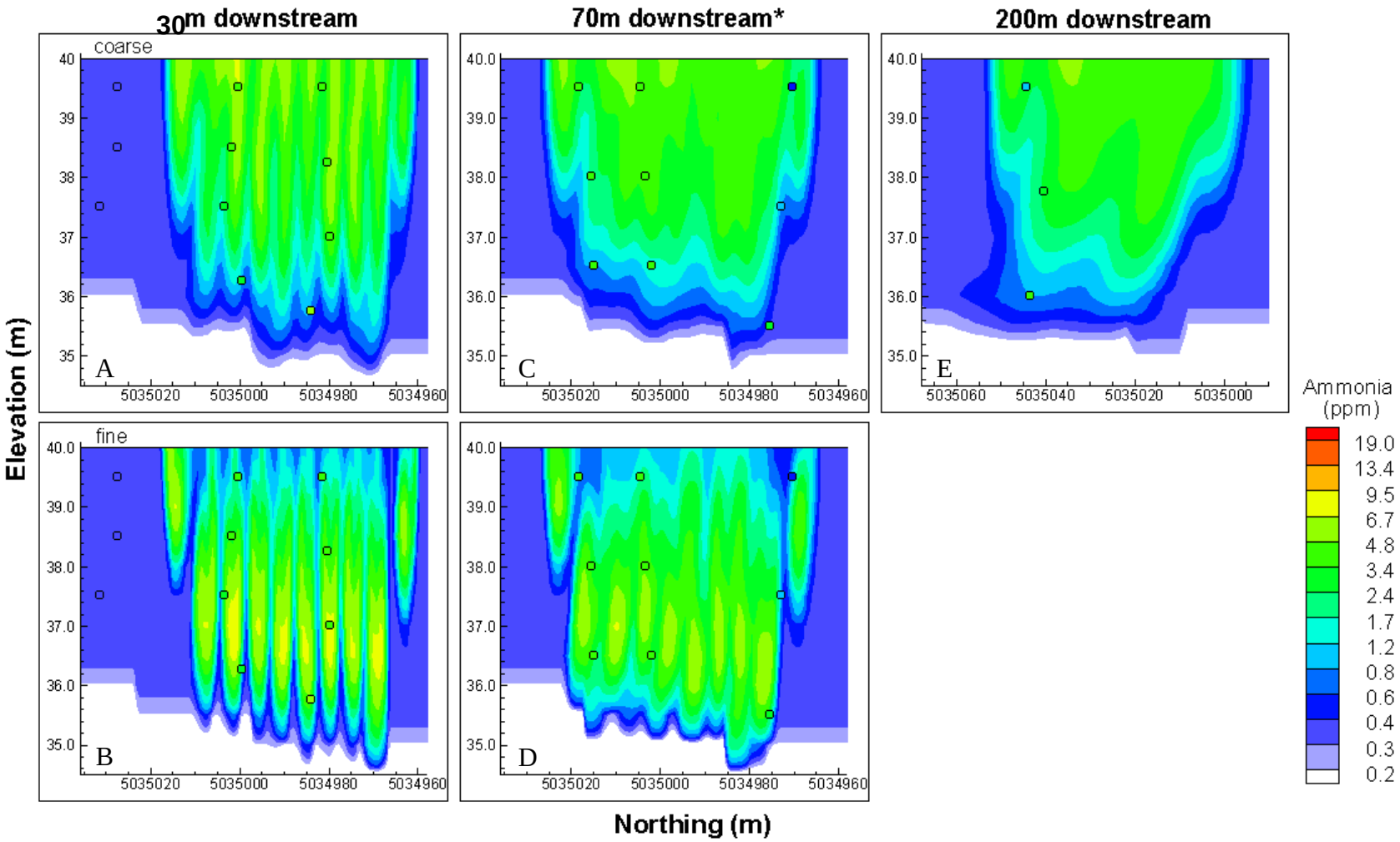

Figure 4.16: Vertical cross-sections of ammonia downstream of the diffuser. Points represent measured data and contours represent FLOW3D *k-ε* model data. Images are provided for CM (graphs on top) and FM (bottom graphs) models. The colour scale was chosen arbitrarily to provide a meaningful picture of the ammonia gradient in the plume. The colour scales between Figures 4.14 and 4.15 are equivalent. The diffuser location is not provided as its positioning is identified by the highest concentration contours of all four images. (*70m contour is a diagonal cross-section, not perpendicular to the river banks as the other cross-sections, in order to capture all of the collected measured data in one plot. See Figure 3.9 for an illustration.)

4.5.2. Graphical comparison

Measured and modelled data were plotted on a scatter plot for comparison, with a 1:1 relationship indicated (Figure 4.17). Two graphs are provided, Figure 4.17A showing all data collected and Figure 4.17B showing only data collected 30m and further downstream of the diffuser. All results depict a positive correlation between measured and modelled ammonia concentrations, as exhibited by the line of best fit (same colour as the data points) for each model. However, correlations are all very weak. The LES model (red) exhibits the strongest correlation for all data.

Regression coefficients (r^2) for all four models are provided in Table 4.3. The r^2 of the LES model is highest for all data and downstream data only, slightly improving in the latter. However, the r^2 values of the *k-ε* models slightly degrade when only downstream data are taken into account.

Regression coefficients for modelling sensitivities tested with the *k-ε*, RNG *k-ε* and CORMIX2 models are also provided in Table 4.3. The sensitivities tested were for differences in effluent discharge rate, effluent ammonia concentrations and bed-roughness (as described in Section 3.4.3). A high effluent discharge and concentration provided best results overall. The r^2 was highest for downstream data with values of 0.6177 and 0.6170 for the *k-ε* and RNG *k-ε* models, respectively. Low effluent discharges resulted in very low r^2, whereas surface roughness sensitivity results for all data were lower than the original model, but showed slightly improved results considering only downstream data.

A scatter plot identifies how well a simulation resembles an actual occurrence. However, it is of limited use if uncertainties lie in the sample data. For example, even though spatial locations for water sampling were pre-determined and were closely monitored, it was impossible to ensure for absolute accuracy of recorded locations. Boat drift due to river current may have caused spatial errors. The use of a manual instrument such as the van Dorn sampler may have caused both spatial and depth errors.

A scatter plot is also of limited use here because the model has to capture all of the minute variations in the field in order to provide good results. For instance, if the model's mesh is

not fine enough, the slight variabilities of concentration changes in the field may not be captured.

The models in this thesis were setup as steady state models, with a constant flow and a constant ammonia concentration discharging from the plant. As shown in the Appendix, neither of those conditions corresponds to the actual discharge dynamics; thus another reason for poor scatter plot results.

Using sensitivity analysis for discharge rate and ammonia concentrations, higher flows and higher concentrations in the base models may have been more appropriate for steady state modelling. At the time of the field campaign, ROPEC's effluent discharge was highly oscillatory (see Appendix, Figure A.1), impacting the mixing between the ambient river flow and the discharge, therefore impacting final ammonia concentrations in the river. Steady-state modelling would not have been able to capture those temporal differences.

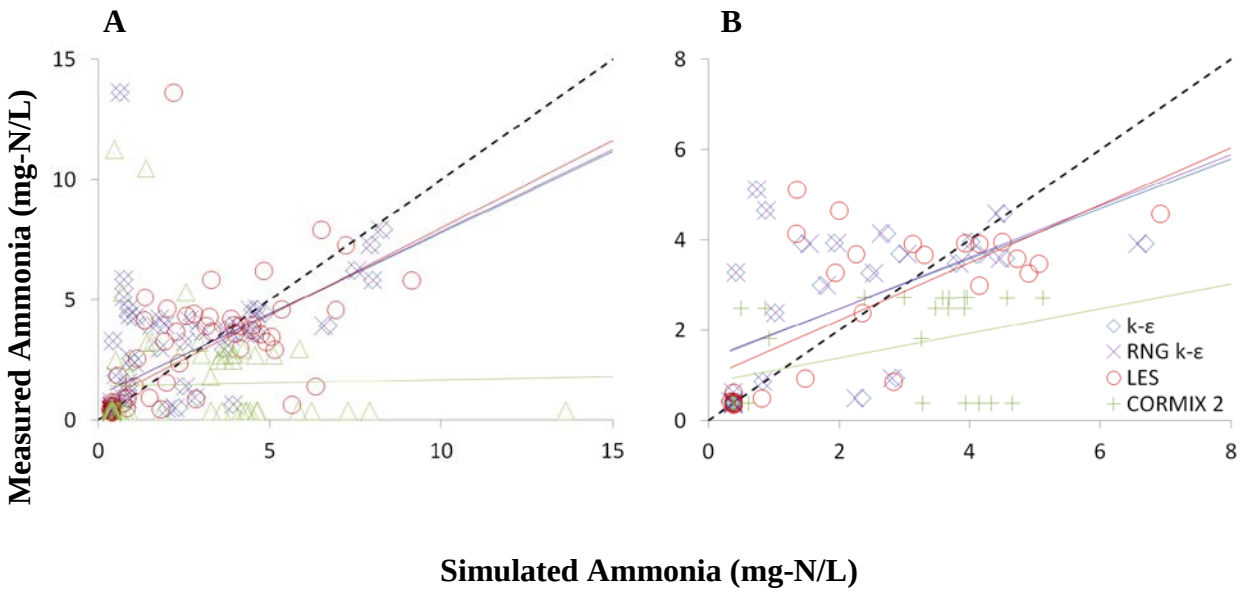

Figure 4.17: Scatter plots of measured ammonia vs modelled (simulated) ammonia concentrations. Graph A contains all data and graph B contains downstream data only (27m+).

Table 4.3: Regression coefficients (r^2) between measured ammonia samples vs. modelled ammonia results from all of the simulations performed under FLOW-3D: *k-ε*, RNG *k-ε* and LES and CORMIX2 including sensitivity analyses.

		r^2					
	Model		**High Q[1] High C[2]**	**Low Q[3] High C**	**Low Q Low C[4]**	**n = 0.025**	**n = 0.035**
All-Data	*k-ε*	0.3490	0.4704	0.2595	0.2597	0.3338	0.3291
	RNG *k-ε*	0.3514	0.4703	0.2624	0.2626	0.3383	0.3337
	LES	0.4227	-	-	-	-	-
	CMX2	0.0012	-	-	-	0.0142	0.0060
Down-stream Data	*k-ε*	0.3128	0.6177	0.2260	0.2266	0.3337	0.3235
	RNG *k-ε*	0.3254	0.6170	0.2318	0.2327	0.3520	0.3418
	LES	0.4876	-	-	-	-	-
	CMX2	0.1807	-	-	-	0.1736	0.3370

[1] **High Q** discharge was a 0.456m^3/s

[2] **High C** concentration was 29mg-N/L

[3] **Low Q** discharge was 0.427m^3/s

[4] **Low C** concentration was 21mg-N/L

4.5.3. Comparison to empirical approximations

The following section uses existing theories to calculate and study the plume characteristics of the ROPEC effluent. Near-field length, dilution and plume width are estimated using empirical equations, modelled results and observed data. The empirical equations for near-field length and dilution are based on results from a study by Tian, *et al.* (2004b), while the plume width is based on discussions from Chanson (2004) and Rutherford (1996).

Near-field characteristics

The ROPEC diffuser is perpendicular to the Ottawa River's streamwise flow with 9 ports discharging vertically into a cross-flow. The flow at the diffuser is dominated by the ambient current, where Froude number F (equation 21) is 38.3. Here, the density of the effluent was assumed to be equivalent to that of freshwater, dependent on the temperature

at the time of the field campaign (21°C for the river/ambient flow and 22°C for the effluent).

ROPEC's diffuser spacing to water depth ratio (s/H) is equal to 1.17. Thus, as discussed in Section 2.3.4, the diffuser belongs in the transition zone between a line and a point plume discharge (for $0.5 < s/H \leq 4.5$).

Tian, *et al*. (2004b) developed equations to approximate the near-field length (x_n – equation 23) and the dilution (S_n – equation 24). These parameters identified the end of the near-field, where mixing due to effluent discharge was no longer significant. Using equation (23), the empirical approximation for the ROPEC diffuser near-field length, x_n, equaled between 71m and 87m. Due to lack of field campaign data, the near-field length was not possible to approximate by means of measured data. For dilution, the empirical approximation for the ROPEC dilution (S_n – equation 24) equaled between 3.8 and 5.7, while the approximation by Chu (1979) (equation 25, where $C_2 = 0.41$), dilution was 6.6. Using measured and modelled data (of the *k-ε* model) dilution was calculated to be 9.4 and 15.5, respectively, by equation (26). Please see Section 3.6.2 for a full explanation.

Both measured and *k-ε* model results were higher for dilution than that of the approximations by Tian *et al.* (2004b) and Chu (1979). As well, the *k-ε* model results were higher than the measured data. Several factors that may have contributed to the differences are listed below.

- The equations used to approximate S_n and x_n relied on average velocities and average depth at the diffuser location. However, for both measured and modelled data the velocities and bathymetry change quite significantly through the course of the approximated near-field length.
- The empirical models only take into account river flow and discharge dynamics, while equation (26) takes into account only concentration values (initial, final and ambient)
- The initial effluent concentration, C_0, used to calculate the measured and modelled S_n is based on an average concentration over several days, which may not have been

the actual concentration discharged from ROPEC during the time of the field campaign. The temporal change in concentration is illustrated by Figure A.4 A.4 in the Appendix, where within a period of 24 hours, the concentration had changed by over 10mg-N/L.

- The plume concentration, C_x, calculated for the k-ε model is based on a steady-state model, not allowing for temporal differences in effluent discharges.
- The k-ε model consistently under-predicted the concentration results near bed bottom, as noted at all cross-sections measured, (see Figure 4.15); thus decreasing the mean concentration, used for C_x to approximate S_n.
- The ratio of port diameter to H is significantly smaller than any of those reported in experiments of Tian, *et al.* (2004b), or for any publications studied by the author up to date, a fact which may be of interest for further study.
- None of the equations compared accounted for the density differences between the ambient and effluent flows.

Finally, CORMIX2 predicted the near-field length at approximately 22m downstream of the diffuser, with a S_n of 9.5, while the S_n at 70m was 10.5. The model predicted the near-field length where it simulated that the effluent impacted the surface. At this point, the model also simulated that the vertical column is completely mixed. However, from observations in the field, the jets impacted the surface within centimeters of the diffuser ports.

Plume width

As discussed in Section 4.4.2, plume width was difficult to estimate from measured results. However, the plume width may be approximated using available empirical equations and the model results. Empirical equation (28) for point-source plume width was used. Figure 4.18 shows the estimated plume widths at given distances (5m, 10m, 18m, 30m, 70m and 200m downstream of the diffuser) using the empirical approximation, the k-ε and CORMIX2 models.

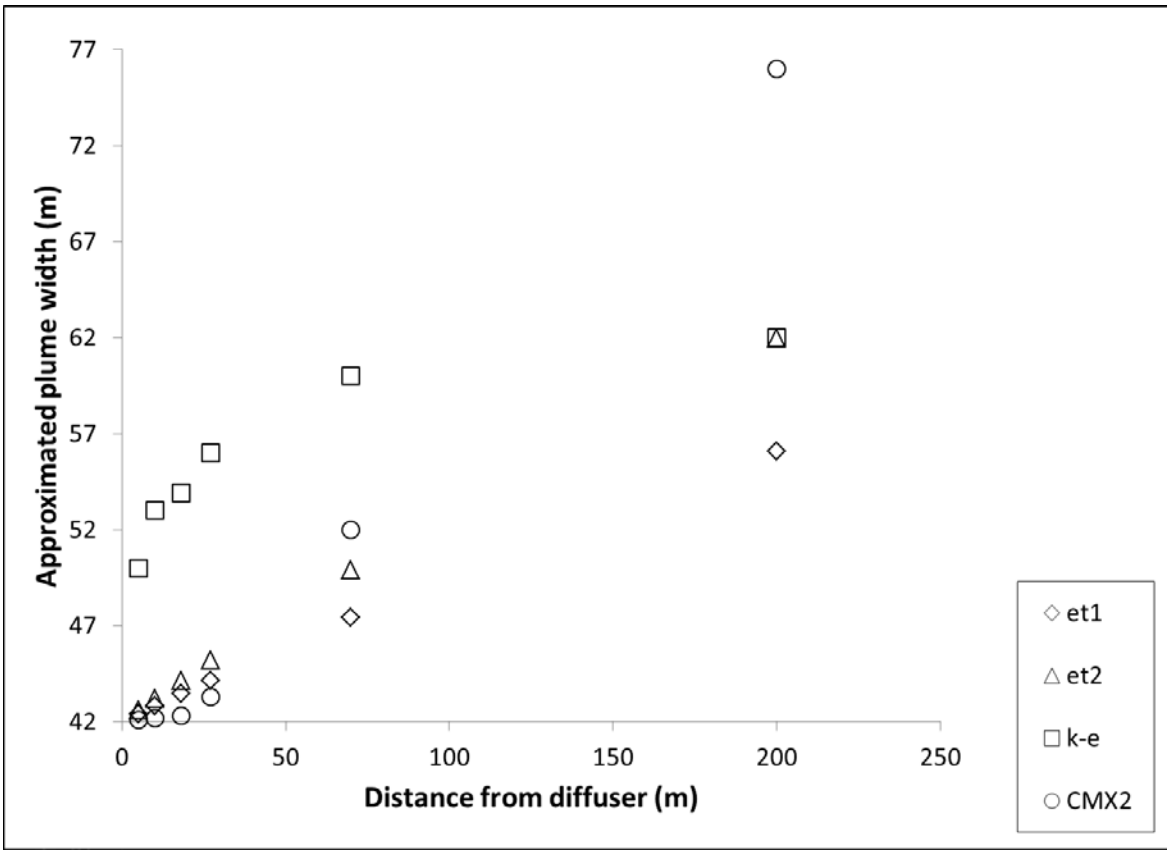

Figure 4.18: Estimated plume width at 5m, 10m, 18m, 30m, 70m and 200m downstream of the diffuser. Shown are width results from equation (28) (using the transverse mixing coefficient ε_t, where ε_{t1} uses an empirical constant of 0.6 and ε_{t2} uses an empirical constant of 0.9), FLOW-3D's *k-ε* and CORMIX2 models.

Figure 4.18 shows that the *k-ε* model consistently over-predicts the plume width for all of the other given approximations until a downstream distance of 200m is reached. Here, the *k-ε* model plume width is equivalent to the empirical equation with C=0.9.

Though model information isn't available further downstream of 200m, it is evident that the plume width beyond this point does not increase at any significant scale (Figure 4.14). The assumption can be made that lateral mixing is quite slow, which was also shown by Pilechi, *et al.* (2014) for a river similar to the conditions found for this thesis. Tian, *et al.* (2004b) suggested that as the ambient current increased, additional mixing decreased due to surface impact. As the high Froude number (F = 38.3) between the Ottawa River and the ROPEC discharge indicates, the dynamics may have prevented significant lateral mixing from occurring; thus, causing a narrow plume width beyond 100m of diffuser discharge.

Several factors that may contribute to the differences in plume width between empirical approximations (equation 28 and CORMIX2) and the *k*-*ε* model are listed below.

- The equations used to approximate ε_t and CORMIX2 results are depth averaged. However, bathymetry maps in Section 4.2 show significant variations through the course of the approximated distances.
- Equation 28:
    - does not consider density variation, whereas CORMIX2 and the *k*-*ε* model do; and,
    - was developed for a point source discharge, where some approximation was involved to employ for a line source discharge in a manner described in Section 3.6.2.
- Both empirical equations rely on an average velocity along the area of interest, which varies in the k-ε model as seen in Section 4.3.

4.5.4. Unionized ammonia prediction by FLOW-3D

Prediction of unionized ammonia by FLOW-3D's *k*-*ε* turbulence closure model is provided in Figure 4.19. The model predicted high unionized ammonia levels more than 250m downstream of the diffuser at both near surface and mid-depth elevations, just as the measured data had shown (Section 4.4.3). Higher concentrations are detected near water surface, but as discussed earlier, the model tended to over predict the concentration of ammonia compared to measured data. Here, the model simulated unionized ammonia levels above 0.100mg-N/L. Thus, the model had shown that the unionized ammonia concentration surpassed the Canadian WSER well beyond the 100m radius downstream of the diffuser discharge.

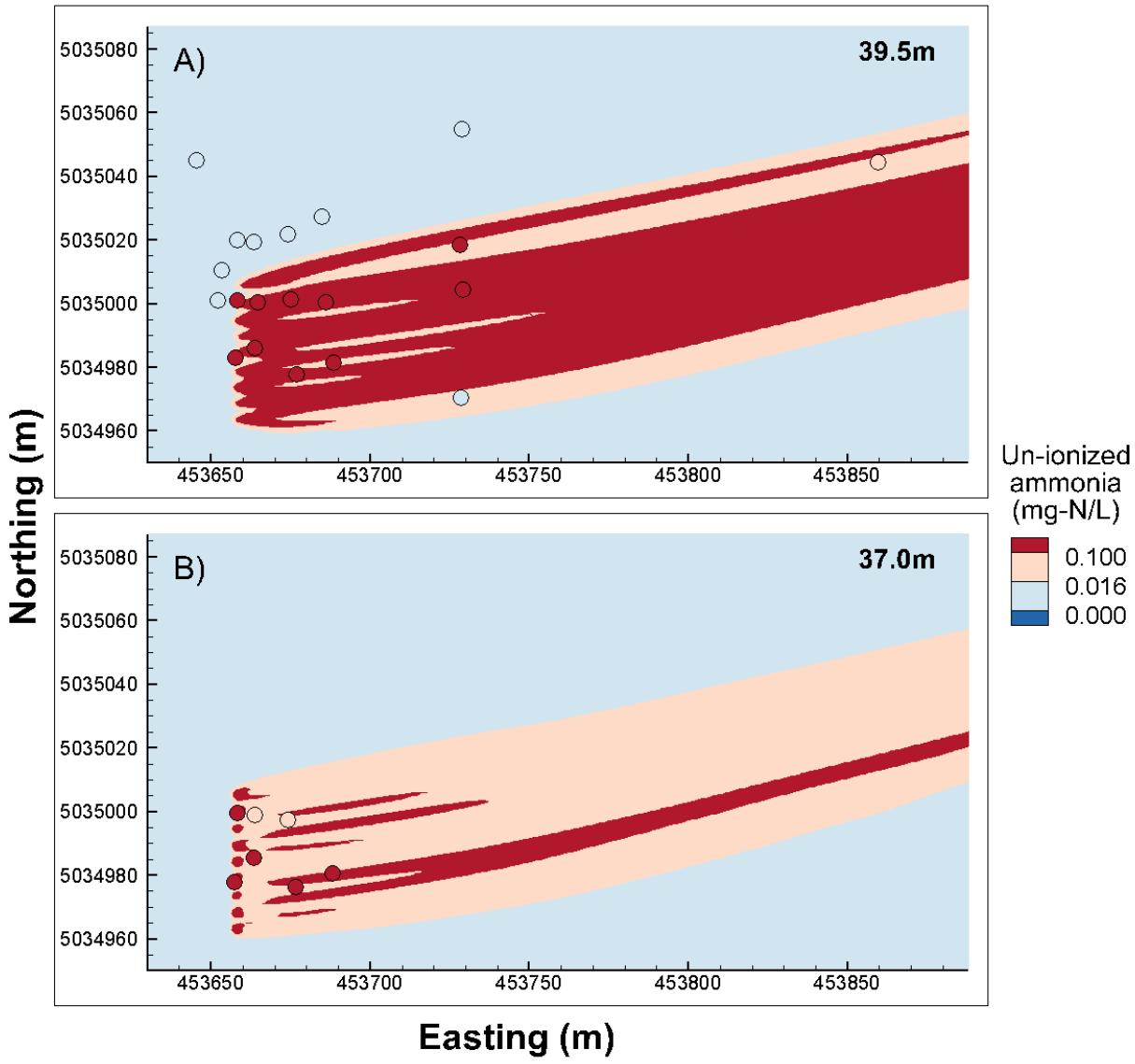

Figure 4.19: Predicted unionized ammonia results by FLOW-3D using the *k-ε* turbulence closure.

4.6. Limitation of the Study

The study completed for this thesis has been validated for the chosen site and the conditions (for ambient and effluent discharges and ammonia concentrations) observed during the time of the study's field campaign. It cannot be expanded to other sites or different conditions. This is mainly due to the fact that steady state modelling was used, where averaged steady-state values were utilized for effluent and ambient discharge flows and concentrations. However, the methods described may be evaluated, considered and further expanded upon instead.

5. Conclusions

5.1. Summary

This study simulated mixing of a WWTP effluent with the discharge environment using an off-the-shelf commercial CFD model. Ammonia already present in the effluent and discharged into the Ottawa River was used as a tracer agent to study the movement and dilution of the effluent. A field campaign was performed to measure the flow field (using an ADP) and ammonia concentration (by collecting water samples from the river) in the study area. The study reach was 1.2km long, where bathymetry and velocity data were collected, as well as basic water surface quality measurements using an ammonia test kit; while water samples were collected over the water column at pre-determined spatial locations within a 200m extent downstream of the diffuser. The collected samples were measured in a laboratory for ammonia. The samples were also measured for nitrite and nitrate to determine whether any kinetics occurred during the sampling period. The results obtained in the field were used towards model setup, field analyses of the effluent's behaviour in the receiving environment and as validation data to the models. The FLOW-3D modelling software was used with the k-ε, RNG k-ε and LES turbulence models to simulate the mixing conditions on the Ottawa River by the ROPEC discharge. CORMIX2 was used to approximate the sampling reach extent and later as a comparison to the turbulence closure models. Empirical equations approximating near-field length, dilution and plume width were also used to better understand the mixing within the sampled reach.

5.2. Conclusions

1. A combination of field and modelling work provided an ability to study the mixing behaviour of a wastewater treatment plant's discharge from a multiport diffuser into a receiving river.
    a. The initial jets originating from the diffuser were vertically oriented. These high momentum effluent jets impinged the water surface immediately downstream of the diffuser. The diffuser jets appeared to force diversion of the ambient flow around the diffuser, resulting in a low speed wake region downstream of the diffuser.

b. The effluent mixed quickly with the ambient river flow at the onset of the discharge, with ammonia concentrations decreasing rapidly. Highest ammonia concentration occurred near the water surface in the wake region immediately downstream of the diffuser. The plume then mixed vertically downward and spread laterally. The field data suggested that full vertical mixing occurred approximately 70m downstream of the diffuser. The plume did not spread laterally very rapidly, with model results suggesting that in 200m downstream of the diffuser it spread to 60m from the diffuser's width of 42m. Significant ammonia concentrations were still measurable in the effluent plume 1 km downstream of the diffuser. Furthermore, although end-of-pipe unionized ammonia concentrations passed the regulation, subsequent concentrations found in the river did not pass the recommended 0.016mg-N/L limit to receiving waters.

2. Based on evidence provided in Section 4, CFD modelling results were comparable to field results.
3. The field data were too limited to provide a 3D interpretation of the processes taking place between the discharged and ambient flow, for both the flow field and effluent concentration. However, combined with numerical modelling, a reasonable 3D interpretation was obtained, as provided in 1) above.
4. The CORMIX2 model was a useful aid in planning for the field campaign. Unfortunately, CORMIX2 did not allow for the estimated diffuser/river configuration and thus could not capture the immediate physics of the flow interaction.
5. Ammonia kinetics were not detected within the 200m sampling reach, thus ammonia was treated like a conservative substance for CFD modelling purposes.
6. Certain approximations augmented inaccuracies in CFD simulations. The end-of-pipe ammonia concentrations in the effluent had to be estimated during the water sampling period. The exact position of the diffuser and the diffuser ports' height were not available and had to be estimated.
7. To simplify the CFD modelling, only steady-state modelling was considered. However, due to lack of data and aforementioned modelling uncertainties, it would not have made sense to do otherwise.

8. Modelling sensitivity analysis illustrated that the results were most sensitive to discharge concentrations. When ammonia discharge concentrations were raised, the regression coefficient between measured and simulated data improved.
9. The *k-ε* and RNG *k-ε* models predicted very similar results. The LES model was treated as a spatially and temporally-averaged model. The prediction of the concentration field by all three models was reasonable and provided better results than the CORMIX2 model; illustrating that CFD modelling was more useful for this case than a model based on empirical and semi-empirical equations.
10. During the second half of August of the year 2011, ROPEC's end-of-pipe discharges passed unionized ammonia regulations of 1.25 mg-N/L as expected. However, according to the measurements and CFD simulations completed for this thesis, on August 23, 2011, unionized ammonia concentrations greatly exceeded the chronic toxicity limit of 0.016mg-N/L well beyond a 100m radius downstream of the diffuser (a regulatory limitation consideration if the primary regulation fails).

5.3. Recommendations for future work

1. In order to provide a better interpolation of the flow field, a denser network of ADP transects should be collected. In order to provide a good interpretation of the 3D flow field around the diffuser, tight transects, perpendicular to the river banks immediately upstream and downstream of the diffuser should be collected.
2. A method for collecting effluent concentration with continuous sampling and high frequency would be useful to ensure for a much larger tracer dataset. Employing a Conductivity-Temperature-Depth (CTD) scanner with a fluorometer and Rhodamine-WT injection from the outfall is a common such method (Pilechi *et al.*, 2014). Another method may be to use a CTD scanner with a sensor attachment for ammonia, nitrite and nitrate (Masserini & Fanning, 2000), the employment of which needs further research before deployment.
3. An effort to establish the exact location of the diffuser and the diffuser ports' height is recommended to improve model simulation. Another alternative would be to

model the diffuser position at both suggested locations (see Section 3.1.3) and include the port height in the sensitivity analysis.

4. If the work is to include far field investigations using ammonia, more descriptive kinetics should be analyzed.
5. A different model should be employed (such as OpenFoam – modelling software more readily used at University of Ottawa), which includes turbulence models such as the k-ω and LRR not available in FLOW-3D v. 10.0 used in the thesis.
6. Computing power has increased since the simulations for this thesis were performed, therefore configuration of the computational mesh could be improved. For instance, in FLOW-3D, nested meshes with a higher resolution at and near the diffuser to properly capture each port should be employed. As well, a finer overall mesh resolution should be tested to enable free-surface modelling utilizing the VOF functionality. In OpenFoam, the use of an unstructured mesh in the horizontal plane would be useful for improving the computational analysis.
7. Non-steady state modelling should be considered, where river discharge (or velocity) varies across the model's initial boundary; and effluent discharges and ammonia concentrations vary with time. Effluent discharges are already measured daily, in 1-minute intervals by ROPEC's operations. Ammonia concentration sampling, as described in the Appendix, would require collaboration and a coordinated effort between ROPEC (and most likely approval from the City of Ottawa) and University of Ottawa.

6. References

ABAD, J.D., RHOADS, B.L., GÜNERALP, I., GARCIA, M.H., 2008. Flow Structure at Different Stages in a Meander-Bend with Bendway Weirs. *Journal of Hydraulic Engineering*, **134**(8), pp. 1052-1063.

ADMIRAAL, W., BOTERMANS, Y.J.H., 1989. Comparison of Nitrification Rates in Three Branches of the Lower River Rhine. *Biogeochemistry*, **8**, pp. 135-151.

ALI, J.A., FIELDHOUSE, J.D., 2014. Effects of the Discharge Pipe Structure on Plume Profile Using Software Fluent. *Scientific Journal of Computer Science*, **4**(2), pp. 20-27.

ADVANCED AMERICAN DIVING SERVICE, INC. (AADS), 2004. Georgia Pacific Wauna Mill Outfall – Diiffuser Flow Testing. Report prepared for Georgia Pacific Corp., AADS Portland, Ore.

APHA, 1995. APHA METHOD 4500-NH_3 C. Nesslerization Method (Direct and Following Distillation). Standard Methods for the Examination of Water and Wastewater, 17th ed. American Public Health Association-American Water Works Association-Water Pollution Control Federation (APHA-AWWA-WPCF), APHA, Washington, DC.

APHA, 2005a. 4500-NO_2^- B. Colorimetric Method, Standard Methods for the Examination of Water and Wastewater, 20th ed., American Public Health Association-American Water Works Association-Water Pollution Control Federation (APHA-AWWA-WPCF), APHA, Washington, DC.

APHA, 2005b. 4500-NO_3^- B. Ultraviolet Spectrophotometric Screening Method, Standard Methods for the Examination of Water and Wastewater, 20th ed., American Public Health Association-American Water Works Association-Water Pollution Control Federation (APHA-AWWA-WPCF), APHA, Washington, DC.

AZIZ, T.N., KHAN, A.A., 2011. Research Article: Simulation of Vertical Plane Turbulent Jet in Shallow Water. *Advances in Civil Engineering*, **2011**, 10 pp.

BAPTIST, M.J., UIJTTEWAAL, W.S.J., 2005. Transport and Mixing of Cooling Water: Guidelines and Modelling Practice. Delft, Netherlands, 23 pp.

BARKHUDAROV, M.R., 1997. Advanced Simulation of the Flow and Heat Transfer Processes in Simultaneous Engineering. International ADI and Simulation Conference, Helsinki, Finland, May 28-30, 15 pp.

BENIDICKSON, J., 2007, The Culture of Flushing: A Social and Legal History of Sewage, UBC Press, Vancouver, Canada, 432 pp.

BLUMBERG, A.F. and MELLOR, G.L., 1987. Description of a Three-Dimensional Coastal Ocean Circulation Model. HEAPS, N.S., (ed.). Three Dimensional Coastal Oceans Model. American Geophysical Union, Washington, DC, 17 pp.

BRION, D., BILLEN, G., GUEZENNEC, L., FICHT, A., 2000. Distribution of Nitrifying Activity in the Seine River (France) from Paris to the Estuary. *Estuaries*, **23**(5), pp. 669-682.

CAMARGO, J.A., ALONSO, A., SALAMANCA, A., 2005. Nitrate Toxicity to Aquatic Animals: A Review with New Data for Freshwater Invertebrates. *Chemosphere*, **58**, pp. 1255-1267.

CCME (CANADIAN COUNCIL OF MINISTERS OF THE ENVIRONMENT), 2003. Canadian Water Quality Guidelines for the Protection of Aquatic Life: Nitrate-Ion. In: Canadian Environmental Quality Guidelines, 1999, Canadian Council of Ministers of the Environment, Winnipeg, 8 pp.

CCME (CANADIAN COUNCIL OF MINISTERS OF THE ENVIRONMENT), 2010. Canadian Water Quality Guidelines for the Protection of Aquatic Life: Ammonia. In: Canadian Environmental Quality Guidelines, 1999, Canadian Council of Ministers of the Environment, Winnipeg, 8 pp.

CEDERWALL, K., 1971. Buoyant Slot Jets into Stagnant or Flowing Environments, California Institute of Technology, Division of Engineering and Applied Science, W.M.Keck Laboratory for Hydraulic and Water Resources.

CHANSON, H., 2004. Environmental Hydraulics of Open Channel Flows. Elsevier, Burlington, MA, 430 pp.

CHEN, Y.P., LI, C.W., ZHANG, C.K., 2006. Large Eddy Simulation of Vertical Jet Impingement with a Free Surface. *Journal of Hydrodynamics*, **18**(2), pp. 148-155.

CHOI, K.W., LEE, J.H.W., 2007. Distributed Entrainment Sink Approach for Modeling Mixing and Transport in the Intermediate Field, *Journal of Hydraulic Engineering*, **133**(7), pp. 804-815.

CHU, V.H., 1979. L.N. Fan's Data on Buoyant Jets in Crossflow. *Journal of Hydraulics Division*, **105**(5), pp. 612-617.

COOPER, A.B., 1983. Population Ecology of Nitrifiers in a Stream Receiving Geothermal Inputs of Ammonium. *Applied and Environmental Microbiology*, **45**, pp. 1170-1177.

CRAIG, G.R., MIDDELRAAD, I., 2003. Risk Management for Ammonia: Determination of a Site-Specific Ammonia Limit in Municipal Wastewater Effluent (MWWE). *Prepared for Environment Canada by G.R. Craig & Associates Inc. Environmental Toxicology*, 62 pp.

DANESHFAR, B., 2011. Data Transformation (PowerPoint slides). Retrieved from lecture notes: GEO5153B Computer Techniques in Earth Sciences, University of Ottawa.

DAVIERO, G.J., ROBERTS, P.J.W., 2006. Marine Wastewater Discharges from Multiport Diffusers III: Stratified Stationary Water. *Journal of Hydraulic Engineering*, **132**(4), 404-410.

DONEKER, R.O., JIRKA, G.H., 2007. CORMIX User Manual: A Hydrodynamic Mixing Zone Model and Decision Support System for Pollutant Discharges into Surface Waters. US Environmental Protection Agency, EPA-823-K-07-001, Washington, D.C., 236 pp.

EC (ENVIRONMENT CANADA), 1990. Biological Test Method: Acute Lethality Test Using Rainbow Trout. Conservation and Protection, Ottawa, Ontario, Report EPS 1/RM/9 including May 1996 Amendments, 51 pp.

EC (ENVIRONMENT CANADA), 2012. Daily Data Report for August 2011. url: www.climate.weatheroffice.gc.ca, accessed: July 11, 2012.

EC (ENVIRONMENT CANADA), 2013. Guideline for the Release of Ammonia Dissolved in Water Found in Wastewater Effluents. url: http://www.ec.gc.ca/lcpe-cepa/default.asp?lang=En&n=B7CE1A5E-1&offset=1&toc=show, accessed: Nov. 17, 2014.

EC (ENVIRONMENT CANADA), 2015. Daily Discharge Data for Ottawa River at Brittania (02KF005). url: www.wateroffice.ec.gc.ca accessed: March 14, 2015.

EC (ENVIRONMENT CANADA), HC (HEALTH CANADA), 2000. Ammonia in the Aquatic Environment. CEPA 1999, Priority Substances List Assessment Report, En40–215/55E, pp. 103.

EMERSON, K., RUSSO, R.C., LUND, R.E., THURSTON, R.V., 1975. Aqueous Ammonia Equilibrium Calculations: Effect of pH and Temperature. *Journal of Fisheries Research Board of Canada,* **32**(12), pp. 2379-2383.

ETEMAD-SHAHIDI, A. and AZIMI, A.H., 2007. Simulation of Thermal Discharges Using Two Mixing Zone Models. *Journal of Coastal Research,* (Special issue 50), pp. 663-667.

FISHERIES ACT, 1985. Wastewater Systems Effluent Regulations (SOR/2012-139). Canada, url: http://www.gazette.gc.ca/rp-pr/p2/2012/2012-07-18/html/sor-dors139-eng.html, accessed: December 23, 2014.

FLOW SCIENCE, 2010. FLOW-3D Model User Manual, v. 10.0. Flow Science, Inc.

FLOW SCIENCE, 2012. CFD-101: The Basics of Computational Fluid Dynamics Modeling. Simulating Fluid Flows with Free Surfaces, Flow Science, Inc., url: http://www.flow3d.com/cfd-101/cfd-101-free-surface-fluid-flow.html, accessed: August 8, 2012.

FLOW SCIENCE, 2014. FLOW-3D^{V11} Water & Environment Training: Lectures. Flow Science, Inc.

FRANZINI, J.B., FINNEMORE, E.J., 1997. Fluid Mechanics with Engineering Applications, 9th ed. McGraw-Hill, Toronto, Canada, 807 pp.

GOOGLE MAPS, 2012. url: Not Available, accessed: February 23, 2012.

HARLEMAN, D.R.F., JIRKA, G.H., 1974. Buoyant Discharges from Submerged Multiport Diffusers. *Proceedings of the 14th ASCE Coastal Engineering Conference.* Copenhagen, Denmark, June 24-28.

HE, S., XU, Z., JACKSON, J. D., 2002. An Experimental Investigation of Buoyancy-Opposed Wall Jet Flow." *International Journal of Heat and Fluid Flow*, **23**, pp. 487–496.

HIRT, C.W., SICILIAN, J.M., 1985. A Porosity Technique for the Definition of Obstacles in Rectangular Cell Meshes. Proc. 4th Intl. Conf. Ship Hydro-dynamics, 1–19. National Academy of Science, Washington, DC.

HOLETON, C., CHAMBERS, P.A., GRACE, L., 2011. Wastewater Release and its Impacts on Canadian Waters. *Canadian Journal of Fisheries and Aquatic Sciences,* **68**, pp. 1836-1859.

HUAI, W.X., XIAO, Q.H., ZENG, Y.H., YANG, Z.H., QIAN, Z.D., 2008. Behavior of Near-Field Dilution of Thermal Buoyant Jet Discharged Horizontally in Compound Open-Channel. *Applied Mathematics and Mechanics – English Edition,* **29**(2), pp. 263-271.

HUAI, W.X., LI, Z.W., QIAN, Z.D., ZENG, Y.H., HAN, J., 2010. Numerical Simulation of Horizontal Buoyant Wall Jet. *Journal of Hydrodynamics*, **22**(10), pp. 58-65.

ICH (INTERNATIONAL CONFERENCE ON HARMONISATION OF TECHNICAL REQUIREMENTS FOR REGISTRATION OF PHARMACEUTICALS FOR HUMAN USE), 2005. Validation of Analytical Procedures: Text and Methodology Q2(R1), 17 pp.

JAMIESON, E.C., RENNIE, C.D., JACOBSON, R.B., TOWNSEND, R.D., 2011. 3-D Flow and Scour Near a Submerged Wing Dike: ADCP Measurements on the Missouri River. *Water Resources Research* **47** W07544, DOI:10.1029/2010WR010043, 20 pp.

JIRKA, G.H., 1982. Multiport Diffusers for Heat Disposal: A Summary. *Journal of the Hydraulics Division* **108**(12), pp. 1425-1468.

JIRKA, G.H., 2006. Integral Model for Turbulent Buoyant Jets in Unbounded Stratified Flows Part 2: Plane Jet Dynamics Resulting from Multiport Diffuser Jets. *Environmental Fluid Mechanics,* **2006**(6), pp. 43–100.

JIRKA, G.H., HARLEMAN, D.R.F., 1979. Stability and Mixing of a Vertical Plane Buoyant Jet in Confined Depth. *Journal of Fluid Mechanics,* **94**(2), pp. 275-304.

JIRKA, G.H., DONEKER, R.L., HINTON, S.W., 1996. User's Manual for CORMIX: A Hydrodynamic Mixing Zone Model and Decision Support System for Pollutant Discharges into Surface Waters, Office of Science and Technology, U.S. Environmental Protection Agency, Washington, DC, 164 pp.

KENNEDY, K. J., MCHARG, A. M., 2007. Optimization of Municipal Wastewater Biological Nutrient Removal Using ASM2d. *Journal of Environmental Engineering and Science*, 6, pp. 31-43.

KHEIRKHAH GILDEH, H., MOHAMMADIAN, A., NISTOR, I., QIBLAWEY, H., 2015. Numerical Modeling of 30° and 45° Inclined Dense Turbulent Jets in Stationary Ambient. *Environmental Fluid Mechanics*, **15**(3), pp.537-562.

KIM, G.D., CHO, H.Y., 2006. Modeling the Buoyant Flow of Heated Water Discharged from Surface and Submerged Side Outfalls in Shallow and Deep Water with a Cross Flow. *Environmental Fluid Mechanics*, **6**, pp. 501-518.

KIM, G.D., SEO, I.W., 2000. Modeling the Mixing of Heated Water Discharged from a Submerged Multiport Diffuser. *Journal of Hydraulic Research*, **38**(4), pp. 259-270.

KUANG, C. P., AND LEE, J. H. W., 2001. Effect of Downstream Control on Stability and Mixing of a Vertical Plane Buoyant Jet in Confined Depth. *Journal of Hydraulic Research*, **39**(4), pp. 375-391.

KUANG, C. P., AND LEE, J. H. W., 2006. Stability and Mixing of a Vertical Axisymmetric Buoyant Jet in Shallow Water. *Environmental Fluid Mechanics*, **6**(2), pp. 153-180.

LAI, A.C.H, LEE, J.H.W., 2012. Dynamic Interaction of Multiple Buoyant Jets. *Journal of Fluid Mechanics*, **708**, pp. 539-575.

LEE, J.H.W., 2012, Mixing of Multiple Buoyant Jets. *Journal of Hydraulic Engineering*, **138**(12), pp. 1008-1021.

LEE, J.H., JIRKA, G.H., HARLEMAN, D.R.F., 1977. Modelling of Unidirectional Thermal Diffusers in Shallow Water. MIT Dep Civ Eng Ralph M. Parsons Lab Water Resour Hydrodyn Rep, 308 pp.

LI, Z.W., HUAI, W.X., QIAN, Z.D., 2012. Study on the Flow Field and Concentration Characteristics of the Multiple Tandem Jets in Crossflow. *Science China Technological Sciences*, **55**(10), pp. 2778-2788.

LI, S.S., HODGINS, D.O., 2010. Modelling Wastewater Effluent Mixing and Dispersion in a Tidal Channel. *Canadian Journal of Civil Engineering*, **37**, pp. 99-111.

LOWE, S.C., SCHUEPFER, F., DUNNING, D.J., 2009. Case Study: Three-Dimensional Hydrodynamic Model of a Power Plant Thermal Discharge. *Journal of Hydraulic Engineering*, **135**(4), pp. 247-256.

MARSDEN, R., 2012. Performance of Several ADCP Internal Magnetic Compasses. In Hydraulic Measurements and Experimental Methods 2012, CD edited by D.M. Admiraal and D.F Hill, 2012 Hydraulic Measurements and Experimental Methods Conference, Snowbird, Utah, August 12-15, ASCE, 6 pp.

MASSERINI, R.T., FANNING, K.A., 2000. A Sensor Package for the Simultaneous Determination of Nanomolar Concentrations of Nitrite, Nitrate, and Ammonia in Seawater by Fluorescence Detection. *Marine Chemistry*, **68**(4), pp. 323-333.

NRCAN (NATURAL RESOURCES CANADA), 2010. Ottawa River. url: http://www.nrcan.gc.ca/earth-sciences/products-services/mapping-product/geoscape/ottawa/6040, accessed: March 8, 2013.

ONTARIO WATER RESOURCES ACT, 1990. Ontario Regulation 129/04: Licensing of Sewage Works Operators. url: http://www.e-laws.gov.on.ca/html/regs/english/elaws_regs_040129_e.htm, accessed: June 19, 2012.

PARK, Y.W., SEONG, G.H., KWUN, S.K., 2007. Interfacing Near- and Far-Field Models to Simulate Submerged Freshwater Discharge Mixing in Seawater. *Coastal Engineering Journal*, **49**(3), pp. 337-356.

PAUER, J.J., AUER, M.T., 2009. Formulation and Testing of a Novel River Nitrification Model. *Ecological Modeling*, **220**, pp. 857-866.

PILECHI, A., RENNIE, C. D., MOHAMMADIAN, A., ZHU, D. Z., 2014. *In Situ* Spatially Distributed Field Measurements of Transverse Dispersion of a Wastewater Effluent in an Extended Natural Meandering River. *Journal of Hydraulic Research*, DOI: 10.1080/00221686.2014.950611

POCERNICH, M., LITKE, D.W., (1997). Nutrient Concentrations in Wastewater Treatment Plant Effluents, South Platte River Basin. *Journal of the American Water Resources Association*. **33**(1), pp. 205-214.

RENNIE, C.D., CHURCH, M., 2010. Mapping Spatial Distribution and Uncertainty of Water and Sediment Flux in a Large Gravel Bed River Reach Using an Acoustic Doppler Current Profiler. *Journal of Geophysical Research*, **115**(3), 27 pp.

ROBERTS, P.J.W., 1979. Line Plume and Ocean Outfall Dispersion. *Journal of Hydraulics Division*, **105**(4), pp. 313-330.

ROBERTS, P.J.W., HUNT, C.D., MICKELSON, M.J., TIAN, X., 2011a. Field and Model Studies of the Boston Outfall, *Journal of Hydraulic Engineering*, **137**(11), pp. 1415-1425.

ROBERTS, P.J.W., TIAN, X., JUNG, Y., 2011b. Physical Model Study of an Alternating Diffuser for Thermal Discharge, *Journal of Hydraulic Engineering*, **137**(9), pp. 1027-1036.

RODI, W., 1993. Turbulence Models and Their Application in Hydraulics: A State-of-the-Art Review, 3rd ed. A. A. Balkema, Rotterdam, 124 pp.

RUTHERFORD, J.C., 1994. River mixing. John Wiley & Sons Ltd., Chichester, England.

SIMPSON, M.R., 2001. Discharge Measurements Using a Broad-Band Acoustic Doppler Current Profiler. U.S. Geological Survey Open-File Report 01-1, Sacramento, California, 134 pp.

SOCOLOFSKY, S.A. and JIRKA, G.H., 2005. Special Topics in Mixing and Transport Processes in the Environment. Engineering Lecture Notes, 5th ed. Coastal and Ocean Engineering Division, Texas A&M University, Texas.

STAMOU, A.I., NIKIFORAKIS, I.K., 2013. Integrated Modelling of Single Port, Steady-State Thermal Discharges in Unstratified Coastal Waters. *Environmental Fluid Mechanics*, **13**(4), pp. 309-336.

TECPLOT, INC., 2011. Tecplot 360 2011 User's Manual. Tecplot, Inc., Bellevue, Washington, 586 pp.

TOOMBES, L., CHANSON, H., 2011. Numerical Limitations of Hydraulic Models. 34th IAHR World Congress, Brisbane, Australia, June 26 – July 1, 8 pp.

TANG, H.S., PAIK, J., SOTIROPOULOS, F., KHANGAONKAR, T., 2008. Three-Dimensional Numerical Modeling of Initial Mixing of Thermal Discharges at Real-Life Configurations. *Journal of Hydraulic Engineering*, **134**(9), pp. 1210-1224.

TIAN, X., ROBERTS, P.J.W., DAVIERO, G.J., 2004a. Marine Wastewater Discharges from Multiport Diffusers. I: Unstratified Stationary Water. *Journal of Hydraulic Engineering*, **130**(12), pp. 1137–1146.

TIAN, X., ROBERTS, P.J.W., DAVIERO, G.J., 2004b. Marine Wastewater Discharges from Multiport Diffusers. II: Unstratified Flowing Water. *Journal of Hydraulic Engineering*, **130**(12), pp. 1147–1155.

TIAN, X., ROBERTS, P.J.W., DAVIERO, G.J., 2006. Marine Wastewater Discharges from Multiport Diffusers IV: Stratified Flowing Water. *Journal of Hydraulic Engineering*, **132**(4), 411-419.

TIAN, X., ROBERTS, P.J.W., 2011. Experiments on Marine Wastewater Diffusers with Multiport Rosettes. *Journal of Hydraulic Engineering*, **137**(10), pp. 1148–1159.

USACE (U.S. ARMY CORPS OF ENGINEERS), 2001. Simulation of Tailrace Hydrodynamics Using Computational Fluid Dynamics Models. Report Number: PNNL-13467, 35 pp.

USEPA (U.S. ENVIRONMENTAL PROTECTION AGENCY), 1981. Hourly Diurnal Flow Variations in Publicly-Owned Wastewater Treatment Facilities [Project Summary]. Washington, D.C., no. 600-S2-81-218, 4 pp.

USEPA (U.S. ENVIRONMENTAL PROTECTION AGENCY), 2013. Aquatic Life Ambient Water Quality Criteria for Ammonia – Freshwater. Office of Science and Technology, Washington, DC. EPA 822-R-13-001, 255 pp.

VERSTEEG, H.K., MALALASEKERA, W., 2007. An Introduction to Computational Fluid Dynamics: The Finite Volume Method, 2nd ed. Longman Scientific & Technical, Essex, England, 503 pp.

VIOLLET, P.L., 1980. Turbulent Mixing in a Two Layer Stratified Shear Flow. *Proc., 2nd Int. Symp. on Stratified Flows*, Trondheim, Norway, pp. 315–325.

WADE, A., MAHER, B., LAWRENCE, I., DAVIS, N., ZOPPOU, C., BELL, C., 1988. Estimating the Allowable Ammonia Concentrations in Wastewater Treatment Plant Discharge to Ensure Protection of Aquatic Biota. *Environmental Technology*, **19**, pp. 749-754.

WAGNER, C.R., MUELLER, D.S., 2011. Comparison of Bottom-Track to Global Positioning System Referenced Discharges Measured Using an Acoustic Doppler Current Profiler. *Journal of Hydrology*, **401**, pp. 250-258.

WATER ENVIRONMENT FEDERATION, 2008. Operation of Municipal Wastewater Treatment Plants: MoP No.11, 6th ed. WEF Press, Toronto. McGraw-Hill Professional publication.

WATER ENVIRONMENT FEDERATION, 2011. Nutrient Removal: WEF MoP No. 34. WEF Press, Toronto. McGraw-Hill Professional publication.

WEPP (WATER ENVIRONMENT PROTECTION PROGRAM), 2007. Pollution Prevention Plan for Inorganic Chloramines and Chlorinated Wastewater Effluents in the City of Ottawa, Appendix D, Environmental Effects Monitoring Report for 2005/2006. Prepared by Stantec, Ottawa, 112 pp.

WATER SURVEY OF CANADA, 2010. Hydrometric Data.
url: http://www.wsc.ec.gc.ca/applications/H2O/index-eng.cfm, accessed: March 7, 2013.

WETZEL, R. G., 1983. Limnology. 2nd ed., Saunders Press, Philadelphia, PA, 860 pp.

XUE, W.Y., HUAI, W.X., QIAN, Z.D., 2014. Numerical Simulation of Initial Mixing of Marine Wastewater Discharge from Multiport Diffusers. *Engineering Computations*, **31**(7), pp. 1379-1400.

YANNOPOULOS, P.C., 2010. Advanced Integral Model for Groups of Interacting Round Turbulent Buoyant Jets. *Environmental Fluid Mechanics,* **10**, pp. 415-450.

YAKHOT, V., ORSZAG, S.A., 1986. Renormalization Group Analysis of Turbulence. I. Basic Theory. *Journal of Scientific Computing,* **1**(1), pp. 3-51.

ZHANG, X.Y., ADAMS, E.E., 1999. Prediction of Near Field Plume Characteristics Using Far Field Circulation Model. *Journal of Hydraulic Engineering,* **125**(3), pp. 233-241.

ZHANG, W., ZHU, D.Z., 2011. Near-Field Mixing Downstream of a Multiport Diffuser in a Shallow River. *Journal of Environmental Engineering,* **137**(4), pp. 230-240.

ZHAO L., CHEN C., LEE, K., 2011. Modelling the Dispersion of Wastewater Discharges from Offshore Outfalls: A Review. *Environmental Reviews,* **19**(1), pp. 107-120.

A. Appendix

Estimation of ROPEC's ammonia discharge and concentration during the field campaign

Outflows from a municipal diffuser are not constant with time. However, for simplicity, simulations were performed using steady state conditions and thus, constant values were used for effluent discharge and ammonia concentration. This section provides a brief overview of data collection at ROPEC and how constant values for this thesis were derived.

Effluent flow rates from ROPEC are available in 1-minute intervals.

One-day composite wastewater samples were collected by combining samples collected several times an hour by an auto-sampler. These composite samples were used to verify ammonia, nitrite and nitrate levels in the final effluent wastewater and hence the wastewater discharged to the Ottawa River. Composites are collected every other day. Since the field campaign was not synchronized with ROPEC's sampling, variation in effluent ammonia concentrations was not captured during the hours of the field campaign.

Occasionally, hourly concentration data are also collected at the plant. In February 2012 during dry-weather conditions, samples were collected every 10 minutes to make hourly composites. These hourly concentration data originated from the primary treatment effluent. The concentrations here are similar (if not equivalent) to ammonia, nitrite and nitrate concentrations in the final effluent since secondary treatment is not designed to nitrify ammonia (Ranya Sherif, personal communication). Subsequently, these data were used to determine whether a relationship exists between changes in ammonia concentration levels and effluent flow rates from the plant.

Discharge

The field campaign took place on August 23, 2011 between 13:23 and 18:49 hours. The ROPEC effluent discharge (Ranya Sherif, personal communication) on the day of the campaign is shown in Figure A.1, where hours of discharge during hours of sampling are

highlighted by the dotted orange box. An average discharge rate of 4.022m^3/s (0.447m^3/s per port) was calculated to be the mean effluent discharge during the sampling period. Note that the discharge is highly oscillatory throughout the field campaign.

Figure A.1 illustrates an early morning discharge of 3m^3/s until 10:00 hours. For an hour afterwards, discharge significantly increased (to 5m^3/s). Subsequently, the discharge slowly decreased. Between the hours of 13:30 and 15:30 the effluent discharge stabilized (to 3.4m^3/s). From the hours of 15:30 to 19:00 a large variation in discharge ensued having a range of 2 to 7m^3/s.

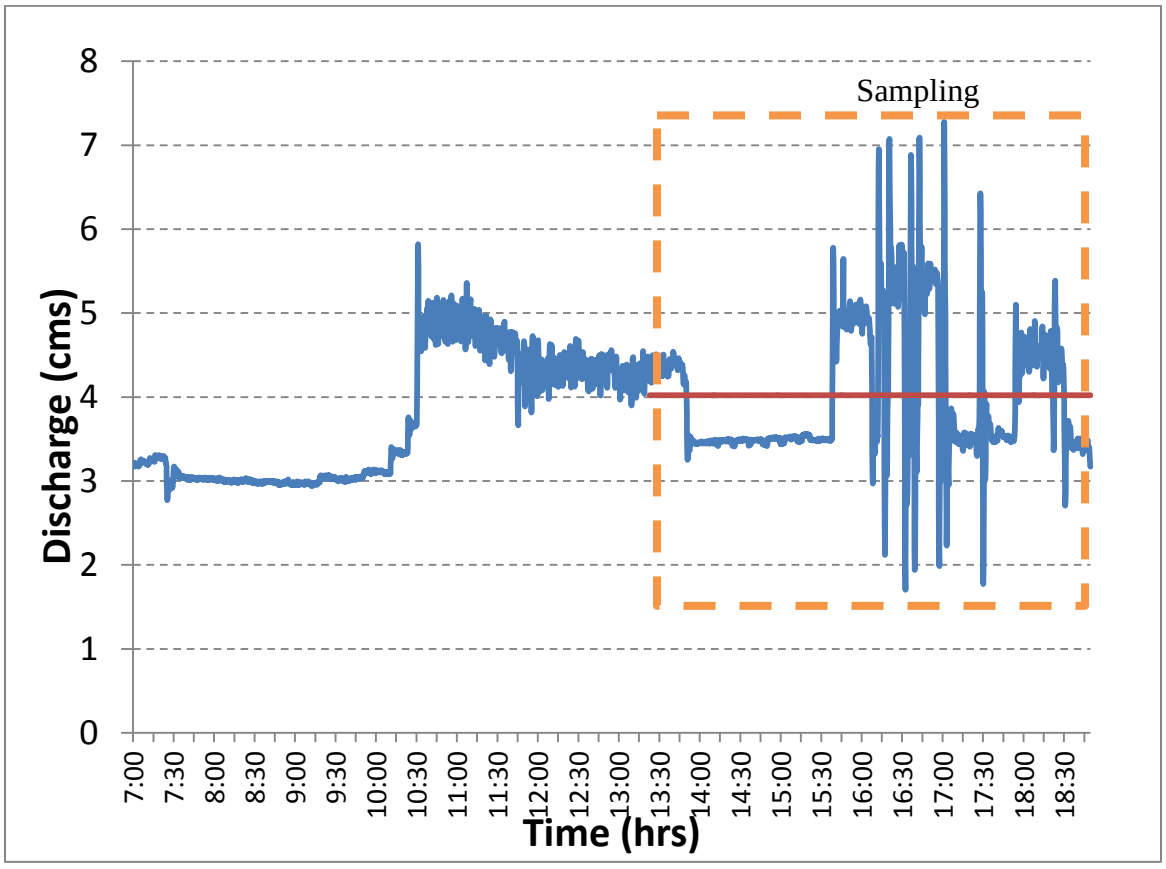

Figure A.1: Effluent discharge from ROPEC between 7am and 6:45pm on August 23, 2011 (Ranya Sherif, personal communication). The straight red line represents the calculated average of the discharges as encapsulated by the orange dotted box which signifies the sampling period.

A simple sensitivity analysis for the change in discharge is presented in

Table A.1, where the time-period within which the average flow rate was calculated is provided. It shows the difference in average discharge depending on which time-period is chosen.

Table A.1: Sensitivity analysis for the changes in discharge of ROPEC's effluent on August 23, 2012.

Time period	Average discharge (m^3/s)
7:00 – 18:49	3.845
9:00 – 18:49	4.029
11:30 – 18:49	4.106
13:23 – 18:49	4.022

A 12 hour average encompassing early morning discharges, resulted in the lowest average value of $3.8 m^3/s$; whereas a 7.25 hour average, encompassing the lunch hour discharge, provided the highest average value of $4.1 m^3/s$.

Ammonia concentration

Ammonia composites (Ranya Sherif, personal communication) are provided in Figure A.2 for every other day between the dates of August 16 and 28, 2011. The water sampling campaign took place on August 23, 2011. Note that the lowest (21mg-N/L) and highest (29mg-N/L) values of ammonia concentrations measured in the 13 day period were one day prior to and one day after sampling, respectively. Otherwise ammonia concentrations ranged between 26 and 28 mg-N/L. From these values, the mean concentration was 26.57mg-N/L (indicated by the solid red line), the median was 27mg-N/L and the standard deviation was 2.44mg-N/L.

Indicated also (in Figure A.2) are ammonia concentrations of ROPEC's final effluent between 2008 and 2010 collected by the City of Ottawa (Adam Bishow, personal communication). Ammonia composites on September 3, 2008 were 25mg-N/L, on August 24, 2009 it was 24mg-N/L and on August 30, 2010 it was 26mg-N/L. All dates fall within the 2 week period of the year as the

sampling period. These data show that the ammonia concentration outputs are fairly consistent year to year during a similar time period.

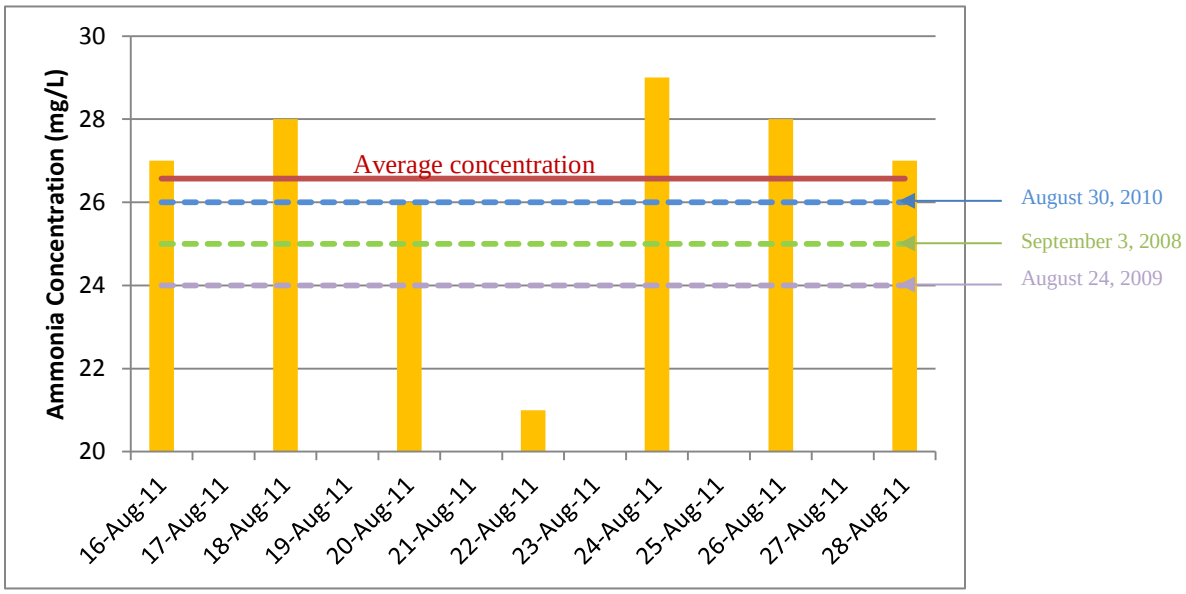

Figure A.2: Ammonia composites (orange bars) at ROPEC between August 16 and 28, 2011. Plotted also are ammonia composites for September 3, 2008 (dashed green line), August 24, 2009 (purple dashed line) and August 30, 2010 (blue dashed line). Data was made available by ROPEC (Ranya Sherif, personal communication). The average concentration of the bar data is shown by the solid red line. Note that the water sampling for this study occurred on August 23, 2011.

Relationship between effluent discharge and ammonia concentration

Brief examination was performed to show correlation between effluent discharge rates and ammonia concentrations in the plant and at the outflow.

Using available data provided by ROPEC (during the time of the field campaign and water sampling) provided no evidence of a relationship between average effluent discharges and ammonia concentration. Figure A.3 provides a comparison of the average effluent discharge with ammonia concentration for all even dates between August 18 and 28 (dates for which ammonia concentration levels are available). Discharge values are averages from 13:23 to 18:49 hours for all of the dates provided. The highest discharge of 6.2m^3/s corresponds to 28mg-N/L of ammonia, while the highest ammonia concentration of 29mg-N/L corresponds to 4.6m^3/s. The lowest discharge of 4.1m^3/s corresponds to 28mg-N/L of ammonia, while the lowest ammonia concentration of 21mg-N/L corresponds to 4.3m^3/s discharge.

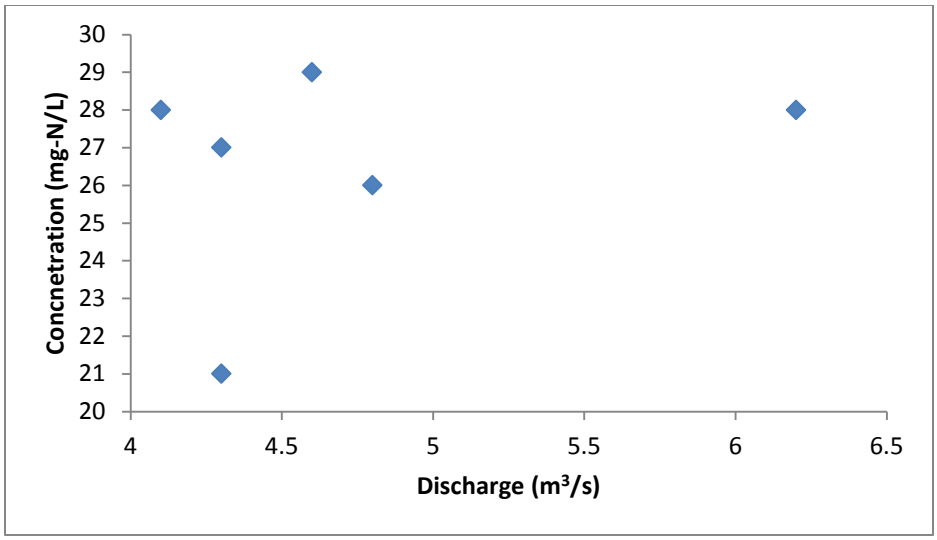

Figure A.3: Ammonia concentrations versus average effluent flows every other day, between August 18 and August 28, 2011.

Another method was used to check for a correlation between effluent discharges and ammonia concentration. This also provided no evidence of a relationship as discussed below. Hourly effluent flows and composites of ammonia concentrations were collected for a short period of time in February 2012 at ROPEC (Ranya Sherif, personal communication). Data were collected from 12:00, February 15th to 11:00, February 16th and from 8:00, February 18th to 7:00, February 20th. Hours given are in a 24hr time frame. Results are provided in Figure A.4. Note that the data are not continuous time-series data. In total 72 hours (24 hours for the first series and 48 hours for the second) are available for analysis.

In the time-series of Figure A.4, ammonia concentrations peaked in the afternoon from 14:00 to 16:00 hours in the afternoon and tended to be lowest around midnight. For the second set of time-series data, peak flows were at approximately 16:00 hours in the afternoon, whereas the first set of time-series data did not demonstrate an obvious peak. The lowest effluent flows for both sets were consistently exhibited at 8:00 in the morning.

Correlation between ammonia concentration and flow between the 1st and 2nd time-series in the graph of Figure A.4 were 0.26 and 0.41, respectively. A cross-correlation time lag test was conducted for each time-series set to identify any trends between ammonia and effluent flow. A single time lag correlation could not be calculated as the time-series has to be continuous. Thus, two time lag tests were performed. For the first set, the peak

correlation of 0.8 occurred at a lag of 8 hours (ammonia peak lagged the discharge peak). For the second set, the peak correlation of 0.75 occurred 1 hour ahead (ammonia peak was ahead of the discharge peak). The second set also exhibited a dip-peak correlation of 0.8 where a dip in ammonia was exhibited 7 hours following a peak in discharge.

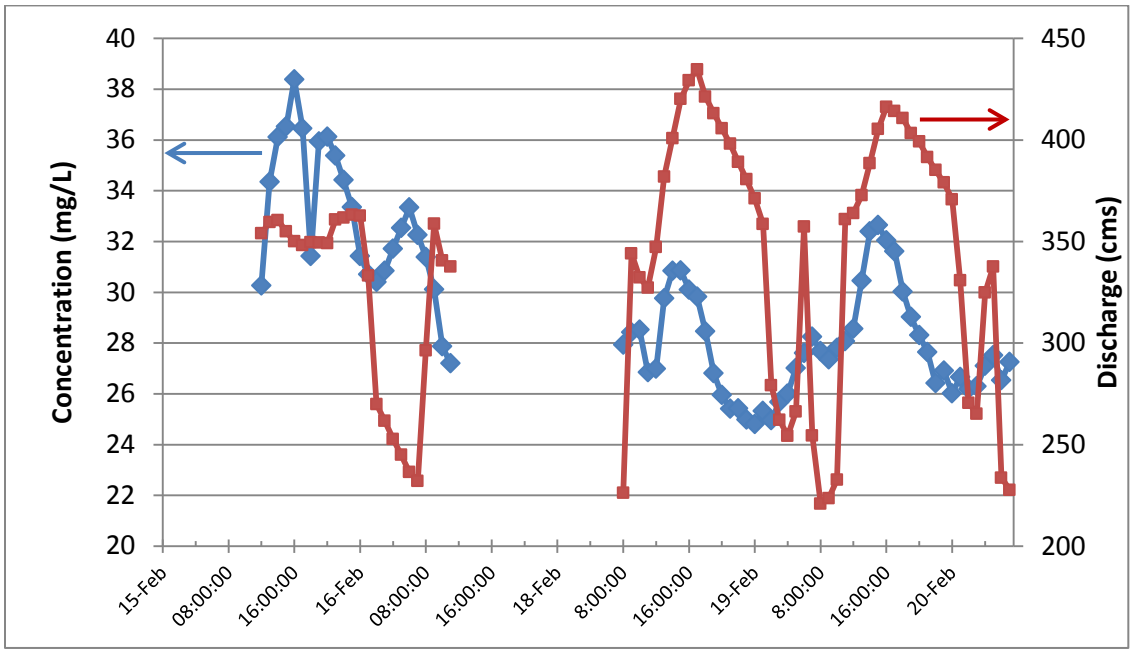

Figure A.4: Hourly ammonia concentration (blue) and effluent flow (red). Data was made available by ROPEC (Ranya Sherif, personal communication). The vertical axis on the left is a scale of concentration and the axis on the right is a scale of discharge. The horizontal axis shows the time period in hours over a 5 day range.

Final estimates

Average flows and concentrations are used for modelling purposes as steady-state flow is simulated in this thesis. An average discharge rate of 4.022m^3/s (0.447m^3/s per port) and an average ammonia concentration of 26.57mg-N/L were used for simulations.